



저작자표시-비영리-동일조건변경허락 2.0 대한민국

이용자는 아래의 조건을 따르는 경우에 한하여 자유롭게

- 이 저작물을 복제, 배포, 전송, 전시, 공연 및 방송할 수 있습니다.
- 이차적 저작물을 작성할 수 있습니다.

다음과 같은 조건을 따라야 합니다:



저작자표시. 귀하는 원저작자를 표시하여야 합니다.



비영리. 귀하는 이 저작물을 영리 목적으로 이용할 수 없습니다.



동일조건변경허락. 귀하가 이 저작물을 개작, 변형 또는 가공했을 경우에는, 이 저작물과 동일한 이용허락조건하에서만 배포할 수 있습니다.

- 귀하는, 이 저작물의 재이용이나 배포의 경우, 이 저작물에 적용된 이용허락조건을 명확하게 나타내어야 합니다.
- 저작권자로부터 별도의 허가를 받으면 이러한 조건들은 적용되지 않습니다.

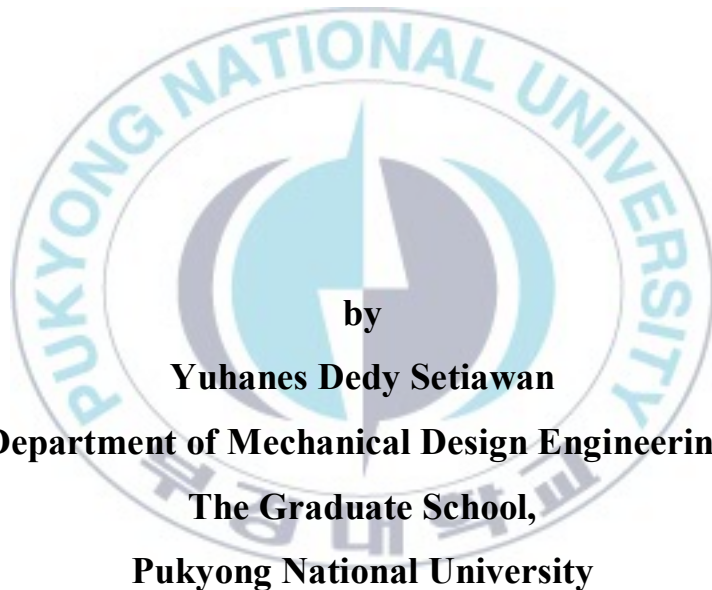
저작권법에 따른 이용자의 권리는 위의 내용에 의하여 영향을 받지 않습니다.

이것은 [이용허락규약\(Legal Code\)](#)을 이해하기 쉽게 요약한 것입니다.

[Disclaimer](#)

Thesis for the Degree of Master of Engineering

**Development and Controller Design of
Four Wheel Independent Steering
Automatic Guided Vehicles**



February 2015

**Development and Controller Design of
Four Wheel Independent Steering
Automatic Guided Vehicles**

**4 른 독립제어 조향 무인차량의
개발 및 제어기설계**

Advisor: Professor Sang Bong Kim

by

Yuhanes Dedy Setiawan

A thesis submitted in partial fulfillment of the requirements
for the degree of

Master of Engineering

in Department of Mechanical Design Engineering, The Graduate
School, Pukyong National University

February 2015

Development and Controller Design of Four Wheel Independent Steering Automatic Guided Vehicles

A thesis

by

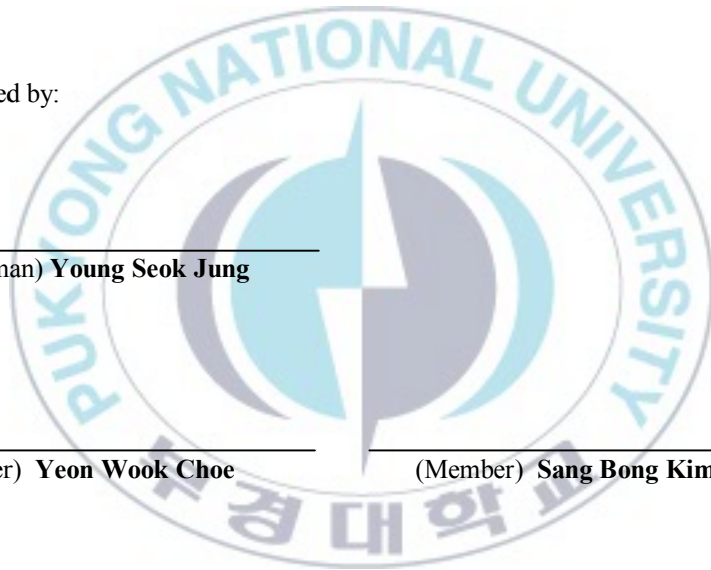
Yuhanes Dedy Setiawan

Approved by:

(Chairman) **Young Seok Jung**

(Member) **Yeon Wook Choe**

(Member) **Sang Bong Kim**



February 27, 2015

Acknowledgements

First of all, I would like to give my highest praise to God for all helps and guidance that have been given such that I could finish all my research and thesis in Master program very well. All achievement and success that have been granted to me only can I return to the One who owns them. In this right moment of time, I would like to express my deep gratitude to all people who helped me during my study and meaningful life in South Korea.

Firstly, I would like to express my deepest gratitude to my professor, Professor Sang Bong Kim, who has helped me significantly in completing my Master program. I really appreciate his kindness and helps that he has shown to me during my study in his excellent laboratory.

Secondly, I would like to express my sincere gratitude to the members of my thesis committee, Professor Young Seok Jung and Professor Yeon Wook Choe, for their helpful comments and suggestions for my thesis.

Thirdly, I would like to express my profound gratitude to Professor Hak Kyeong Kim for his great help and advice such that I could finish my research project and my master thesis very well.

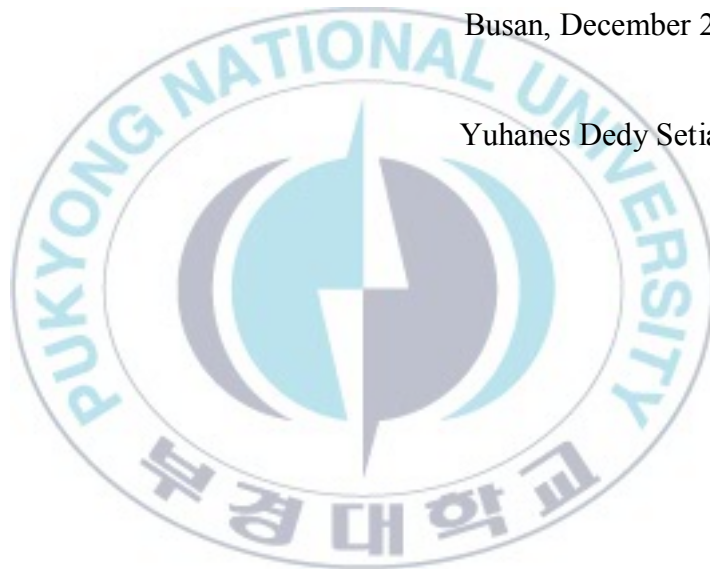
Furthermore, I would like to express my gratitude to all members of Computer Integrated Manufacturing Electronics Commerce (CIMEC) laboratory for their cooperation, kindness and friendship, Dr. Phuc Thinh Doan, Dr. Bui Thanh Luan, Dr. Hoang Giang, Mr. Pandu Sandi Pratama, Mr. Van Tu Duong, Mr. Nguyen Tron Hai, Mr. Quang Tuyen Tran, Mr. Min Jung Hu, Miss. Amruta Vinod Gulalkari,

Mr. Jin Wook Kim, Mr. Husam Hasan Khudhir El-dulaimi, Mr. Ding Xingkun, Mr. Jeong Jae Hoon and Mr. Sheng Dongbo.

Last but not least, I would like to express my deepest gratitude to my father, Liauw Joeng Ji, my mother, Go Erlani, my sister, Ciska Yuni Setiawan and all my relatives for their love, endless prayers, encouragement and support for me not only in completing Master program but also in the whole of my life.

Busan, December 22, 2014

Yuhanes Dedy Setiawan



Contents

Acknowledgements

Contents	i
Abstract	iii
List of Figures	v
List of Tables	xi
Chapter 1: Introduction	1
1.1 Background and motivation	1
1.2 Objective and research method	4
1.3 Outline and contribution of thesis	6
Chapter 2: System Modeling and Controller Design	8
2.1 Basic terminologies.....	8
2.2 Four wheel steering vehicle maneuvers	11
2.2.1 Parallel steering maneuver	11
2.2.2 Zero-sideslip maneuver	13
2.3 Kinematic modeling.....	22
2.4 Controller design based on Backstepping method.....	29
Chapter 3: Controller Implementation and Hardware	
Description	34
3.1 Mechanical design	34
3.1.1 Body configuration	36
3.1.2 Wheel configuration.....	40
3.2 Electrical design.....	43
3.2.1 DC motors.....	44
3.2.2 Encoders	45
3.2.3 Industrial PC	46
3.2.4 Battery	49

3.2.5 Microcontrollers AVR ATmega128	50
3.2.6 Motor drivers	51
3.2.7 Monitor	51
3.2.8 Laser Navigation System NAV200.....	53
3.3 Graphical Unit Interface (GUI) software	57
Chapter 4: Simulation and Experimental Results.....	60
4.1 Simulation results.....	60
4.1.1 Reference trajectory with sharp edges	60
4.1.2 Circular reference trajectory	76
4.2 Experimental results.....	94
4.2.1 Reference trajectory with sharp edges	94
4.2.2 Circular reference trajectory	101
Chapter 5: Conclusions	115
5.1 Conclusions	115
5.2 Future works.....	117
References.....	118
Publication and Conferences	128
Appendix A: Proof of Eq. (2.10)	131
Appendix B: Proof of Eqs. (2.12) - (2.15).....	152
Appendix C: Proof of Eqs. (2.53) and (2.54).....	159
Appendix D: Proof of Eq. (2.62)	161
Appendix E: Mechanical design drawing.....	164

Development and Controller Design of Four Wheel
Independent Steering Automatic Guided Vehicles

Yuhanes Dedy Setiawan

Department of Mechanical Design Engineering, The Graduate School,
Pukyong National University

Abstract

Development of Automated Guided Vehicles (AGVs) has been an interesting research topic over decades not only for researchers in university but also for AGV manufacturers. The goal is to improve AGVs' efficiency in fulfilling the given task such as material handling. Several kinds of wheel configuration for AGVs have been developed such as differential drive configuration and tricycle wheel configuration. To get higher maneuverability and flexibility, four wheel independent steering configuration have been proposed for development of AGVs, hereafter referred to as four wheel independent steering AGVs (4WIS-AGVs).

The objective of this thesis is to present a new type of 4WIS-AGV for carrying heavy baggage and propose a controller that is designed for the 4WIS-AGV to track given trajectories like omnidirectional tracking using Backstepping method. To do this task, the followings are done. First, a 4WIS-AGV is designed and manufactured for experimental purpose. Eight DC motors are used in this system: four motors for steering motor and the others for driving motor. Second, a kinematic modeling of the 4WIS-AGV is created based on a single track vehicle model. This model is obtained by

reducing an ordinary four wheel vehicle model into a two wheel vehicle model with the wheels at the centerline of the vehicle. Third, based on the modeling, a trajectory tracking controller is designed based on Backstepping method for the 4WIS-AGV to track a given trajectory omnidirectionally. Fourth, to implement the designed controller, a control system is developed using industrial PC and AVR ATmega128 microcontrollers. Industrial PC is used as the main controller which collects data from sensors, generates control signal and controls Graphical User Interface (GUI) of the system. AVR ATmega128 microcontrollers are used to convert control signal from industrial PC to Pulse Width Modulation (PWM). This PWM signal is then converted to voltage signals by motor drivers. A monitor is used to display the GUI to users. Laser navigation system NAV200 for getting position data of the vehicle and eight encoders for getting angular velocity data of eight motors for 4 steering motors and 4 driving motors are used. Two 12V batteries are used to supply power to the system. Finally, simulations and experiments are conducted to verify the effectiveness and the performances of the proposed controller for tracking two reference trajectories: a trajectory with sharp edges for parallel steering maneuver and a circular trajectory for zero-sideslip maneuver. The results show that the proposed controller makes the 4WIS-AGV track the reference trajectory with sharp edges for parallel steering maneuver and the reference circular trajectory for zero-sideslip maneuver very well.

Keywords: Automated Guided Vehicles, Four wheel independent steering, Controller design, Backstepping.

List of Figures

Fig. 2.1 Schematic of four wheel steering vehicles.....	9
Fig. 2.2 Parallel steering maneuver.....	11
Fig. 2.3 Zero-sideslip maneuver	14
Fig. 2.4 Configuration for system modeling.....	23
Fig. 2.5 Single-track vehicle model	25
Fig. 2.6 Block diagram of the proposed controller for zero-sideslip maneuver.....	33
Fig. 2.7 Block diagram of the proposed controller for parallel steering maneuver.....	33
Fig. 3.1 4WIS-AGV system.....	35
Fig. 3.2 Body configuration.....	37
Fig. 3.3 Body plate	38
Fig. 3.4 Body frame.....	39
Fig. 3.5 Body cover plate.....	39
Fig. 3.6 Wheel configuration.....	40
Fig. 3.7 Wheel hub.....	41
Fig. 3.8 Nylon plate.....	42
Fig. 3.9 Steering steel plate.....	42
Fig. 3.10 Reduction gear 1:2.....	42
Fig. 3.11 Nylon wheel	43
Fig. 3.12 Electrical configuration of 4WIS-AGV	43
Fig. 3.13 DC motors.....	44
Fig. 3.14 Performance graph of the DC motors.....	45
Fig. 3.15 Encoder E40HB-6-3600-3-V-5	46
Fig. 3.16 Industrial PC TANK-800.....	47
Fig. 3.17 12V battery ATLASBX ITX100.....	49

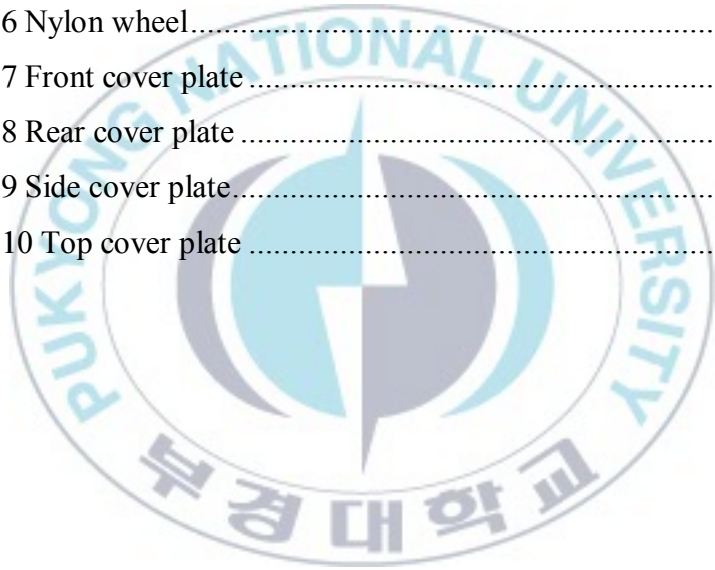
Fig. 3.18 Microcontroller AVR ATmega128	50
Fig. 3.19 Motor drivers.....	51
Fig. 3.20 Monitor MYMO MY-720.....	52
Fig. 3.21 Laser navigation system NAV200 basic principle	53
Fig. 3.22 Position measurement of the NAV200	54
Fig. 3.23 Laser navigation system NAV200.....	56
Fig. 3.24 Manual menu of the 4WIS-AGV GUI.....	58
Fig. 3.25 Automatic menu of the 4WIS-AGV GUI	59
Fig. 4.1 Initial position and reference trajectory with sharp edges ..	61
Fig. 4.2 Illustration of the expected motion.....	62
Fig. 4.3 X-axis reference trajectory	64
Fig. 4.4 Y-axis reference trajectory	64
Fig. 4.5 Reference vehicle linear velocity	65
Fig. 4.6 Reference sideslip angular velocity.....	66
Fig. 4.7 Trajectory tracking result.....	67
Fig. 4.8 Trajectory tracking errors	67
Fig. 4.9 Control law U	69
Fig. 4.10 X-axis reference and simulation	71
Fig. 4.11 Y-axis reference and simulation	71
Fig. 4.12 Error e_x and e_y	72
Fig. 4.13 Vehicle orientation reference and simulation	73
Fig. 4.14 Vehicle sideslip angle reference and simulation	74
Fig. 4.15 Wheel steering angle δ_i	74
Fig. 4.16 Linear velocity of each wheel v_i	75
Fig. 4.17 Angular velocity of each wheel ω_i	76
Fig. 4.18 Initial position and circular reference trajectory	77
Fig. 4.19 Illustration of the expected motion.....	78

Fig. 4.20 X -axis reference trajectory	79
Fig. 4.21 Y -axis reference trajectory	80
Fig. 4.22 Trajectory tracking result	80
Fig. 4.23 Trajectory tracking errors	81
Fig. 4.24 Control law U	82
Fig. 4.25 X -axis reference and simulation	83
Fig. 4.26 Y -axis reference and simulation	83
Fig. 4.27 Error e_x and e_y	84
Fig. 4.28 Vehicle orientation reference and simulation	85
Fig. 4.29 Vehicle sideslip angle reference and simulation	85
Fig. 4.30 Steering angle of the front wheel	86
Fig. 4.31 Steering angle of the rear wheel	86
Fig. 4.32 Steering angle of the front outer wheel	87
Fig. 4.33 Steering angle of the front inner wheel	87
Fig. 4.34 Steering angle of the rear inner wheel	88
Fig. 4.35 Steering angle of the rear outer wheel	88
Fig. 4.36 Linear velocity of the front outer wheel	89
Fig. 4.37 Linear velocity of the front inner wheel	90
Fig. 4.38 Linear velocity of the rear inner wheel	90
Fig. 4.39 Linear velocity of the rear outer wheel	91
Fig. 4.40 Angular velocity of the front outer wheel	92
Fig. 4.41 Angular velocity of the front inner wheel	92
Fig. 4.42 Angular velocity of the rear inner wheel	93
Fig. 4.43 Angular velocity of the rear outer wheel	93
Fig. 4.44 Simulation and experimental trajectory tracking results ..	95
Fig. 4.45 Simulation and experimental trajectory tracking errors ...	95
Fig. 4.46 Simulation and experimental control law	96

Fig. 4.47 Simulation and experimental results of X -axis trajectory tracking	97
Fig. 4.48 Simulation and experimental results of Y -axis trajectory tracking	97
Fig. 4.49 Simulation and experimental errors e_x and e_y	98
Fig. 4.50 Simulation and experimental vehicle orientation.....	98
Fig. 4.51 Simulation and experimental vehicle sideslip angles	99
Fig. 4.52 Simulation and experimental wheel steering angles	100
Fig. 4.53 Simulation and experimental linear velocities of each wheel	100
Fig. 4.54 Simulation and experimental angular velocities of each wheel.....	101
Fig. 4.55 Simulation and experimental results of circular reference trajectory tracking	102
Fig. 4.56 Simulation and experimental trajectory tracking errors .	102
Fig. 4.57 Simulation and experimental control laws U	103
Fig. 4.58 Simulation and experimental results of X -axis trajectory tracking	104
Fig. 4.59 Simulation and experimental results of Y -axis trajectory tracking	104
Fig. 4.60 Simulation and experimental errors e_x and e_y	105
Fig. 4.61 Simulation and experimental vehicle orientation.....	105
Fig. 4.62 Simulation and experimental vehicle sideslip angles	106
Fig. 4.63 Simulation and experimental front wheel steering angles	107
Fig. 4.64 Simulation and experimental rear wheel steering angles	107
Fig. 4.65 Simulation and experimental steering angles of the front outer wheel.....	108

Fig. 4.66 Simulation and experimental steering angles of the front inner wheel.....	108
Fig. 4.67 Simulation and experimental steering angles of the rear inner wheel.....	109
Fig. 4.68 Simulation and experimental steering angles of the front outer wheel.....	109
Fig. 4.69 Simulation and experimental linear velocities of the front outer wheel.....	110
Fig. 4.70 Simulation and experimental linear velocities of the front inner wheel.....	111
Fig. 4.71 Simulation and experimental linear velocities of the rear inner wheel.....	111
Fig. 4.72 Simulation and experimental linear velocities of the rear outer wheel.....	112
Fig. 4.73 Simulation and experimental angular velocities of the front outer wheel.....	112
Fig. 4.74 Simulation and experimental angular velocities of the front inner wheel.....	113
Fig. 4.75 Simulation and experimental angular velocities of the rear inner wheel.....	113
Fig. 4.76 Simulation and experimental angular velocities of the rear outer wheel.....	114
Fig. A.1 Coordinate system configuration of four wheel steering vehicles	131
Fig. A.2 Wheel configuration in two dimension.....	134
Fig. A.3 Triangle <i>PC4</i>	135
Fig. A.4 Triangle <i>P3C</i>	136
Fig. A.5 Triangle <i>PB1</i>	138

Fig. A.6 Triangle $P2B$	139
Fig. A.7 Triangle PBC	141
Fig. A.8 Triangle PAC	142
Fig. A.9 Triangular relationships	146
Fig. E.1 Body plate.....	164
Fig. E.2 Wheel hub.....	164
Fig. E.3 Holder plate	165
Fig. E.4 Nylon plate	166
Fig. E.5 Steering steel plate	167
Fig. E.6 Nylon wheel.....	167
Fig. E.7 Front cover plate.....	168
Fig. E.8 Rear cover plate	168
Fig. E.9 Side cover plate.....	169
Fig. E.10 Top cover plate	169



List of Tables

Table 2.1 Special angle conditions in Eqs. (2.10) and (2.12) - (2.15)	21
Table 2.2 Special angle conditions of ψ_A and β_A	27
Table 3.1 Specification of the vehicle body	37
Table 3.2 Specification of DC motor IG-52GM 04TYPE (24V)	45
Table 3.3 Specification of encoder E40HB-6-3600-3-V-5	46
Table 3.4 Specification of PC TANK-800	48
Table 3.5 Specification of 12V battery ATLASBX ITX100	49
Table 3.6 Specification of microcontroller AVR ATmega128	50
Table 3.7 Specification of monitor MYMO MY-720	52
Table 3.8 Specification of laser navigation system NAV200	56
Table 4.1 Parameter and initial values for the simulation	62
Table 4.2 Parameter and initial values for the simulation	78

Chapter 1: Introduction

1.1 Background and motivation

Automatic Guided Vehicles (AGVs) have been operated in almost every industry due to their high efficiency for material handling [1-8]. Therefore, many AGV research projects have been conducted such as development of laser [9-15], development of vision [16-21], localization [22-31] and navigation [32-44] for the AGV. One of the techniques to improve the performance of AGVs is to improve AGVs' maneuverability and flexibility because the higher these characteristics are, the better the AGVs' performance is. Several kinds of wheel configurations for AGVs have been developed. Pratama et al. [45] developed a differential drive AGV that could work autonomously using laser measurement system. Obstacle avoidance algorithm was also applied in this system. On the other hand, Doan et al. [46] developed a tricycle wheeled AGV. In this vehicle, Doan proposed a path tracking control using camera sensor. To get higher maneuverability and flexibility, four wheel independent steering configuration has been proposed for development of AGVs, hereafter referred to as 4WIS-AGVs.

Four wheel independent steering configuration is a wheel configuration that each wheel orientation is adjusted separately. As a result, 4WIS-AGVs can move to any direction in their work environment. The main advantages of this wheel configuration are small vehicle sideslip angle and better dynamic response characteristics [47]. Nevertheless, controlling the configuration of four wheels to make the 4WIS-AGV move to certain directions is

challenging. This is because the orientation of each wheel has to be adjusted with particular formation such that the vehicle can move in the expected direction. Thus, appropriate controllers are necessary for 4WIS-AGVs.

There have been many researches developing controllers for four wheel steering vehicles. Zhang et al. [48] proposed robust optimal control technology for four-wheel steering vehicle. H_2 optimal controller and Kalman filter were proposed for the two degree of freedom vehicle model. A H_∞ optimal controller was also presented to deal with the model uncertainty. The simulation results showed that the proposed controller was robust and stable. Furthermore, the proposed controller could also improve the vehicle steering performance because it could reduce the model uncertainty and resist the disturbance very well. However, this controller could work only when the parameter uncertainty of the tire could be considered as linear time invariant and the vehicle speed was low.

Amdouni et al. [49] proposed another kind of optimal control for four-wheel active steering vehicles. It was designed using parameter optimization method based on genetic algorithm which combined front and rear wheel steerings to control the front and rear wheel angles. The controller was then proposed and implemented in MATLAB/Simulink. The proposed controller model is comprised of model matching, feedforward and feedback controllers. This controller gave a better control for the vehicle at high speed. Moreover, an optimal control approach was proposed for four wheel active steering vehicle because the computing tools and techniques developed in this paper were general and fully parameterized.

Lam et al. [50] proposed a behavior-based steering control for four wheel independent steering vehicles. This strategy was used to overcome limitations of wheel orientation control. The controller consisting of position controller and kinematic controller worked as virtual linkages among each wheel to minimize wheel slip resulted by the misalignment of the orientations of wheels effectively. The simulation results showed that the proposed controller increased the driving and steering efficiency with little path variation. Nevertheless, they did not show whether the chosen PID parameters in this controller could make optimum performance in real field or not because the effectiveness of the proposed controller was only validated by simulation.

For some conditions, only single control method cannot work properly on four wheel steering vehicles. Thus, Yang et al. [51] suggested a multi-mode control strategy based on fuzzy selector. This fuzzy selector analyzed the steering behavior and chose the appropriate control mode and determined the corresponding control model to improve the vehicle's steering characteristics. The aim of using this type of controller is to achieve optimal yawing angular velocity, centroid edge angle and body heeling angle. Despite that, this control strategy could not make the vehicle with stable sideslip angle, yawing angular velocity and rolling angle as shown in the simulation results.

Another control algorithm is fuzzy logic robust controller based on Sugeno fuzzy model which was developed by Shaout et al. [52]. This controller used the responsiveness and stability of the rear wheel steering in conjunction with front wheel steering using fuzzy logic robust controller based on single track nonlinear vehicle model. The

simulation results showed that the developed controller enhanced the vehicle handling in the presence of noise, steering linkage play and variation in vehicle parameters.

From the above mentions, there is a necessity of conducting research on developing a new type of four wheel independent steering configuration for AGVs. Furthermore, a new good trajectory tracking controller is needed for the AGVs to fulfill the working requirements.

1.2 Objective and research method

The objective of this thesis is to present a Four Wheel Independent Steering Automatic Guided Vehicle (4WIS-AGV) for heavy baggage carriers with omnidirectional maneuver. The application of this system is in the airport and the hotel where people can put their baggage on the 4WIS-AGV and it will bring the baggage to the desired locations. To do this, the followings are done.

First, a 4WIS-AGV is developed for experimental purpose. The 4WIS-AGV with big dimension of 500 mm (height) x 705 mm (width) x 905 mm (length) is designed and manufactured. Four high power DC motors are used to drive its wheels and four additional DC motors are used for its steering purpose. Each motor is controlled independently and industrial PC is used as the main controller. Each motor has a motor driver and an ATmega128 microcontroller. ATmega128 is used to convert desired revolution signals from industrial PC to Pulse Width Modulation (PWM). This PWM is then converted to voltage signals by the motor driver.

Second, a kinematic modeling of 4WIS-AGVs is created based on a single track vehicle model. This model is obtained by reducing an ordinary four wheel vehicle model into a two wheel vehicle model with the wheels at the centerline of the vehicle. This model has been proved to sufficiently represent the four wheel steering vehicles as the more complicated nonlinear two track vehicle model does.

Third, a trajectory tracking controller is designed based on Backstepping method to make the 4WIS-AGV tracks reference trajectories omnidirectionally and accurately.

Fourth, a control system is developed using industrial PC and AVR ATmega128 microcontrollers to implement the designed controller. Industrial PC is used as the main controller which collects the data from sensors, generates control signal and controls Graphical User Interface (GUI) of the system. AVR ATmega128 microcontrollers are used to convert control signal from industrial PC to PWM. This PWM signal is then converted to voltage signals by motor drivers. A monitor is used to display the GUI to users. Laser navigation system NAV200 to get position data of the vehicle and eight encoders to get angular velocity data of eight motors for 4 steering motors and 4 driving motors are used. Two 12V batteries are used to supply power to the system.

Finally, simulations and experiments are conducted to verify the effectiveness and the performances of the proposed controller for tracking two reference trajectories: a trajectory with sharp edges for parallel steering maneuver and a circular trajectory for zero-sideslip maneuver. The results show that the proposed controller makes the 4WIS-AGV track the reference trajectory with sharp edges for

parallel steering maneuver and the reference circular trajectory for zero-sideslip maneuver very well.

1.3 Outline and contribution of thesis

This section describes the contents of the thesis and their contributions briefly. The contents consist of five sections, i.e. introduction, system modeling and controller design, controller implementation and hardware description, simulation and experimental results and conclusions as follows:

Chapter 1: Introduction

In this chapter, background and motivation of this thesis are presented. The objective and research method of this thesis are then described. Finally, the outline and contribution of this thesis is explained.

Chapter 2: System modeling and controller design

This chapter describes the modeling and controller design of the 4WIS-AGV. To do this, the followings are done. First, basic terminologies and equations of four wheel steering vehicles and their control theories are explained. Second, a kinematic modeling of the 4WIS-AGV based on a single track vehicle model is created. Finally, a trajectory tracking controller is designed for this system to track given reference trajectory based on Backstepping method.

Chapter 3: Controller implementation and hardware description

This chapter describes the hardware structure of the 4WIS-AGV used to implement the designed controller. The hardware structure of the 4WIS-AGV consists of mechanical design, electrical design and GUI of the 4WIS-AGV. The mechanical design of the vehicle is explained in detail, which consists of its body and wheel configurations. All electric hardware used in the system such as steering motors and driving motors, encoders, industrial PC, batteries, ATmega128 microcontrollers, monitor, motor drivers and laser navigation system NAV200 are described. The GUI is comprised of manual and automatic menus. Both of these menus are described in this chapter.

Chapter 4: Simulation and experimental results

Simulation and experimental results are shown. These results are shown to prove the effectiveness, performance and applicability of the designed controller for the 4WIS-AGV to track two reference trajectories: a reference trajectory with sharp edges for parallel steering maneuver and a circular reference trajectory for zero-sideslip maneuver. The simulation and experimental results show that the proposed controller makes the 4WIS-AGV able to track the reference trajectories very well.

Chapter 5: Conclusions

Conclusions from this research and several suggestions for future works are presented.

Chapter 2: System Modeling and Controller Design

This chapter presents a system modeling and a controller design for the 4WIS-AGV system. First, basic terminologies of four wheel steering vehicle are explained in this chapter. Second, two maneuvers of four wheel steering vehicles are explained. Third, a kinematic modeling of the 4WIS-AGV system is created. Finally, a trajectory tracking controller based on Backstepping method is designed.

2.1 Basic terminologies

The schematic of four wheel steering vehicles is shown in Fig.

2.1.



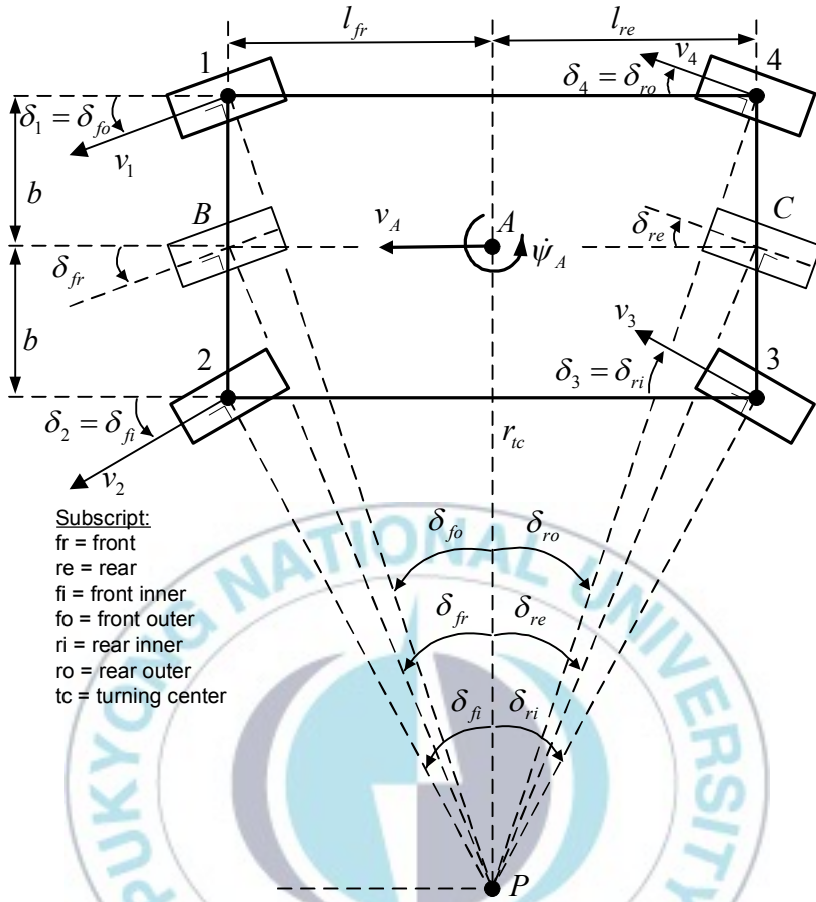


Fig. 2.1 Schematic of four wheel steering vehicles

where,

δ_{fi}, δ_{fo} = Front inner and front outer wheel steering angles, respectively (rad)

δ_{ri}, δ_{ro} = Rear inner and rear outer wheel steering angles, respectively (rad)

δ_{fr}, δ_{re} = Front and rear wheel steering angles, respectively (rad)

Wheel steering angles are measured as angle between the wheel longitudinal axis and vehicle longitudinal axis in counter-clockwise direction.

v_A = Vehicle linear velocity (m/s)

v_i = Each wheel linear velocity, for $i = 1, \dots, 4$ (m/s)

$\dot{\psi}_A$ = Vehicle angular velocity (rad/s)

l_{fr}, l_{re} = Longitudinal distances from vehicle center of gravity (CG) to the front and rear wheels, respectively (m)

r_{tc} = Turning center radius of the vehicle (m)

b = Lateral distances from CG to right or left wheel (m)

r_w = Wheel radius (m)

B = Middle point of the front wheels

C = Middle point of the rear wheels

CG = Vehicle center of gravity

P = Turning center

Four wheel steering vehicles have four wheels that are adjusted separately. Thus, each wheel has wheel steering angle δ_i , wheel linear velocity v_i and wheel angular velocity ω_i ($v_i = \omega_i r_w$). The wheel names are determined when the vehicle moves in curved trajectories as shown in Fig. 2.1. In this condition, there are two wheels which are nearer to the turning center and therefore defined as the inner wheels. The rest of the wheels which are farther to the turning center are called the outer wheels. The wheel numbers are started from the front outer wheel as wheel 1, going in counter-clockwise direction to the front inner wheel as wheel 2, then going to

the rear inner wheel as wheel 3 and the last wheel is the rear outer wheel as wheel 4.

2.2 Four wheel steering vehicle maneuvers

There are two kinds of maneuvers that four wheel steering vehicles have, i.e. parallel steering maneuver and zero-sideslip maneuver [54]. These maneuvers take advantage of the unique kinematic characteristics of four wheel steering vehicles. In this thesis, the experimental 4WIS-AGV will be tested on its capability for these two maneuvers.

2.2.1 Parallel steering maneuver

This maneuver is done when both the front and rear wheels are steered with the same angle, direction and velocity as shown in Fig. 2.2.

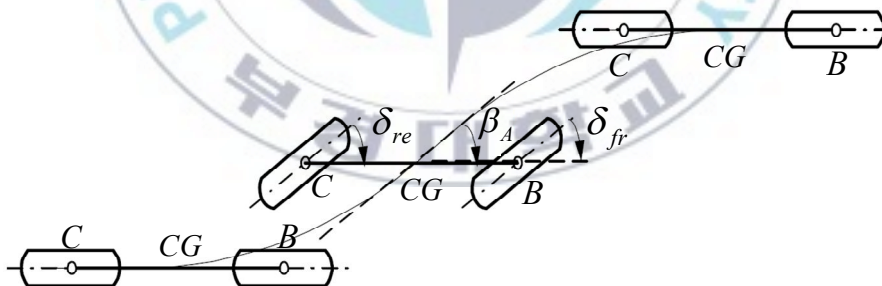


Fig. 2.2 Parallel steering maneuver

In this condition, all wheel steering angles are set to follow the sideslip angle, β_A .

$$\delta_i = \beta_A \quad \text{for } i = 1, \dots, 4, fr, re \quad (2.1)$$

Likewise, the velocity of each wheel follows the vehicle linear velocity, v_A .

$$v_i = v_A \quad \text{for } i = 1, \dots, 4, fr, re \quad (2.2)$$

This condition causes the turning radius of the vehicle motion, r_{tc} , always equal to infinity along the path.

$$r_{tc} = \infty, \quad s : s_0 \rightarrow s_n \quad (2.3)$$

where s represents the path length travelled by CG from the starting point, s_0 , to the ending point, s_n .

Furthermore, in this condition, the vehicle moves without changing its orientation during the motion and mathematically this condition can be written as follows:

$$\psi_A(s) = \psi_A(0), \quad s : 0 \rightarrow s_n \quad (2.4)$$

where $\psi_A(0)$ is the initial orientation of the vehicle.

This maneuver is very practical in vehicle lane-changing and obstacle avoidance. As a result, this maneuver is very useful for AGVs when they have to move in small working space on which ordinary AGVs have limitation to move.

2.2.2 Zero-sideslip maneuver

This maneuver is done when the sideslip angle of the vehicle is kept zero ($\beta_A = 0$) while the vehicle moves. This maneuver is illustrated with Fig. 2.3.

At the point CG on the path, the incremental change, ds , can be expressed as:

$$ds = \sqrt{dX^2 + dY^2} \quad (2.5)$$

where dX and dY are the incremental changes in X and Y directions, respectively. The tangential angle ψ_A at point CG can be expressed as:

$$\psi_A = \tan^{-1} \frac{dY}{dX} \quad (2.6)$$

Subsequently, the path curvature, κ , can be obtained by deriving function $\psi_A(s)$ with respect to s as follows:

$$\kappa = \frac{1}{r_{ic}} = \frac{d\psi_A}{ds} = \frac{d^2Y / dX^2}{\left(1 + (dY / dX)^2\right)^{3/2}} \quad (2.7)$$

When the vehicle moves along the path s , the sideslip angle can be written as follows:

$$\beta_A(s) = 0, \quad s : s_0 \rightarrow s_n \quad (2.8)$$

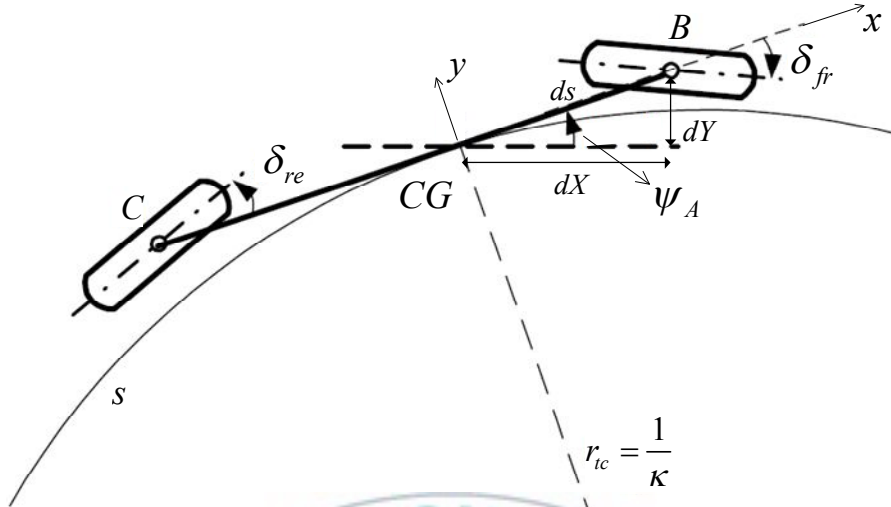


Fig. 2.3 Zero-sideslip maneuver

The orientation of the vehicle $\psi_A(s)$ is set to match the tangential angle of the desired path $\psi_d(s)$.

$$\psi_A(s) = \psi_d(s), \quad s: 0 \rightarrow s_n \quad (2.9)$$

Because the vehicle body is always tangent to the path, this maneuver is desirable for the vehicle motion. By assuming that all angles δ_i , for $i = 1, \dots, 4, A, fr, re$, are limited to be less than $\pm \pi/2$ rad, velocities of each wheel in zero-sideslip maneuver can be formulated as follows [53]:

$$v_i = \begin{cases} \frac{v_A \tan \delta_{fr} \csc \delta_i}{\sqrt{1 + \frac{1}{4} (\tan \delta_{fr} + \tan \delta_{re})^2}}, i = 1, 2; \cos \delta_{fr} \sin \delta_i \neq 0, \delta_i \neq \delta_{fr} \\ \frac{v_A \tan \delta_{re} \csc \delta_i}{\sqrt{1 + \frac{1}{4} (\tan \delta_{fr} + \tan \delta_{re})^2}}, i = 3, 4; \cos \delta_{re} \sin \delta_i \neq 0, \delta_i \neq \delta_{re} \end{cases} \quad (2.10)$$

where

$$\lim_{\delta_x, \delta_y \rightarrow 0} [\tan \delta_x \csc \delta_y] = \lim_{\delta_x, \delta_y \rightarrow 0} \left[\frac{\sin \delta_x}{\sin \delta_y} \sec \delta_x \right] = 1 \quad (2.11)$$

Proof of Eq. (2.10) is written in Appendix A.

Subsequently, the steering angles of each wheel, δ_i , can be calculated as follows:

$$\delta_1 = \cot^{-1} \left(\cot \delta_{fr} + \frac{b}{l_{fr} + l_{re}} \cot \delta_{fr} [\tan \delta_{fr} - \tan \delta_{re}] \right) \quad (2.12)$$

for $\delta_1 \neq \delta_{fr}$, $\delta_{fr} \neq \delta_{re}$, $\cos \delta_{re} \sin \delta_{fr} \neq 0$

$$\delta_2 = \cot^{-1} \left(\cot \delta_{fr} - \frac{b}{l_{fr} + l_{re}} \cot \delta_{fr} [\tan \delta_{fr} - \tan \delta_{re}] \right) \quad (2.13)$$

for $\delta_2 \neq \delta_{fr}$, $\delta_{fr} \neq \delta_{re}$, $\cos \delta_{re} \sin \delta_{fr} \neq 0$

$$\delta_3 = \cot^{-1} \left(\cot \delta_{re} - \frac{b}{l_{fr} + l_{re}} \cot \delta_{re} [\tan \delta_{fr} - \tan \delta_{re}] \right) \quad (2.14)$$

for $\delta_3 \neq \delta_{re}$, $\delta_{fr} \neq \delta_{re}$, $\cos \delta_{fr} \sin \delta_{re} \neq 0$

$$\delta_4 = \cot^{-1} \left(\cot \delta_{re} + \frac{b}{l_{fr} + l_{re}} \cot \delta_{re} \left[\tan \delta_{fr} - \tan \delta_{re} \right] \right) \quad (2.15)$$

for $\delta_4 \neq \delta_{re}$, $\delta_{fr} \neq \delta_{re}$, $\cos \delta_{fr} \sin \delta_{re} \neq 0$

Proof of Eqs. (2.12) - (2.15) is written in Appendix B.

Since Eqs. (2.10) and (2.12) - (2.15) contain sin, cos and tan functions, these equations have special values in particular angles. The following describes the special angle conditions for Eqs. (2.10) and (2.12) - (2.15).

From Eq. (2.10), linear velocity of wheel 1, v_1 , is taken as follows:

$$v_1 = \frac{v_A \tan \delta_{fr} \csc \delta_1}{\sqrt{1 + \frac{1}{4} (\tan \delta_{fr} + \tan \delta_{re})^2}} \quad (2.16)$$

Case 1: In straight direction, $\delta_{fr} = \delta_{re} = 0$ or π and by considering Eq. (2.11), Eqs. (2.12) - (2.15) and (2.16) becomes

$$\delta_i = 0 \quad (2.17)$$

$$v_1 = \frac{v_A \cdot 1}{\sqrt{1 + \frac{1}{4} (0+0)^2}} = v_A, \text{ likewise } v_2 = v_3 = v_4 = v_A \quad (2.18)$$

Case 2: $\delta_{re} = \delta_{fr}$

Eqs. (2.12) - (2.15) becomes

$$\delta_1 = \delta_2 = \delta_3 = \delta_4 = \delta_{fr} = \delta_{re} \quad (2.19)$$

and thus Eq. (2.16) becomes

$$v_1 = \frac{v_A \tan \delta_{fr} \csc \delta_{fr}}{\sqrt{1 + \frac{1}{4} (\tan \delta_{fr} + \tan \delta_{fr})^2}} = \frac{v_A \sec \delta_{fr}}{\sqrt{1 + \tan^2 \delta_{fr}}} = \frac{v_A \sec \delta_{fr}}{\sec \delta_{fr}} = v_A \quad (2.20)$$

likewise $v_2 = v_3 = v_4 = v_A$ (parallel steering maneuver)

Case 3: $\delta_{re} = -\delta_{fr}$

From Eqs. (2.12) - (2.15), the followings are done.

$$\delta_1 = \cot^{-1} \left(\cot \delta_{fr} + \frac{b}{l_{fr} + l_{re}} \cot \delta_{fr} [2 \tan \delta_{fr}] \right) = \cot^{-1} \left(\cot \delta_{fr} + \frac{2b}{l_{fr} + l_{re}} \right) \quad (2.21)$$

$$\delta_2 = \cot^{-1} \left(\cot \delta_{fr} - \frac{b}{l_{fr} + l_{re}} \cot \delta_{fr} [2 \tan \delta_{fr}] \right) = \cot^{-1} \left(\cot \delta_{fr} - \frac{2b}{l_{fr} + l_{re}} \right) \quad (2.22)$$

$$\delta_3 = \cot^{-1} \left(-\cot \delta_{fr} + \frac{b}{l_{fr} + l_{re}} \cot \delta_{fr} [2 \tan \delta_{fr}] \right) = \cot^{-1} \left(-\cot \delta_{fr} + \frac{2b}{l_{fr} + l_{re}} \right) \quad (2.23)$$

$$\delta_4 = \cot^{-1} \left(-\cot \delta_{fr} - \frac{b}{l_{fr} + l_{re}} \cot \delta_{fr} [2 \tan \delta_{fr}] \right) = \cot^{-1} \left(-\cot \delta_{fr} - \frac{2b}{l_{fr} + l_{re}} \right) \quad (2.24)$$

In addition, from Eq. (2.21), the followings are obtained.

$$v_1 = v_A \tan \delta_{fr} \csc \left[\cot^{-1} \left(\cot \delta_{fr} + \frac{2b}{l_{fr} + l_{re}} \right) \right] \quad (2.25)$$

$$v_2 = v_A \tan \delta_{fr} \csc \left[\cot^{-1} \left(\cot \delta_{fr} - \frac{2b}{l_{fr} + l_{re}} \right) \right] \quad (2.26)$$

$$v_3 = -v_A \tan \delta_{fr} \csc \left[\cot^{-1} \left(-\cot \delta_{fr} + \frac{2b}{l_{fr} + l_{re}} \right) \right] \quad (2.27)$$

$$v_4 = -v_A \tan \delta_{fr} \csc \left[\cot^{-1} \left(-\cot \delta_{fr} - \frac{2b}{l_{fr} + l_{re}} \right) \right] \quad (2.28)$$

Case 4: When $\delta_{fr} = \pm\pi/2$, Eqs. (2.10) and (2.12) - (2.15) becomes

$$\begin{aligned} v_{1,2} &= \frac{v_A \tan \delta_{fr} \csc \delta_{1,2}}{\sqrt{1 + \frac{1}{4} (\tan \delta_{fr} + \tan \delta_{re})^2}} \\ &= \frac{v_A \csc \delta_{1,2}}{\frac{1}{\tan \delta_{fr}} \sqrt{1 + \frac{1}{4} \tan^2 \delta_{fr} + \frac{1}{2} \tan \delta_{fr} \tan \delta_{re} + \frac{1}{4} \tan^2 \delta_{re}}} \\ &= \frac{v_A \csc \delta_{1,2}}{\sqrt{\frac{1}{\tan \delta_{fr}} + \frac{1}{4} \tan \delta_{fr} + \frac{1}{2} \tan \delta_{re} + \frac{1}{4} \frac{\tan^2 \delta_{re}}{\tan \delta_{fr}}}} \\ \therefore \lim_{\delta_{fr} \rightarrow \pm\pi/2} v_{1,2} &= 0 \end{aligned} \quad (2.29)$$

$$\begin{aligned} v_{3,4} &= \frac{v_A \tan \delta_{re} \csc \delta_{3,4}}{\sqrt{1 + \frac{1}{4} (\tan \delta_{fr} + \tan \delta_{re})^2}} \\ \therefore \lim_{\delta_{fr} \rightarrow \pm\pi/2} v_{3,4} &= 0 \end{aligned} \quad (2.30)$$

$$\begin{aligned}
\delta_1 &= \cot^{-1} \left(\cot \delta_{fr} + \frac{b}{l_{fr} + l_{re}} \cot \delta_{fr} [\tan \delta_{fr} - \tan \delta_{re}] \right) \\
&= \cot^{-1} \left(\cot \delta_{fr} + \frac{b}{l_{fr} + l_{re}} - \frac{b}{l_{fr} + l_{re}} \cot \delta_{fr} \tan \delta_{re} \right) \\
\therefore \lim_{\delta_{fr} \rightarrow \pm\pi/2} \delta_1 &= \cot^{-1} \left(\frac{b}{l_{fr} + l_{re}} \right), \text{ likewise } \lim_{\delta_{fr} \rightarrow \pm\pi/2} \delta_2 = \cot^{-1} \left(-\frac{b}{l_{fr} + l_{re}} \right)
\end{aligned} \tag{2.31}$$

$$\begin{aligned}
\delta_3 &= \cot^{-1} \left(\cot \delta_{re} - \frac{b}{l_{fr} + l_{re}} \cot \delta_{re} [\tan \delta_{fr} - \tan \delta_{re}] \right) \\
\therefore \lim_{\delta_{fr} \rightarrow \pm\pi/2} \delta_3 &= -\infty, \text{ likewise } \lim_{\delta_{fr} \rightarrow \pm\pi/2} \delta_4 = \infty
\end{aligned} \tag{2.32}$$

Case 5: When $\delta_{re} = \pm\pi/2$, Eqs. (2.10) and (2.12) - (2.15) becomes

$$\begin{aligned}
v_{1,2} &= \frac{v_A \tan \delta_{fr} \csc \delta_{1,2}}{\sqrt{1 + \frac{1}{4} (\tan \delta_{fr} + \tan \delta_{re})^2}} \\
\therefore \lim_{\delta_{re} \rightarrow \pm\pi/2} v_{1,2} &= 0
\end{aligned} \tag{2.33}$$

$$v_{3,4} = \frac{v_A \tan \delta_{re} \csc \delta_{3,4}}{\sqrt{1 + \frac{1}{4} (\tan \delta_{fr} + \tan \delta_{re})^2}}$$

$$\begin{aligned}
&= \frac{v_A \csc \delta_{1,2}}{\frac{1}{\tan \delta_{re}} \sqrt{1 + \frac{1}{4} \tan^2 \delta_{fr} + \frac{1}{2} \tan \delta_{fr} \tan \delta_{re} + \frac{1}{4} \tan^2 \delta_{re}}} \\
&= \frac{v_A \csc \delta_{1,2}}{\sqrt{\frac{1}{\tan \delta_{re}} + \frac{1}{4} \frac{\tan^2 \delta_{fr}}{\tan \delta_{re}} + \frac{1}{2} \tan \delta_{fr} + \frac{1}{4} \tan \delta_{re}}}
\end{aligned}$$

$$\therefore \lim_{\delta_{re} \rightarrow \pm\pi/2} v_{3,4} = 0 \quad (2.34)$$

$$\begin{aligned}
\delta_1 &= \cot^{-1} \left(\cot \delta_{fr} + \frac{b}{l_{fr} + l_{re}} \cot \delta_{fr} \left[\tan \delta_{fr} - \tan \delta_{re} \right] \right) \\
\therefore \lim_{\delta_{re} \rightarrow \pm\pi/2} \delta_1 &= -\infty, \text{ likewise } \lim_{\delta_{re} \rightarrow \pm\pi/2} \delta_2 = \infty \quad (2.35)
\end{aligned}$$

$$\begin{aligned}
\delta_3 &= \cot^{-1} \left(\cot \delta_{re} - \frac{b}{l_{fr} + l_{re}} \cot \delta_{re} \left[\tan \delta_{fr} - \tan \delta_{re} \right] \right) \\
&= \cot^{-1} \left(\cot \delta_{re} - \frac{b}{l_{fr} + l_{re}} \cot \delta_{re} \tan \delta_{fr} + \frac{b}{l_{fr} + l_{re}} \right) \\
\therefore \lim_{\delta_{re} \rightarrow \pm\pi/2} \delta_3 &= \cot^{-1} \left(\frac{b}{l_{fr} + l_{re}} \right), \text{ likewise } \lim_{\delta_{re} \rightarrow \pm\pi/2} \delta_4 = \cot^{-1} \left(-\frac{b}{l_{fr} + l_{re}} \right) \quad (2.36)
\end{aligned}$$

Case 6: When $\delta_i = \delta_{fr}$, Eqs. (2.10) and (2.12) - (2.15) becomes

$$v_{1,2} = \frac{v_A \sec \delta_{fr}}{\sqrt{1 + \frac{1}{4} (\tan \delta_{fr} + \tan \delta_{re})^2}} \quad (2.37)$$

$$v_{3,4} = \frac{v_A \tan \delta_{re} \csc \delta_{fr}}{\sqrt{1 + \frac{1}{4} (\tan \delta_{fr} + \tan \delta_{re})^2}} \quad (2.38)$$

$$\delta_1 = \delta_2 = \delta_3 = \delta_4 = \delta_{fr} \quad (2.39)$$

Case 7: When $\delta_i = \delta_{re}$, Eqs. (2.10) and (2.12) - (2.15) becomes

$$v_{1,2} = \frac{v_A \tan \delta_{fr} \csc \delta_{re}}{\sqrt{1 + \frac{1}{4} (\tan \delta_{fr} + \tan \delta_{re})^2}} \quad (2.40)$$

$$v_{3,4} = \frac{v_A \sec \delta_{re}}{\sqrt{1 + \frac{1}{4} (\tan \delta_{fr} + \tan \delta_{re})^2}} \quad (2.41)$$

$$\delta_1 = \delta_2 = \delta_3 = \delta_4 = \delta_{re} \quad (2.42)$$

These special angle conditions are summarized in Table 2.1.

Table 2.1 Special angle conditions in Eqs. (2.10) and (2.12) - (2.15)

Special Angles	Eq. (2.10)	Eqs. (2.12) - (2.15)
$\delta_{fr} = \delta_{re}$ $= \delta_i = 0, \pi$	$v_1 = v_2 = v_3 = v_4 = v_A$	$\delta_1 = \delta_2 = \delta_3 = \delta_4 = 0$
$\delta_{re} = \delta_{fr}$	$v_1 = v_2 = v_3 = v_4 = v_A$	$\delta_1 = \delta_2 = \delta_3 = \delta_4 = \delta_{fr}$
$\delta_{re} = -\delta_{fr}$	$v_1 = v_A \tan \delta_{fr} \csc \left[\cot^{-1} \left(\cot \delta_{fr} + \frac{2b}{l_{fr} + l_{re}} \right) \right]$ $v_2 = v_A \tan \delta_{fr} \csc \left[\cot^{-1} \left(\cot \delta_{fr} - \frac{2b}{l_{fr} + l_{re}} \right) \right]$ $v_3 = -v_A \tan \delta_{fr} \csc \left[\cot^{-1} \left(-\cot \delta_{fr} + \frac{2b}{l_{fr} + l_{re}} \right) \right]$ $v_4 = -v_A \tan \delta_{fr} \csc \left[\cot^{-1} \left(-\cot \delta_{fr} - \frac{2b}{l_{fr} + l_{re}} \right) \right]$	$\delta_1 = \cot^{-1} \left(\cot \delta_{fr} + \frac{2b}{l_{fr} + l_{re}} \right)$ $\delta_2 = \cot^{-1} \left(\cot \delta_{fr} - \frac{2b}{l_{fr} + l_{re}} \right)$ $\delta_3 = \cot^{-1} \left(-\cot \delta_{fr} + \frac{2b}{l_{fr} + l_{re}} \right)$ $\delta_4 = \cot^{-1} \left(-\cot \delta_{fr} - \frac{2b}{l_{fr} + l_{re}} \right)$

$\delta_{fr} = \pm\pi/2$	$\lim_{\delta_{fr} \rightarrow \pm\pi/2} v_{1,2} = 0$ $\lim_{\delta_{fr} \rightarrow \pm\pi/2} v_{3,4} = 0$	$\lim_{\delta_{fr} \rightarrow \pm\pi/2} \delta_1 = \cot^{-1} \left(\frac{b}{l_{fr} + l_{re}} \right)$ $\lim_{\delta_{fr} \rightarrow \pm\pi/2} \delta_2 = \cot^{-1} \left(-\frac{b}{l_{fr} + l_{re}} \right)$ $\lim_{\delta_{fr} \rightarrow \pm\pi/2} \delta_3 = -\infty$ $\lim_{\delta_{fr} \rightarrow \pm\pi/2} \delta_4 = \infty$
$\delta_{re} = \pm\pi/2$	$\lim_{\delta_{re} \rightarrow \pm\pi/2} v_{1,2} = 0$ $\lim_{\delta_{re} \rightarrow \pm\pi/2} v_{3,4} = 0$	$\lim_{\delta_{re} \rightarrow \pm\pi/2} \delta_1 = -\infty$ $\lim_{\delta_{re} \rightarrow \pm\pi/2} \delta_2 = \infty$ $\lim_{\delta_{re} \rightarrow \pm\pi/2} \delta_3 = \cot^{-1} \left(\frac{b}{l_{fr} + l_{re}} \right)$ $\lim_{\delta_{re} \rightarrow \pm\pi/2} \delta_4 = \cot^{-1} \left(-\frac{b}{l_{fr} + l_{re}} \right)$
$\delta_i = \delta_{fr}$	$v_{1,2} = \frac{v_A \sec \delta_{fr}}{\sqrt{1 + \frac{1}{4} (\tan \delta_{fr} + \tan \delta_{re})^2}}$ $v_{3,4} = \frac{v_A \tan \delta_{re} \csc \delta_{fr}}{\sqrt{1 + \frac{1}{4} (\tan \delta_{fr} + \tan \delta_{re})^2}}$	$\delta_1 = \delta_2 = \delta_3 = \delta_4 = \delta_{fr}$
$\delta_i = \delta_{re}$	$v_{1,2} = \frac{v_A \tan \delta_{fr} \csc \delta_{re}}{\sqrt{1 + \frac{1}{4} (\tan \delta_{fr} + \tan \delta_{re})^2}}$ $v_{3,4} = \frac{v_A \sec \delta_{re}}{\sqrt{1 + \frac{1}{4} (\tan \delta_{fr} + \tan \delta_{re})^2}}$	$\delta_1 = \delta_2 = \delta_3 = \delta_4 = \delta_{re}$

2.3 Kinematic modeling

The configuration of the 4WIS-AGV for system modeling is shown in Fig. 2.4. The coordinate of OXY is a global coordinate whereas the coordinate of Axy is a local coordinate.

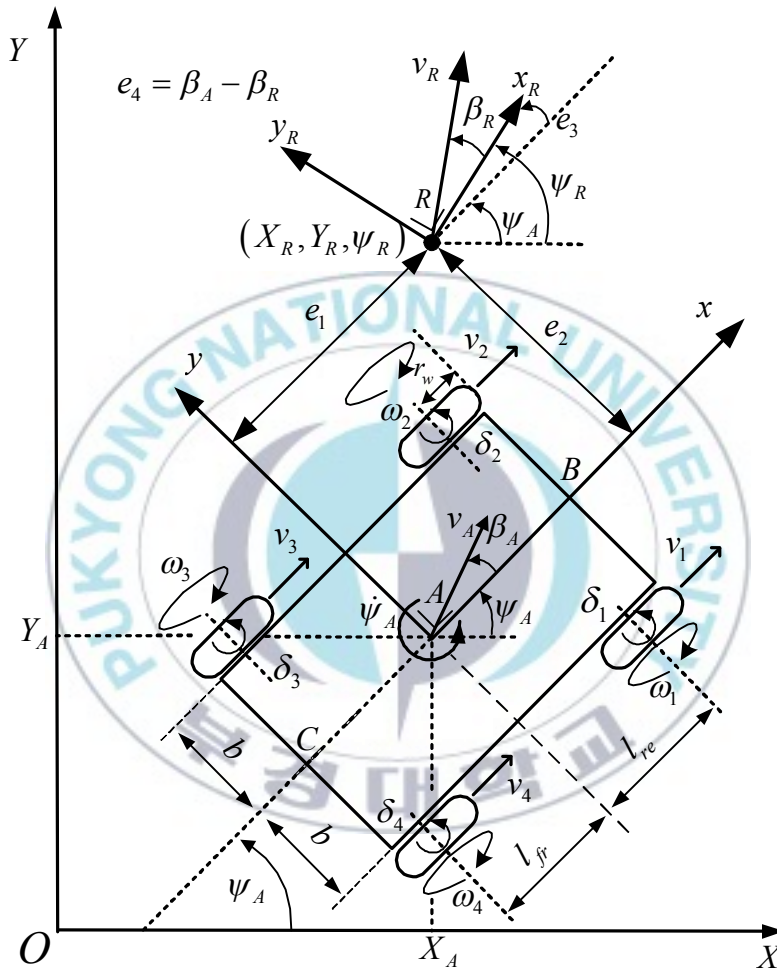


Fig. 2.4 Configuration for system modeling

where,

e_1 = Error in local coordinate x -axis (m)

e_2 = Error in local coordinate y -axis (m)

e_3 = Vehicle orientation error with respect to the reference orientation (rad)

e_4 = Vehicle sideslip angle error with respect to the reference sideslip angle (rad)

r_w = Wheel radius (m)

ω_i = i^{th} wheel angular velocity, for $i = 1, \dots, 4$ (rpm)

δ_i = i^{th} wheel steering angle, for $i = 1, \dots, 4$ (rad)

β_A = Vehicle sideslip angle between vehicle local coordinate x -axis and the vehicle velocity direction measured in counter-clockwise direction (rad)

X_A, Y_A = Current positions of the center point of the 4WIS-AGV (m)

ψ_A = Vehicle orientation between global coordinate X axis and vehicle local coordinate x -axis measured in counter-clockwise direction (rad)

Subscript A represents the current condition, whereas R represents the reference condition.

In this design, a kinematic modeling of 4WIS-AGVs is proposed for the controller design based on a single track vehicle model as shown in Fig. 2.5. This modeling is obtained by reducing an ordinary four wheel vehicle model into a two wheel vehicle model with the wheels at the centerline of the vehicle. This model has been proved to sufficiently represent the four wheel steering vehicles as the more complicated nonlinear two track vehicle model does. Accordingly, this model has been widely adopted as the model for all-four wheel steering [55-61].

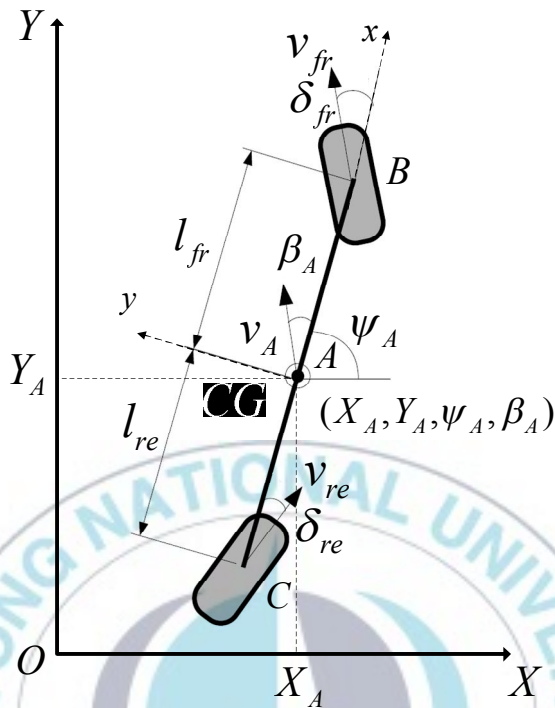


Fig. 2.5 Single-track vehicle model

where,

v_{fr}, v_{re} = Front and rear wheel linear velocities (m/s), respectively

From Figs. 2.4 and 2.5, the kinematic modeling of the 4WIS-AGV is written as follows [54]:

$$\begin{bmatrix} \dot{X}_A \\ \dot{Y}_A \\ \dot{\psi}_A \\ \dot{\beta}_A \end{bmatrix} = \begin{bmatrix} v_A \cos(\psi_A + \beta_A) \\ v_A \sin(\psi_A + \beta_A) \\ \dot{\psi}_A \\ \dot{\beta}_A \end{bmatrix} \quad (2.43)$$

The angular velocity $\dot{\psi}_A$ and sideslip angle β_A of the 4WIS-AGV in the single-track vehicle model in Fig. 2.5 are reduced as follows:

$$\dot{\psi}_A = \frac{v_A \cos \beta_A (\tan \delta_{fr} - \tan \delta_{re})}{l_{fr} + l_{re}} \quad (2.44)$$

$$\beta_A = \tan^{-1} \left(\frac{l_{fr} \tan \delta_{re} + l_{re} \tan \delta_{fr}}{l_{fr} + l_{re}} \right) \quad (2.45)$$

These equations apply to both parallel steering maneuver and zero-sideslip maneuver.

Since Eqs. (2.44) and (2.45) contain cos and tan functions, these equations have special values in particular angles. The following describes the special angle conditions for Eqs. (2.44) and (2.45).

Case 1: $\beta_A = 0$

Eq. (2.44) becomes

$$\dot{\psi}_A = \frac{v_A (\tan \delta_{fr} - \tan \delta_{re})}{l_{fr} + l_{re}} \quad (2.46)$$

Case 2: $\beta_A = \pi/2$

Eq. (2.44) becomes

$$\dot{\psi}_A = 0 \quad (2.47)$$

Case 3: $\delta_{fr} = \delta_{re} = 0$

Eqs. (2.44) and (2.45) become

$$\dot{\psi}_A = \beta_A = 0 \quad (2.48)$$

Case 4: $\delta_{re} = \delta_{fr}$

Eqs. (2.44) and (2.45) become

$$\dot{\psi}_A = 0 \quad (2.49)$$

$$\beta_A = \tan^{-1} \left(\frac{l_{fr} \tan \delta_{fr} + l_{re} \tan \delta_{fr}}{l_{fr} + l_{re}} \right) = \tan^{-1} \left(\frac{\tan \delta_{fr} (l_{fr} + l_{re})}{l_{fr} + l_{re}} \right) = \delta_{fr} \quad (2.50)$$

Case 5: $\delta_{re} = -\delta_{fr}$

Eqs. (2.44) and (2.45) become

$$\dot{\psi}_A = \frac{2v_A \cos \beta_A \tan \delta_{fr}}{l_{fr} + l_{re}} \quad (2.51)$$

$$\beta_A = \tan^{-1} \left(\frac{-l_{fr} \tan \delta_{fr} + l_{re} \tan \delta_{fr}}{l_{fr} + l_{re}} \right) = \tan^{-1} \left(\frac{\tan \delta_{fr} (l_{re} - l_{fr})}{l_{fr} + l_{re}} \right) \quad (2.52)$$

These special angle conditions are summarized in Table 2.2 below.

Table 2.2 Special angle conditions of $\dot{\psi}_A$ and β_A

Special Angles	$\dot{\psi}_A$	β_A
$\beta_A = 0$	$\frac{v_A (\tan \delta_{fr} - \tan \delta_{re})}{l_{fr} + l_{re}}$	0

$\beta_A = \pi/2$	0	$\pi/2$
$\delta_{re} = \delta_{fr} = 0$	0	0
$\delta_{re} = \delta_{fr}$	0	δ_{fr}
$\delta_{re} = -\delta_{fr}$	$\frac{2v_A \cos \beta_A \tan \delta_{fr}}{l_{fr} + l_{re}}$	$\tan^{-1} \left(\frac{\tan \delta_{fr} (l_{re} - l_{fr})}{l_{fr} + l_{re}} \right)$

Steering angles and velocities of each wheel of the 4WIS-AGV, δ_i and v_i , are different when the vehicle move in parallel steering maneuver and zero-sideslip maneuver. For parallel steering maneuver case, the steering angles and velocities of 4WIS-AGV wheels are calculated using Eqs. (2.1) and (2.2), respectively. On the other hand, the steering angles and velocities of 4WIS-AGV wheels in zero-sideslip maneuver are calculated based on the steering angles of the front and rear wheels δ_{fr} and δ_{re} of the single track vehicle model as follows:

$$\delta_{re} = \tan^{-1} \left(\frac{-l_{re} \tan \delta_{fr}}{l_{fr}} \right) \quad (2.53)$$

$$\delta_{fr} = \tan^{-1} \left(\frac{\dot{\psi}_A l_{fr}}{v_A} \right) \quad (2.54)$$

The proof of Eqs. (2.53) and (2.54) is written in Appendix C.

Eqs. (2.53) and (2.54) have constraint that they go to infinity when $v_A = 0$. Therefore, to avoid this condition, v_A is set to have small value (such as 0.000001 m/s) when $v_A = 0$.

2.4 Controller design based on Backstepping method

This section introduces the controller design based on Backstepping method. This method uses stability theory based on Lyapunov function to find suitable controllers. First, the system stability is checked based on Lyapunov stability theory. Subsequently, based on the limitation of controller range that can be applied while the system is stable, the suitable controller can be chosen. In this thesis, the kinematic modeling of the 4WIS-AGV is used and its stability is examined.

The controller is designed for the 4WIS-AGV model to track a reference position $(X_R(t), Y_R(t))$, a reference orientation $\psi_R(t)$ and a reference sideslip angle $\beta_R(t)$ with a reference linear velocity $v_R(t)$, a reference angular velocity $\dot{\psi}_R(t)$ and a reference sideslip angular velocity $\dot{\beta}_R(t)$.

The reference linear velocity $v_R(t)$ of a reference point R on the reference trajectory is expressed as follows:

$$\begin{cases} v_R = \dot{X}_R \cos \psi_R + \dot{Y}_R \sin \psi_R \\ v_A = \dot{X}_A \cos \psi_A + \dot{Y}_A \sin \psi_A \end{cases} \quad (2.55)$$

When vehicles are controlled to track given reference trajectories, tracking errors in Fig. 2.4 are expressed as follows:

$$e_1 = (X_A - X_R) \cos \psi_A + (Y_A - Y_R) \sin \psi_A \quad (2.56)$$

$$e_2 = -(X_A - X_R) \sin \psi_A + (Y_A - Y_R) \cos \psi_A \quad (2.57)$$

$$e_3 = \psi_A - \psi_R \quad (2.58)$$

$$e_4 = \beta_A - \beta_R \quad (2.59)$$

The tracking error vector of Eqs. (2.56) - (2.59) can be written in the state space form as follows:

$$\mathbf{e} = \begin{bmatrix} e_1 \\ e_2 \\ e_3 \\ e_4 \end{bmatrix} = \begin{bmatrix} \cos \psi_A & \sin \psi_A & 0 & 0 \\ -\sin \psi_A & \cos \psi_A & 0 & 0 \\ 0 & 0 & 1 & 0 \\ 0 & 0 & 0 & 1 \end{bmatrix} \begin{bmatrix} X_A - X_R \\ Y_A - Y_R \\ \psi_A - \psi_R \\ \beta_A - \beta_R \end{bmatrix} \quad (2.60)$$

Because 4WIS-AGVs cannot move sideways without steering the wheel to the side direction, a nonholonomic constraint is given as:

$$\begin{cases} \dot{X}_R \sin \psi_R - \dot{Y}_R \cos \psi_R = 0 \\ \dot{X}_A \sin \psi_A - \dot{Y}_A \cos \psi_A = 0 \end{cases} \quad (2.61)$$

From Eqs. (2.55) - (2.61), the time derivative of the tracking error vector is as follows:

$$\dot{\mathbf{e}} = \begin{bmatrix} -v_R \cos e_3 \\ v_R \sin e_3 \\ -\dot{\psi}_R \\ -\dot{\beta}_R \end{bmatrix} + \begin{bmatrix} 1 & e_2 & 0 \\ 0 & -e_1 & 0 \\ 0 & 1 & 0 \\ 0 & 0 & 1 \end{bmatrix} \begin{bmatrix} v_A \\ \dot{\psi}_A \\ \dot{\beta}_A \end{bmatrix} \quad (2.62)$$

Proof of Eq. (2.62) is written in Appendix D.

Subsequently, the stability of the system is checked by Lyapunov stability theory. First, a Lyapunov function is chosen as follows:

$$V = \frac{1}{2}e_1^2 + \frac{1}{2}e_2^2 + \frac{1}{k_2}(1 - \cos e_3) + \frac{1}{2}e_4^2 \text{ for } k_2 > 0 \quad (2.63)$$

Stability checking is used to find a control law U that can make the system stable and track the reference trajectory successfully. From the error dynamic in Eq. (2.63), the time derivative of the Lyapunov function equation, \dot{V} , is obtained as follows:

$$\begin{aligned} \dot{V} &= e_1\dot{e}_1 + e_2\dot{e}_2 + \frac{1}{k_2}\sin e_3\dot{e}_3 + e_4\dot{e}_4 \\ &= e_1(v_A + \dot{\psi}_A e_2 - v_R \cos e_3) + e_2(v_R \sin e_3 - \dot{\psi}_A e_1) + \frac{1}{k_2}\sin e_3(\dot{\psi}_A - \dot{\psi}_R) \\ &\quad + e_4(\dot{\beta}_A - \dot{\beta}_R) \\ &= e_1v_A + e_1\dot{\psi}_A e_2 - e_1v_R \cos e_3 + e_2v_R \sin e_3 - e_2\dot{\psi}_A e_1 + \frac{1}{k_2}\sin e_3(\dot{\psi}_A - \dot{\psi}_R) \\ &\quad + e_4(\dot{\beta}_A - \dot{\beta}_R) \\ &= e_1v_A - e_1v_R \cos e_3 + e_2v_R \sin e_3 + \frac{1}{k_2}\sin e_3(\dot{\psi}_A - \dot{\psi}_R) + e_4(\dot{\beta}_A - \dot{\beta}_R) \\ &= e_1(v_A - v_R \cos e_3) + \frac{1}{k_2}\sin e_3(\dot{\psi}_A - \dot{\psi}_R + e_2k_2v_R) + e_4(\dot{\beta}_A - \dot{\beta}_R) \quad (2.64) \end{aligned}$$

According to the Lyapunov stability criterion, if $\dot{V} \leq 0$, the system is stable. Therefore, to meet this condition, a control law U can be chosen as follows:

$$U = \begin{bmatrix} v_A \\ \dot{\psi}_A \\ \dot{\beta}_A \end{bmatrix} = \begin{bmatrix} -k_1 e_1 + v_R \cos e_3 \\ \dot{\psi}_R - e_2 k_2 v_R - k_3 \sin e_3 \\ \dot{\beta}_R - k_4 e_4 \end{bmatrix} \quad (2.65)$$

where k_1, k_2, k_3 and k_4 are positive constants.

Substituting Eq. (2.65) to Eq. (2.64) yields

$$\dot{V} = -k_1 e_1^2 - \frac{k_3}{k_2} \sin^2 e_3 - k_4 e_4^2 \quad (2.66)$$

This means that value of \dot{V} is always negative by using the chosen control law. Furthermore, $\dot{V} = 0$ from Barbalat's lemma, therefore, $e_1, e_3, e_4 \rightarrow 0$ as $t \rightarrow \infty$. From Eqs. (2.62) and (2.65), the following are attained as:

$$\begin{bmatrix} v_A \\ \dot{\psi}_A \\ \dot{\beta}_A \end{bmatrix} = \begin{bmatrix} v_R \\ \dot{\psi}_R - e_2 k_2 v_R \\ \dot{\beta}_R \end{bmatrix} \quad (2.67)$$

$$\dot{e}_1 = -v_R + v_A + e_2 \dot{\psi}_A = e_2 \dot{\psi}_A = 0 \quad (2.68)$$

$$\dot{e}_2 = -e_1 \dot{\psi}_A = 0 \quad (2.69)$$

$$\dot{e}_3 = \dot{\psi}_A - \dot{\psi}_R = -e_2 k_1 v_R = 0 \quad (2.70)$$

$$\dot{e}_4 = \dot{\beta}_A - \dot{\beta}_R = 0 \quad (2.71)$$

From Eqs. (2.68) - (2.71), $e_2 \rightarrow 0$ as $t \rightarrow \infty$ because of $v_R \neq 0$. \mathbf{e} is globally asymptotically stable.

The block diagram of the proposed controller in zero-sideslip maneuver is shown in Fig. 2.6. In parallel steering maneuver, the controller does not use Eqs. (2.10), (2.12) - (2.15), (2.53) and (2.54) to find v_i , δ_i , δ_{fr} and δ_{re} , respectively. The block diagram of the proposed controller for the 4WIS-AGV to move in parallel steering maneuver is shown in Fig. 2.7. In parallel steering maneuver, Eqs. (2.1) and (2.2) are used to find δ_i and v_i (for $i = 1, \dots, 4, fr, re$).

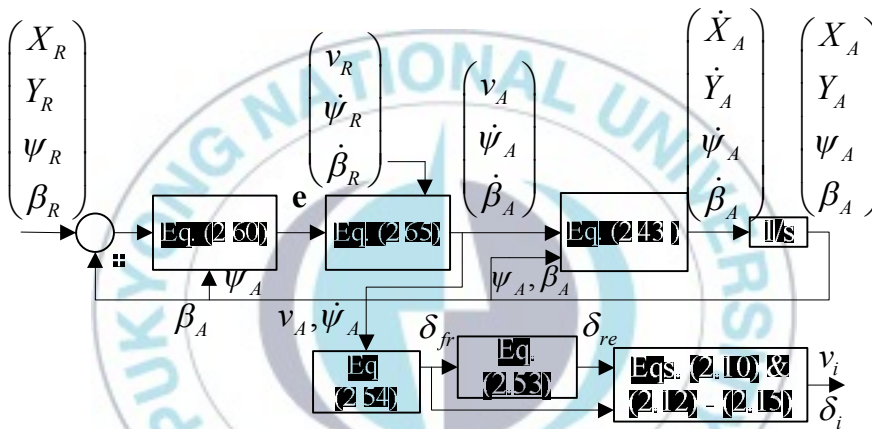


Fig. 2.6 Block diagram of the proposed controller for zero-sideslip maneuver

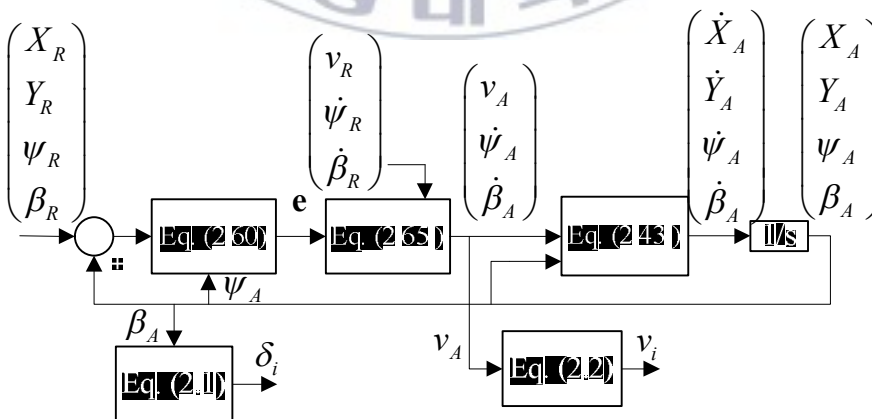


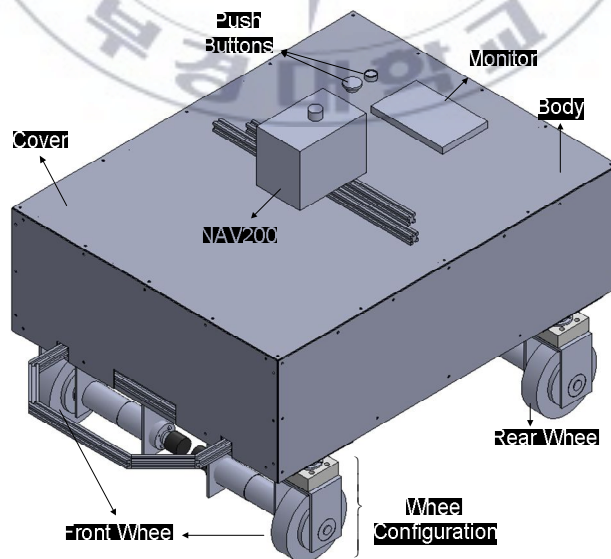
Fig. 2.7 Block diagram of the proposed controller for parallel steering maneuver

Chapter 3: Controller Implementation and Hardware Description

This chapter describes the designed and experimental of the 4WIS-AGV that consists of mechanical design, electrical design and Graphical Unit Interface (GUI) software. The mechanical design is comprised of the body and wheel configurations. The electrical design consists of motors, encoders, industrial PC, battery, ATmega128 microcontrollers, motor drivers, monitor and laser navigation system NAV200. The GUI software explains the software used to control the 4WIS-AGV.

3.1 Mechanical design

The 4WIS-AGV system developed in this thesis is shown in Fig. 3.1.



(a) Designed 4WIS-AGV system



(b) Real system

Fig. 3.1 4WIS-AGV system

It consists of body configuration, laser navigation system NAV200 and wheel configuration. The body and wheel configurations are explained in more detail in the next section. Laser navigation system NAV200 is used to obtain the vehicle position data in addition to data from encoders. The position data is then sent to the trajectory tracking controller in industrial PC. Monitor displays the data from the controller and position of the AGV during experiment. Push buttons are provided to connect and disconnect the system electricity. Moreover, these buttons are included for safety purposes. In case the vehicle has to be turned off, this button works as the emergency button which disconnects all electricity in the system if it is pushed.

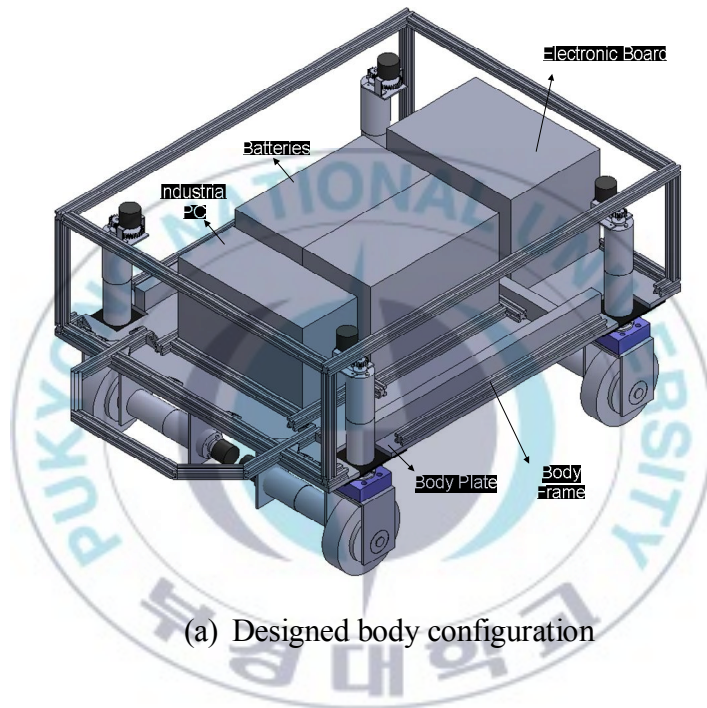
The 4WIS-AGV has dimension of 500 mm (height) x 705 mm (width) x 905mm (length). The electrical components are explained

in detail in the next section. The detailed mechanical drawings of each component are listed in Appendix E.

3.1.1 Body configuration

The body configuration of the 4WIS-AGV is shown in Fig.

3.2.



(a) Designed body configuration



(b) Real body configuration

Fig. 3.2 Body configuration

The specification of the vehicle body is listed in Table 3.1. The body configuration consists of body frame, body plate, electronic board including microcontrollers and motor drivers, batteries and industrial PC. The body plate used in this system is shown in Fig. 3.3.

Table 3.1 Specification of the vehicle body

Descriptions	Symbols	Values
Distance from <i>CG</i> to front wheels	l_{fr}	0.34 m
Distance from <i>CG</i> to rear wheels	l_{re}	0.34 m
Distance from <i>CG</i> left and right wheels	b	0.3125 m

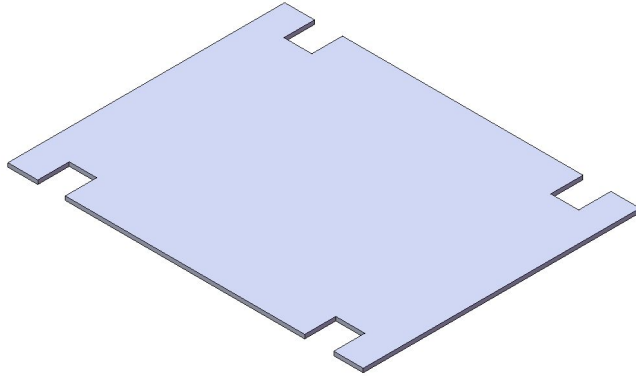


Fig. 3.3 Body plate

All equipments are placed on top of this body plate. Since the AGV is designed for baggage carrier purpose, the body uses big dimension aluminum plate, 100 mm (height) x 705 mm (width) x 905 mm (length), such that it can support the system well. Industrial PC and batteries used in this system are explained in more detail in the electrical design section. The body frame and body cover plate of the vehicle are shown in Fig. 3.4 and 3.5, respectively. The body frame is made of 20 mm x 20 mm aluminum profiles. On the other hand, the body cover plate consists of top cover plate, front cover plate, two side cover plates and rear cover plate. The cover plate uses 2 mm-thickness aluminum plate and is shown in Appendix E for detailed dimension.

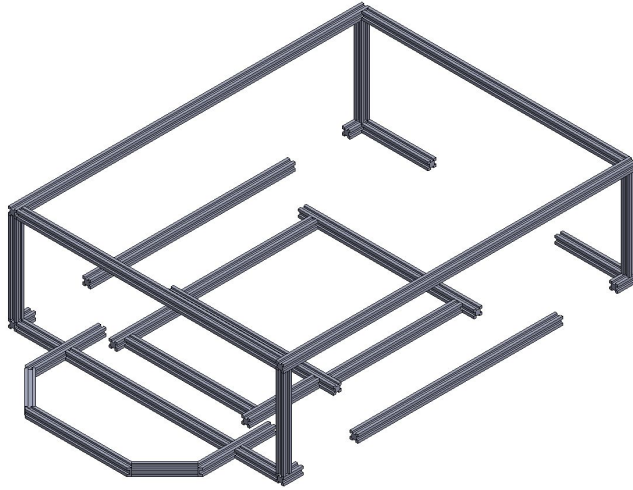


Fig. 3.4 Body frame

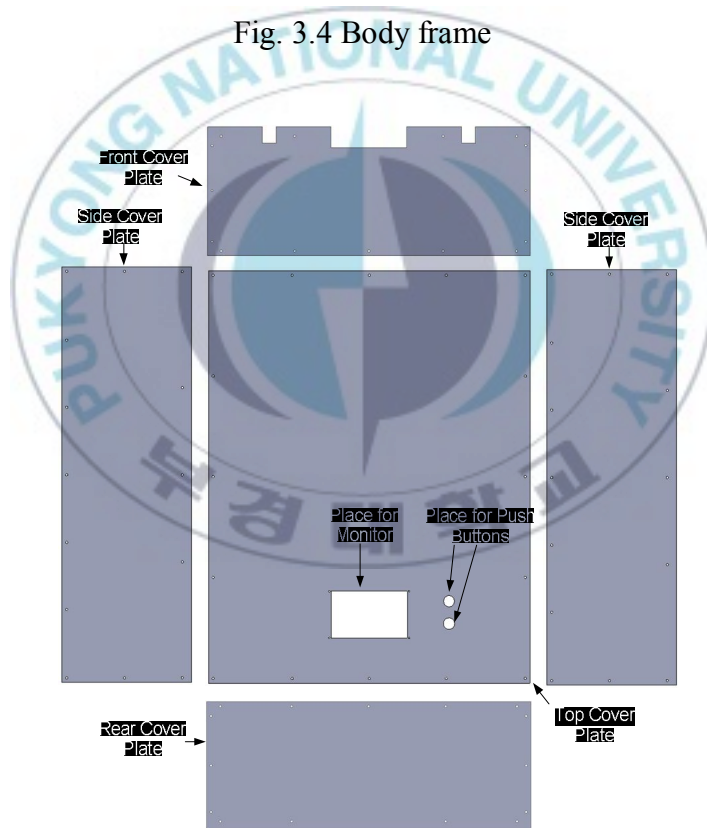


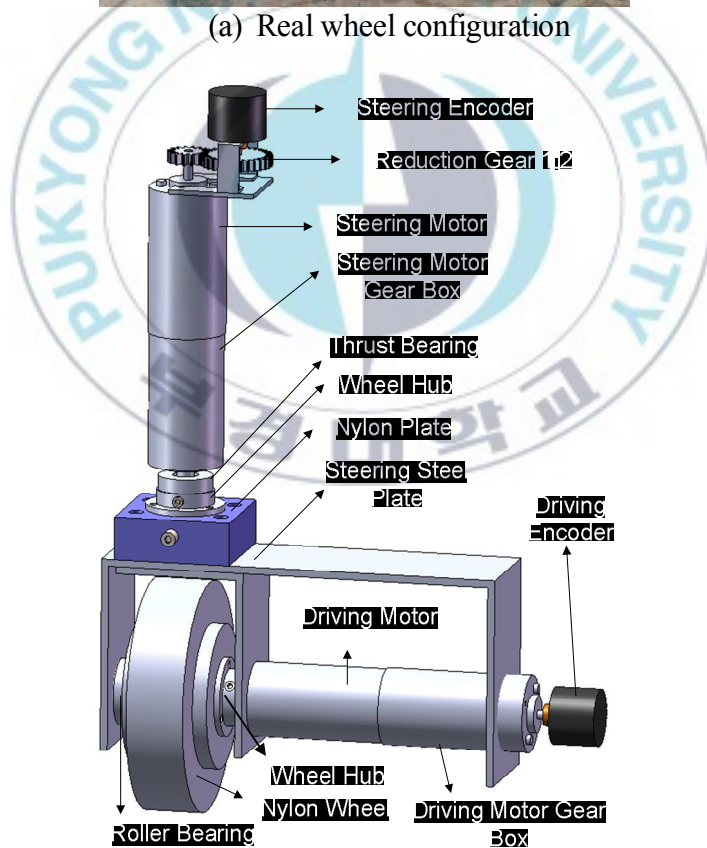
Fig. 3.5 Body cover plate

3.1.2 Wheel configuration

The wheel configuration of this system is shown in Fig. 3.6.



(a) Real wheel configuration



(b) Designed wheel configuration

Fig. 3.6 Wheel configuration

This configuration is comprised of two DC motors for driving and steering purposes. Both driving and steering motors use 48.6 W DC motors with driving motor gear box 1:100 for driving purpose and steering motor gear box 1:150 for steering purpose. Each motor is coupled with an encoder used for positioning of the vehicle. Two wheel hubs as shown in Fig. 3.7 are used: one to connect the steering motor shaft to the nylon plate and the other is to connect the driving motor shaft and nylon wheel. Roller bearing with 20mm (inner diameter) x 46mm (outer diameter) x 13mm (thickness) is used to hold the nylon wheel at the steering steel plate. Nylon plate is used to hold the nylon wheel at the steering steel plate. Nylon plate is used to connect the steering motor with the steering steel plate. Nylon plate and steering steel plate are shown in Figs. 3.8 and 3.9, respectively. Because the steering steel plate has to also support vehicle weight, thrust bearing is used. Reduction gear 1:2 is used to couple the steering motor and steering encoder as shown in Fig. 3.10. Nylon wheel is used for the driving wheel as shown in Fig. 3.11.



Fig. 3.7 Wheel hub

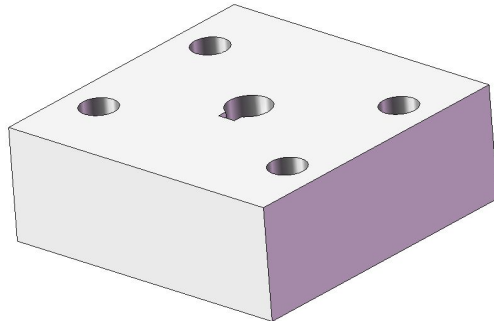


Fig. 3.8 Nylon plate



Fig. 3.9 Steering steel plate



Fig. 3.10 Reduction gear 1:2

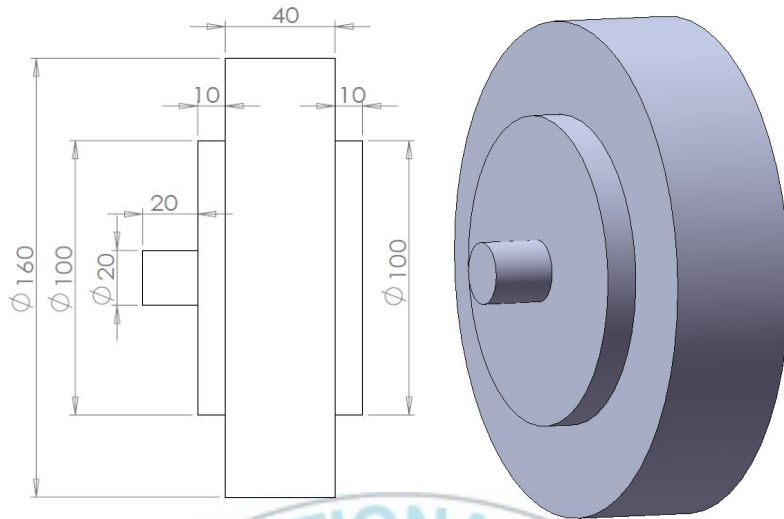


Fig. 3.11 Nylon wheel

3.2 Electrical design

The electrical configuration of the 4WIS-AGV is shown in Fig. 3.12.

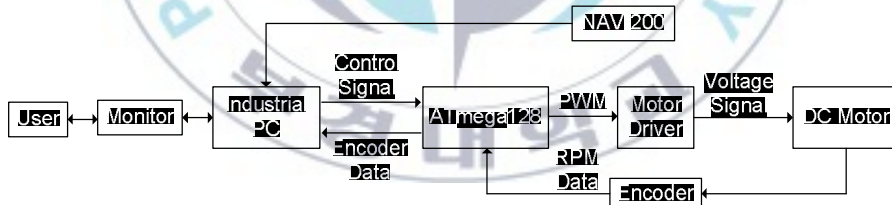


Fig. 3.12 Electrical configuration of 4WIS-AGV

The main controller is industrial PC with RS-232 communication. Users give commands to the 4WIS-AGV through the GUI in industrial PC. The control signals generated from the controller are then sent to ATmega128 microcontrollers in the electronic board of the vehicle. Subsequently, these signals are

converted to Pulse Width Modulation (PWM) signals which are then converted to voltage signals by motor driver for driving DC motor. The feedback data are obtained from sensors such as NAV200 and encoders. NAV200 generates position data which is then sent to the industrial PC. On the other hand, the encoders count the revolution of DC motor shaft which are then used to find the position of the vehicle. The following sections describe these components with detailed specification and figures.

3.2.1 DC motors

DC motors used in the 4WIS-AGV are 48.6 W DC motors as shown in Fig. 3.13. These motors are used for driving and steering purposes. Driving DC motors use 1/100 gear reduction ratio, whereas steering DC motors use 1/150 gear reduction ratio. The motor performance graph is shown in Fig 3.14 and its detailed specification is listed in Table 3.2.



Fig. 3.13 DC motors

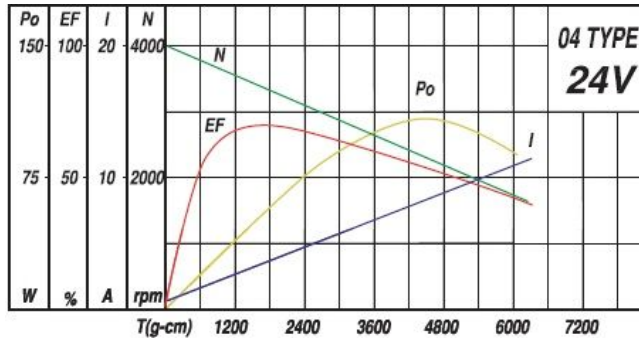


Fig. 3.14 Performance graph of the DC motors [62]

Table 3.2 Specification of DC motor IG-52GM 04TYPE (24V)

No	Parameters	Values	
		Motor with 1/100 gear reduction ratio	Motor with 1/150 gear reduction ratio
1	Gear head (mm)	84	99.5
2	Weight (g)	1,770	1,940
3	Rated torque (kgf-cm)	78	98
5	Rated speed (RPM)	35	23.5
6	No load speed (RPM)	40	26

3.2.2 Encoders

In the 4WIS-AGV system, high-resolution encoders are used instead of built-in encoder from the DC motors. The encoder is rotary encoder E40HB-6-3600-3-V-5 as shown in Fig. 3.15. The specification of the encoder is listed in Table 3.3.



Fig. 3.15 Encoder E40HB-6-3600-3-V-5

Table 3.3 Specification of encoder E40HB-6-3600-3-V-5

No	Parameters	Values
1	Shaft diameter (mm)	6
2	Resolution (pulse /1 revolution)	3600
3	Output phase	A, B, Z
4	Output	Voltage output
5	Power supply (V)	5
6	Weight (g)	120

These encoders are used to measure the revolution of the driving and steering wheels. The data from encoders are sent to the controller such that the movement of the vehicle can be controlled properly.

3.2.3 Industrial PC

Industrial PC TANK-800 is used as the main controller. The overall view of the industrial PC is given in Fig. 3.16. Industrial PCs are basically personal PCs designed for industrial application. Thus, Industrial PCs are very suitable for the 4WIS-AGVs because these

systems need rugged controllers to operate reliably in harsh usage environments and conditions. Moreover, Industrial PC can perform high complexity calculation and collect high-frequency data from sensors. In this system, all the calculation of the controller and collecting data from positioning sensors are conducted in this industrial PC.

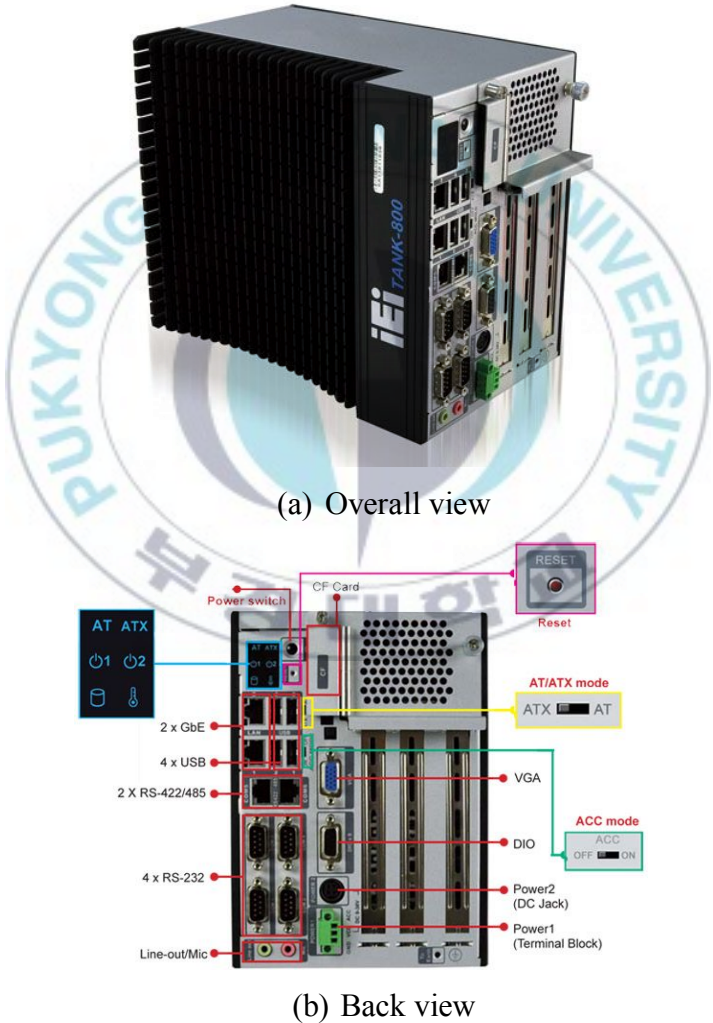


Fig. 3.16 Industrial PC TANK-800

The specification of Industrial PC TANK-800 is shown in Table 3.4.

Table 3.4 Specification of PC TANK-800

No	Parameters		Values
1	Chassis	Dimensions	136 mm x 219 mm x 188 mm
2	Motherboard	CPU	Intel® Atom™ D525 1.8 GHz dual-core processor
		Chipset	Intel® ICH8M
		Ethernet	Dual Realtek RTL8111E PCIe GbE controllers support ASF 2.0
3	Storage	SATA	2.5'' SATA HDD bay
4	System Function	USB	4 x USB 2.0
		Ethernet	2 x RJ-45
		RS-232	4 x DB-9
		RS-422/485	2 x RJ-45
		Display	1 x VGA
		Resolution	Up to 2048 x 1536
		Audio	1 x Mic-in, 1 x Line-out
		DIO	1 x DB-9
		Interior Expansions	One PCIe x4 (physical one PCIe x16 slot) and two PCI slots
5	Power	Power Supply	10.5 V (+/-0.3 V) - 36 V
		Power Consumption	33 W (without add-on card)
6	Reliability	Operating	-20°C - 70°C

		Temperature	
		Weight	3.0 Kg

3.2.4 Battery

In the 4WIS-AGV system, all motors need 24V power supply. Therefore, two ATLASBX ITX100 12V batteries are used as shown in Fig. 3.17. The specification of this battery is listed in Table 3.5.



Fig. 3.17 12V battery ATLASBX ITX100

Table 3.5 Specification of 12V battery ATLASBX ITX100

No	Parameters	Values
1	Nominal Voltage (V)	12 V 100Ah
2	Weight	24.2 kg
3	Terminal type	Bolt terminal
4	Dimension (mm)	330 x 171 x 217

3.2.5 Microcontroller AVR ATmega128

Microcontroller AVR ATmega128 are used to convert control signals generated by the controller to PWM signals which are then converted to voltage signal by motor drivers. The microcontroller is shown in Fig. 3.18 and its specification is listed in Table 3.6.

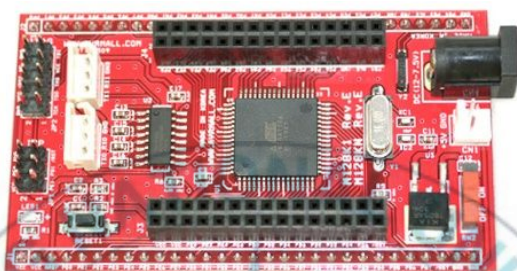


Fig. 3.18 Microcontroller AVR ATmega128

Table 3.6 Specification of microcontroller AVR ATmega128

No	Parameters	Remarks
1	Clock	16MHz
2	RS232 channel interface	Two
3	Operating power	4.5 to operate at 5.5V
4	Board size	4.6 x 7.9 cm
5	RTC-32.768KH	Available
6	ATMEL ISP port, JTAG port	Available
7	All PORT Pin Extension	Available
8	RESET switch	Available
9	Power LED (RED)	Available
10	External input power supply	Available: DC jack (power supply 7.5 - 12V Input)

In this system, eight ATmega128 microcontrollers are used to control four steering motors and four driving motors.

3.2.6 Motor drivers

The overall view and circuit of motor drivers used in the system are shown in Fig. 3.19. Like microcontrollers, eight motor drivers are used in the system. This motor driver can work in the range of 12 - 24 VDC.

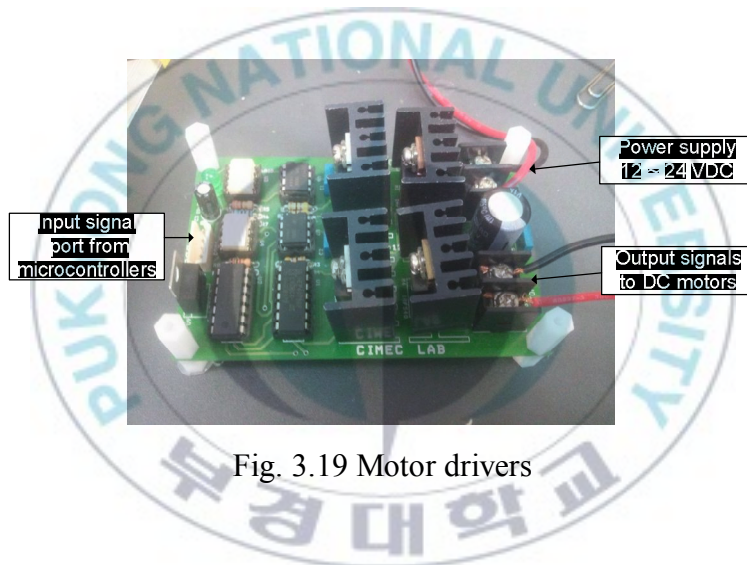


Fig. 3.19 Motor drivers

3.2.7 Monitor

MYMO MY-720 touch screen monitor as shown in Fig. 3.20 is used to display the data of the controller to users. It has 7 inch screen size and its detailed specification is listed in Table 3.7.



Fig. 3.20 Monitor MYMO MY-720

Table 3.7 Specification of monitor MYMO MY-720

No	Specification	TSP Model
1	Screen size	7.0 inch wide
2	Resolution	WVGA (800 × 480)
3	Display colors	16.7 M
4	Brightness	250 cd/m ²
5	Contrast ratio	350 : 1
6	Response time	30 msec
7	Touch input	Touch screen panel
8	Video input	USB2.0 high speed
9	Connector	USB mini B type
10	Power input	USB power (5 V, 500 mA)
11	Power consumption	3.3 - 4.9 W
12	UI, Pivot	Pivot (Landscape, Portrait)
13	Product dimension (mm)	194 (W) x 133 (L) x 180 (H)

3.2.8 Laser Navigation System NAV200

Laser navigation system NAV200 is used to obtain the position of the vehicle and thus it is installed at the center point of the vehicle. The basic principle of the NAV200 is shown in Fig. 3.21. The NAV200 transmits pulse laser signals using a laser diode. The signals are reflected when they detect objects. The reflected signal is received by the laser measurement system receiver which uses a photodiode. Distance from the sensor to the object is calculated from the propagation time (dt) between sent pulse and received pulse.

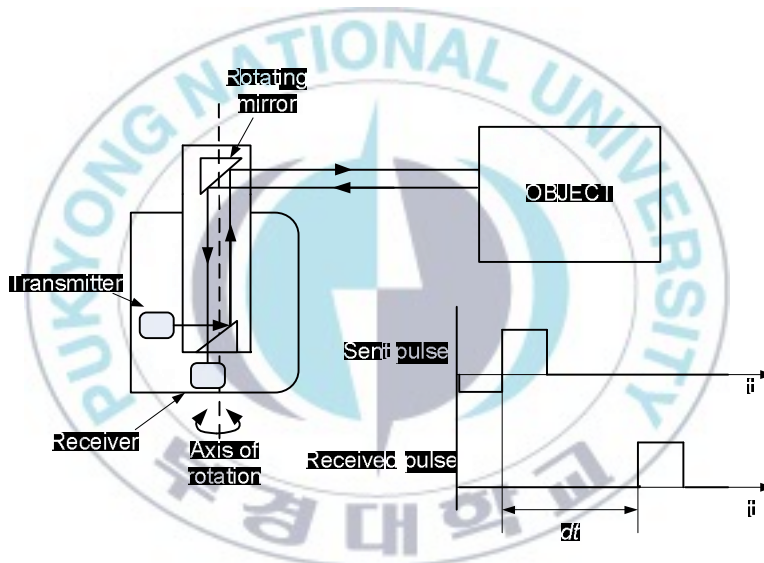


Fig. 3.21 Laser navigation system NAV200 basic principle

The calculation of the position and orientation of the NAV200 is shown in Fig. 3.22. The NAV200 position and orientation are obtained based on the fixed reflectors located at the environment ($R_1, R_2, R_3, \dots, R_n$), where n is number of detected reflectors. One revolution of the scanner head is equivalent to one scanning and each revolution generates one reading per detected reflectors. The

measurement results are distances between sensors and reflectors ($d_1, d_2, d_3, \dots, d_n$) and measurement angles ($\theta_1, \theta_2, \theta_3, \dots, \theta_n$).

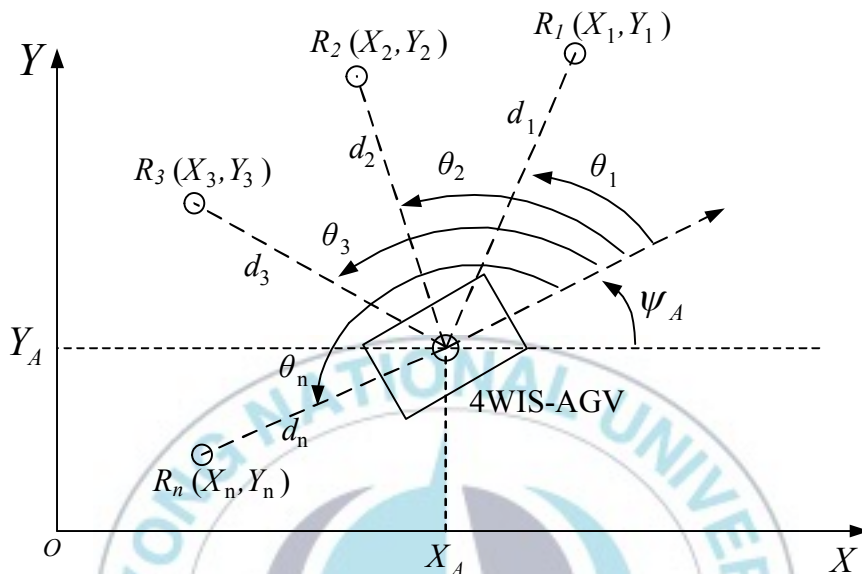


Fig. 3.22 Position measurement of the NAV200

The coordinates of the reflectors are then saved in the nonvolatile reflector memory of the NAV200 as references. At least three reflectors are detected to measure position of the vehicle. In the position measurement, the NAV200 measures the distances and angles of the reflectors and calculates its own position from this data. By comparing the reflector data in the NAV200 memory and the measurement result, the position and orientation of the 4WIS-AGV can be determined.

The coordinate of the 4WIS-AGV (X_A, Y_A) and orientation ψ_A in Fig. 3.22 can be obtained from [60] as follows:

$$X_A = \left[\frac{1}{(m_2 - m_1)(1 + m^2)} \right] \left\{ (m_2 m - 1) \times [(m_1 + m)X_1 + (m_1 m - 1)Y_1] - (m_1 m - 1) \times [(m_2 + m)X_2 + (m_2 m - 1)Y_2] \right\} \quad (3.1)$$

$$Y_A = \left[\frac{1}{(m_2 - m_1)(1 + m^2)} \right] \left\{ (m_1 + m) \times [(m_2 + m)X_2 + (m_2 m - 1)Y_2] - (m_2 + m) \times [(m_1 + m)X_1 + (m_1 m - 1)Y_1] \right\} \quad (3.2)$$

$$\psi_A = \text{atan2}(Y_1 - Y_A, X_1 - X_A) - \theta_1 \quad (3.3)$$

where $m_1 = \tan \theta_1$, $m_2 = \tan \theta_2$, $m_3 = \tan \theta_3$ and $m = \tan \psi_A$. From Eqs. (3.1) - (3.3), m is given by:

$$m = \frac{(m_3 - m_1)(Y_1 - Y_2 - m_1 X_1 + m_2 X_2) - (m_2 - m_1)(Y_1 - Y_3 - m_1 X_1 + m_3 X_3)}{(m_3 - m_1)(m_1 Y_1 + X_1 - m_2 Y_2 - X_2) - (m_2 - m_1)(m_1 Y_1 + X_1 - m_3 Y_3 - X_3)} \quad (3.4)$$

The structure of the NAV200 is shown in Fig. 3.23.



Fig. 3.23 Laser navigation system NAV200

The specification of the NAV200 is listed in Table 3.8.

Table 3.8 Specification of laser navigation system NAV200

No	Parameters	Values
1	Light source	Infrared (855 nm)
2	Laser class	1
3	Field of view	360 °
4	Scanning frequency	8 Hz
5	Angular resolution	0.1°

6	Operating range	1.2 m – 28.5 m
7	Max. range 10 % reflectivity	28.5 m
8	Data communication	Serial (RS-232)
9	Data transmission rate	19,200 Hz
10	Operating voltage:	$\geq 24 \text{ V DC} \pm 25\%$
11	Power consumption:	24 W
12	Weight	3.3 kg
13	Dimensions (mm)	176 x 178 x 115

3.3 Graphical Unit Interface (GUI) software

The software to control the 4WIS-AGV is created using Microsoft Visual Studio 2008 with C# programming language. The Graphical Unit Interface (GUI) for the 4WIS-AGV is shown in Fig. 3.24 and 3.25 for manual menu and automatic menu, respectively. In the GUI manual menu, users can control the 4WIS-AGV manually. Each wheel of the vehicle can be adjusted separately and uniformly as shown in Fig. 3.24.

Fig. 3.24 shows four boxes named Front Left, Rear Left, Rear Right and Front Right. These boxes are used to control adjustment of the front left, rear left, rear right and front right wheels. These boxes also have driving and steering sliders which enable users to adjust driving control and steering control independently. The box at the middle center is all-control box which controls all the wheels within one slider. There are two sliders in this box. One is D slider for driving which enables users to adjust driving control of each wheel and another is S slider for steering which can adjust steering angle of each angle simultaneously.

The right side box with many arrows is used to control the wheels at the specified angles, 0° , $\pm 45^\circ$, $\pm 90^\circ$ and forward and backward motion. Five arrows at the top are used to adjust the direction of each wheel. Stop button, up arrow and down arrow under the five arrows are used to control the angular velocity of the driving motor of each wheel.

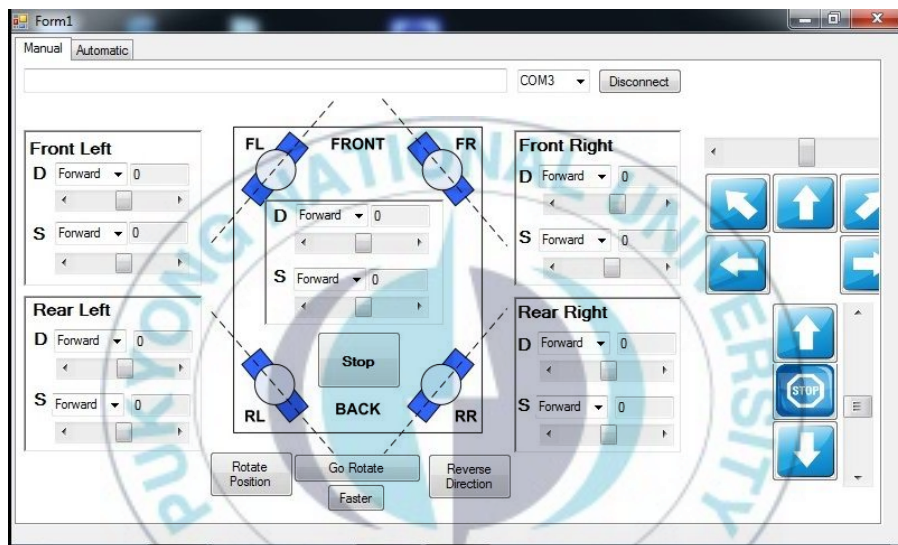


Fig. 3.24 Manual menu of the 4WIS-AGV GUI

In the automatic menu in Fig. 3.25, users can control the vehicle automatically to track reference trajectories. The left box is the map indicating the position of the 4WIS-AGV. The vehicle is illustrated as a circle with one line to show the heading direction. The circular line shows the trajectory that the vehicle is expected to track. The view of the map can be zoomed in and out using plus (+) and minus (-) buttons beside the map box.

The box in the right side is the NAV200 measurement data which shows the 4WIS-AGV X and Y positions and orientation. The

number of reflectors and validity are also shown below the position data. The validity value is dependent on the number of the detected reflectors. The higher the number of detected reflectors is, the higher the validity value is.

Moreover, this menu presents error and wheel measurements. Two numbers at the left side inside wheel measurement box are front and rear wheel steering angles δ_{fr} and δ_{re} in degree unit which are located at the top and bottom, respectively. The eight numbers at the right side inside the wheel measurement box are angular velocity of each wheel ω_i and each wheel steering angle δ_i . The chosen controller gains are shown at left middle side of the GUI. Gains can be adjusted also in this GUI.

To start experiments, users should specify a reference trajectory from which the 4WIS-AGV must track by using Load button, next, click the record button to save all recorded position data, finally, press track button to start the trajectory tracking.

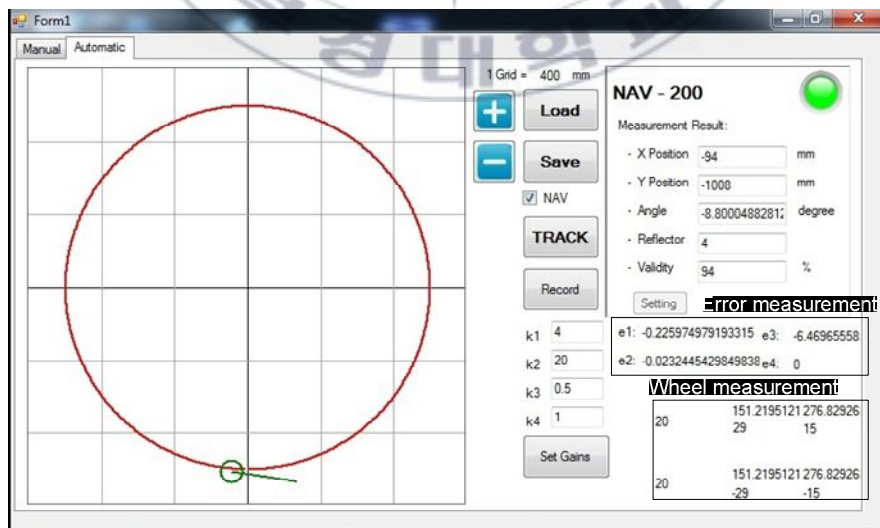


Fig. 3.25 Automatic menu of the 4WIS-AGV GUI

Chapter 4: Simulation and Experimental Results

To verify the effectiveness and performance of the mathematical modeling and the designed controller of the 4WIS-AGV, simulations and experiments are conducted by assigning the 4WIS-AGV to track two reference trajectories, i.e. a reference trajectory with sharp edges and a circular reference trajectory. These two reference trajectories are taken for the verification of two maneuvers that four wheel steering vehicles have, i.e. parallel steering maneuver and zero-sideslip maneuver.

4.1 Simulation results

Simulations are conducted by using two reference trajectories to show the designed controller performance as follows:

- A reference trajectory with sharp edges for parallel steering maneuver
- A circular reference trajectory for zero-sideslip maneuver

4.1.1 Reference trajectory with sharp edges

Fig. 4.1 shows the reference trajectory with sharp edges which is used to verify the 4WIS-AGV can move omnidirectionally. Furthermore, this case is taken to show the experimental 4WIS-AGV's ability to move with parallel steering maneuver.

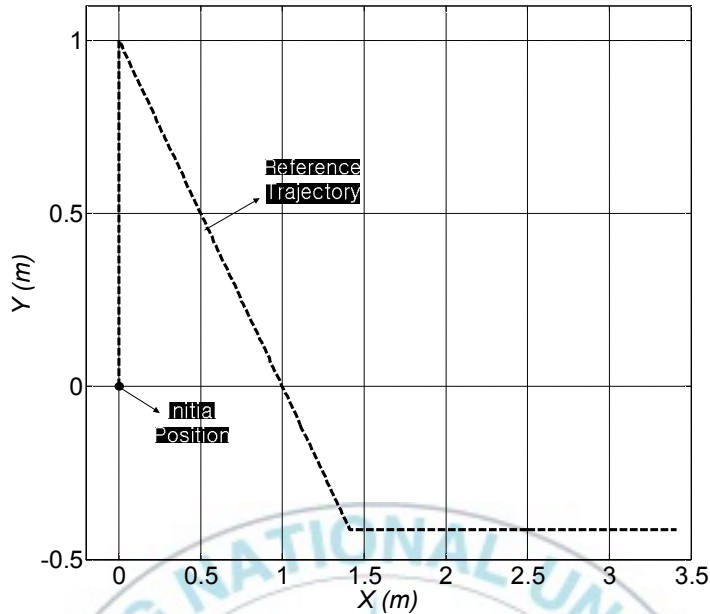


Fig. 4.1 Initial position and reference trajectory with sharp edges

In this simulation, the 4WIS-AGV has to track the trajectory with sharp edges. The trajectory consists of 1 meter in the direction of Y axis, 2 meter line with the slope of 45° and 2 meter line in the direction of X axis. This reference is given to show the flexibility of the 4WIS-AGV that it can turn at the sharp edge accurately. This is the advantage of four wheel steering configuration where the four wheels can be adjusted at the same direction. The simulation was conducted within 73 s.

An illustration on how the vehicle is expected to move is shown in Fig. 4.2. This figure also shows the reference sideslip angle, β_R , that is given to show how the system is supposed to move. In this instance, the reference vehicle orientation, ψ_R , is kept at $\pi/2$ rad. Parameters and initial values of the simulation are listed in Table 4.1.

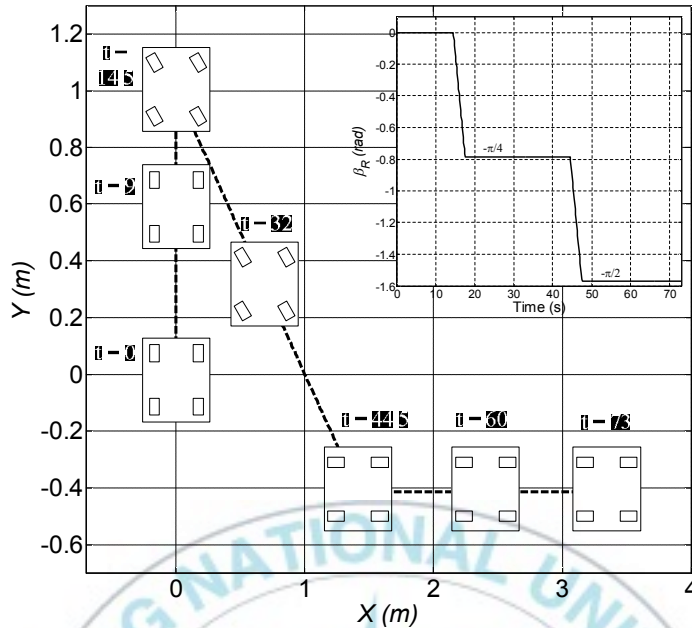


Fig. 4.2 Illustration of the expected motion

Table 4.1 Parameter and initial values of the simulation

Descriptions	Symbols	Values
Initial position of the vehicle	(X_0, Y_0)	$(0, 0)$
Initial position of reference	(X_R, Y_R)	$(0, 0)$
Initial value of vehicle orientation	$\psi_A(0)$	$\pi/2$ rad
Initial value of sideslip angle	$\beta_A(0)$	0
Initial value of wheel steering angles	$\delta_i(0)$	0
Reference vehicle orientation	ψ_R	$\pi/2$ rad
Reference vehicle angular velocity	$\dot{\psi}_R$	0
Limit value of vehicle linear velocity	v_A	± 0.2 m/s
Limit value of vehicle angular velocity	$\dot{\psi}_A$	± 0.15 rad/s
Limit value of vehicle sideslip angular velocity	$\dot{\beta}_A$	± 0.28 rad/s
Controller gain 1	k_1	0.1 s^{-1}
Controller gain 2	k_2	2 rad/m^2
Controller gain 3	k_3	0.5 rad/s
Controller gain 4	k_4	2 s^{-1}

Figs. 4.3 - 4.6 show the reference values of the 4WIS-AGV in the simulation. Figs. 4.3 and 4.4 show the reference X axis and Y axis trajectories, respectively. The reference linear velocity of the 4WIS-AGV is shown in Fig. 4.5. From $t=0$ s to $t=2$ s, the vehicle accelerates with 0.04 m/s^2 . At $t=2$ s, the vehicle reaches $v=0.08$ m/s and the vehicle keeps the velocity until $t=12.5$ s. During this time, the vehicle moves in Y direction. At $t=12.5$ s, the vehicle decelerates with -0.04 m/s^2 for 2 s. At $t=14.5$ s, the vehicle reaches $X = 0$ m, $Y = 1$ m and stays for 3 s to adjust its wheel angles.

Subsequently, the vehicle accelerates with 0.04 m/s^2 in opposite direction at $t=17.5$ s for 2 s. The vehicle reaches -0.08 m/s (minus due to opposite direction) at $t=19.5$ s and keep the velocity for 23 s. At this time, the vehicle moves in -45° slope line (minus means clockwise). At $t=42.5$ s, the vehicle decelerates with -0.04 m/s^2 for 2 s. At $t=44.5$ s, the vehicle reaches $X = 1.41$ m, $Y = -0.41$ m and stays for 3 s to adjust its wheel angles.

Then, the vehicle accelerates with 0.04 m/s^2 at the same direction with the previous movement at $t=47.5$ s for 2 s. The vehicle reaches -0.08 m/s (minus due to opposite direction) at $t=49.5$ s and keep the velocity for 23.5 s. At this time, the vehicle reaches $X = 3.36$ m, $Y = -0.41$ m and moves in X direction.

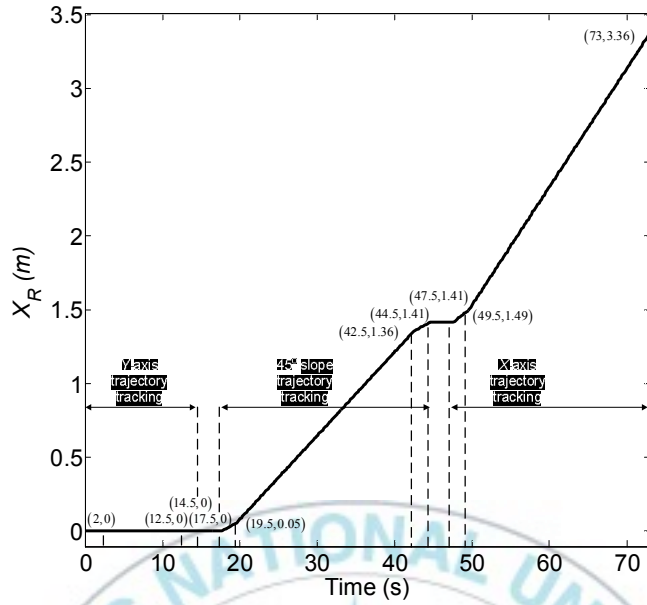


Fig. 4.3 X-axis reference trajectory

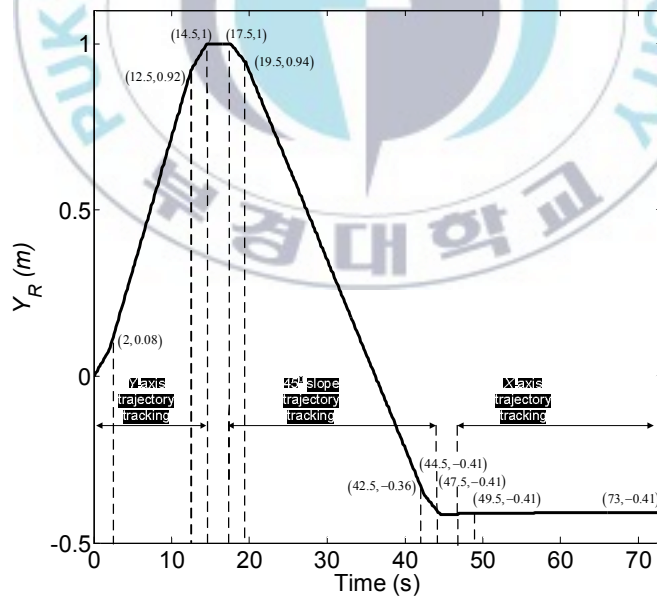


Fig. 4.4 Y-axis reference trajectory

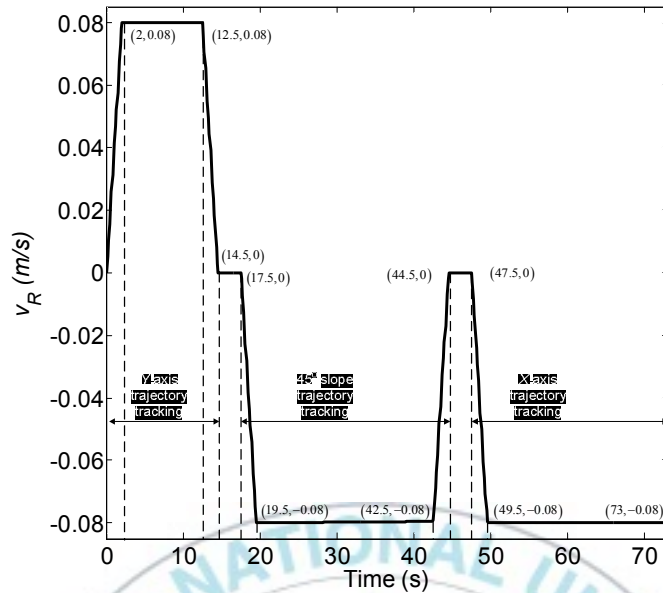


Fig. 4.5 Reference vehicle linear velocity

Subsequently, reference sideslip angular velocity of the 4WIS-AGV is shown in Figs. 4.6. The vehicle has the reference sideslip angular velocity of 0.26 rad/s for 3 s at $t=14.5$ s and $t=44.5$ s that it rotates to adjust its wheels.

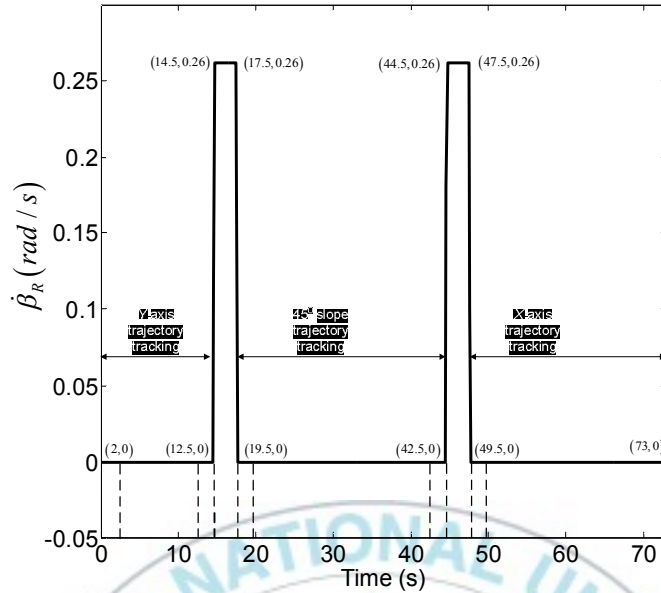


Fig. 4.6 Reference sideslip angular velocity

The trajectory tracking result is shown in Fig. 4.7. It shows that the 4WIS-AGV can track the reference trajectory with sharp edges very well. Fig. 4.8 shows the trajectory tracking errors. Although the errors are relatively very small, there are small peak values when the 4WIS-AGV passes sharp edges. For example, when the vehicle starts to move, error in local coordinate x axis direction, e_1 , instantly decreases to -0.018 m and quickly increases to 0.003 m and decrease slowly approaching to zero. At $t=12.5$ s when the vehicle decelerates, e_1 instantly increases to 0.02 m and quickly decreases to -0.002 m. The same condition happen at $t=14.5$ s, 17.5 s, 44.5 s, and 47.5 s which are the conditions when the vehicle changes its velocity. These phenomena happen because the vehicle needs time to be accelerated and decelerated which is not considered

in the reference values. Thus, every time the vehicle starts and stops, such errors exist which are then minimized by the controller.

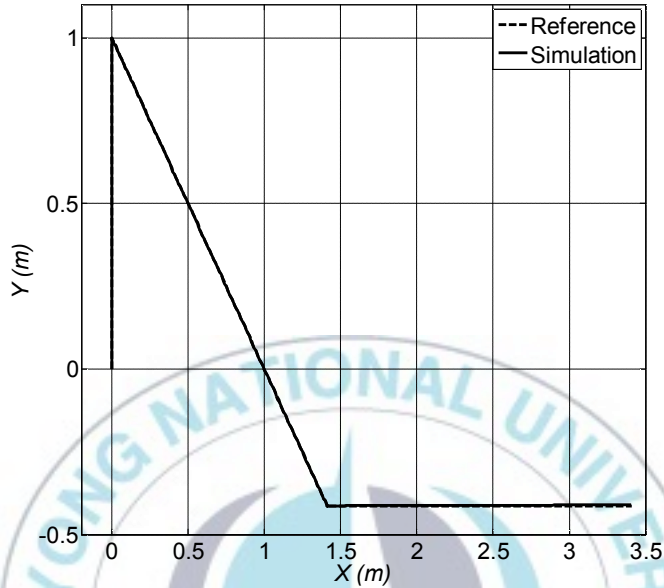


Fig. 4.7 Trajectory tracking result

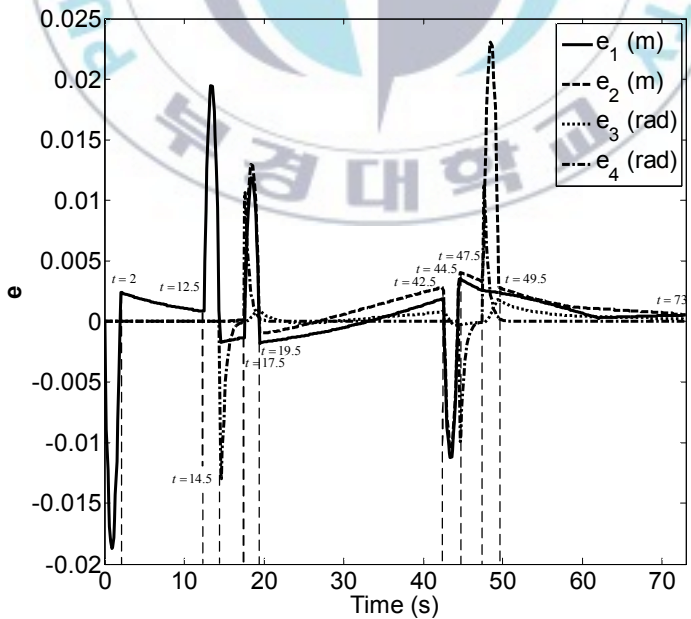


Fig. 4.8 Trajectory tracking errors

The control law U for this trajectory tracking is shown in Fig. 4.9. This figure shows the linear velocity, angular velocity and the sideslip angular velocity of the 4WIS-AGV. The linear velocity of the 4WIS-AGV has values of 0.08 m/s in Y directional motion, -0.08 m/s in 45° slope and X directional motions and 0 m/s for 3 s at the first sharp edge between $t= 14.5$ s and $t=17.5$ s and at the second sharp edge between $t= 44.5$ s and $t=47.5$ s, respectively. Vehicle angular velocity shows 0 rad/s except at $t=17.5$ s, 42.5 s and 47.5 s. At $t=17.5$ s, the vehicle wheel steering angles are already changed and therefore when it starts to move, there is a movement direction change that make the vehicle angular velocity increases with very small value of 0.001 rad/s, which is then minimized by the controller. At $t=42.5$ s, the vehicle angular velocity decreases to -0.001 rad/s and minimized to zero when the vehicle decelerates. The same phenomenon with the vehicle at $t=17.5$ s happens again at $t=47.5$ s when the vehicle changes its wheel steering angles.

When the vehicle moves, the sideslip angular velocity is kept zero as shown in the figure. When the vehicle stays, the controller adjusts each wheel steering angle and thus the sideslip angular velocity increase to 0.26 rad/s for 3 s at $t=17.5$ s and $t=44.5$ s. During the motion, the vehicle angular velocity is kept zero as shown in the figure.

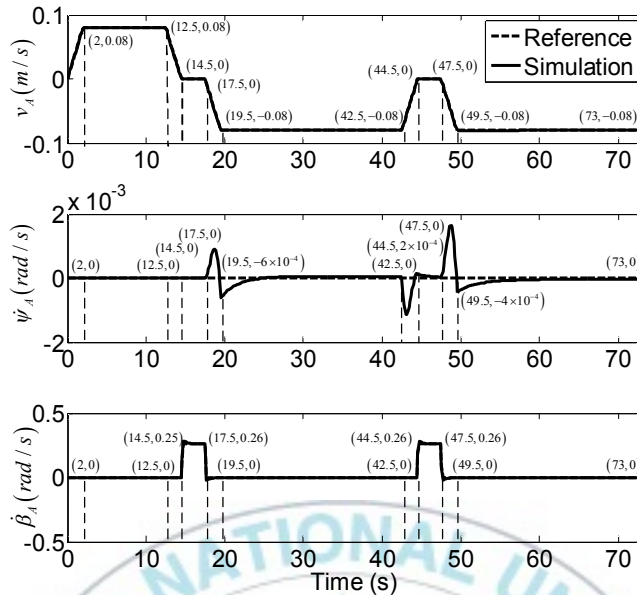


Fig. 4.9 Control law U

Initially the vehicle starts with zero velocity and accelerates until reaching 0.08 m/s at $t=2$ s. The vehicle keeps the vehicle linear velocity for 10.5 s before it decelerates to zero at $t=14.5$ s. For these times, the vehicle tracks 1 m line in Y direction. The vehicle stays for 3 s to adjust the wheel steering angles to be $-\pi/4$ rad from $t=14.5$ s. The vehicle then starts and reaches the reference linear velocity at -0.08 m/s at $t=19.5$ s. For this time, the vehicle tracks the second trajectory line which has $-\pi/4$ rad slope from the first reference line. The vehicle keeps the vehicle linear velocity of -0.08 m/s for 23 s until it decelerates for 2 s. The vehicle stays for 3 s again to change the wheel steering angles to be $-\pi/2$ rad. The vehicle starts again and reaches -0.08 m/s at $t=49.5$ s. The vehicle keeps the vehicle linear velocity of -0.08 m/s again for 23 s before it reaches the goal point.

Figs. 4.10 and 4.11 show the comparison of simulation results and reference of X -axis and Y -axis trajectory tracking. It can be seen that the simulation results are very close with the reference tracking trajectories. The trajectory tracking errors in the X and Y directions, $e_X = X_A - X_R$ and $e_Y = Y_A - Y_R$, are shown in Fig. 4.12. This figure shows that there are errors with $e_X = \pm 0.025$ m and $e_Y = \pm 0.02$ m in X -axis and Y -axis positions. When the vehicle starts to move, error in global coordinate X axis, e_X , instantly decreases to -0.018 m and quickly increases to 0.003 m and decrease slowly approaching to zero. At $t=12.5$ s when the vehicle decelerates, error in global coordinate Y axis, e_Y , instantly increases to 0.02 m and quickly decreases to -0.002 m. The same conditions happen at $t=17.5$ s, 44.5 s, and 47.5 s which are the conditions when the vehicle changes its velocity. These phenomena happen because the vehicle needs time to be accelerated and decelerated which is not considered in the reference values. Thus, every time the vehicle stops and starts, such errors exist which are then minimized by the controller.

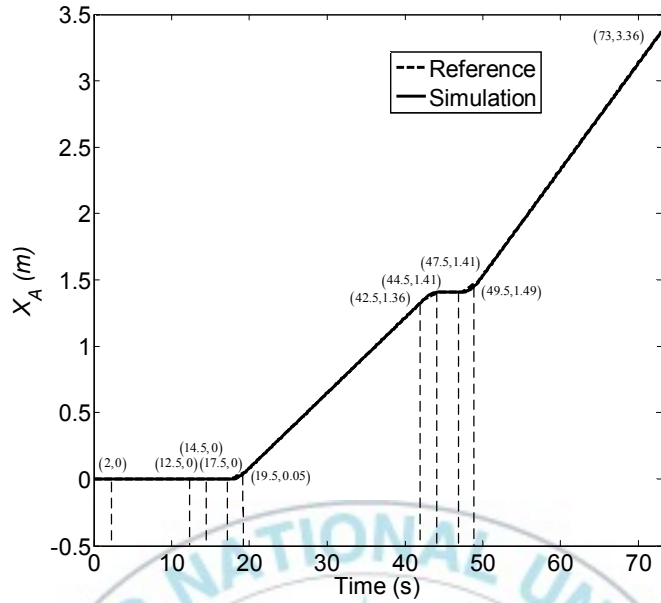


Fig. 4.10 X-axis reference and simulation

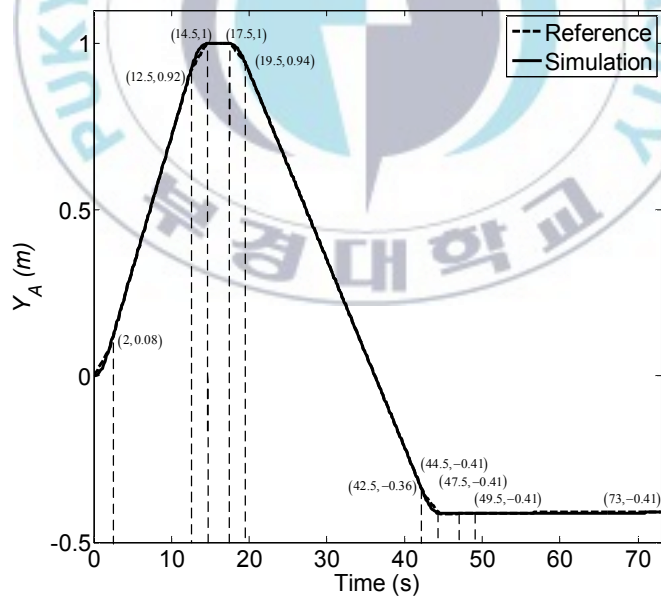


Fig. 4.11 Y-axis reference and simulation

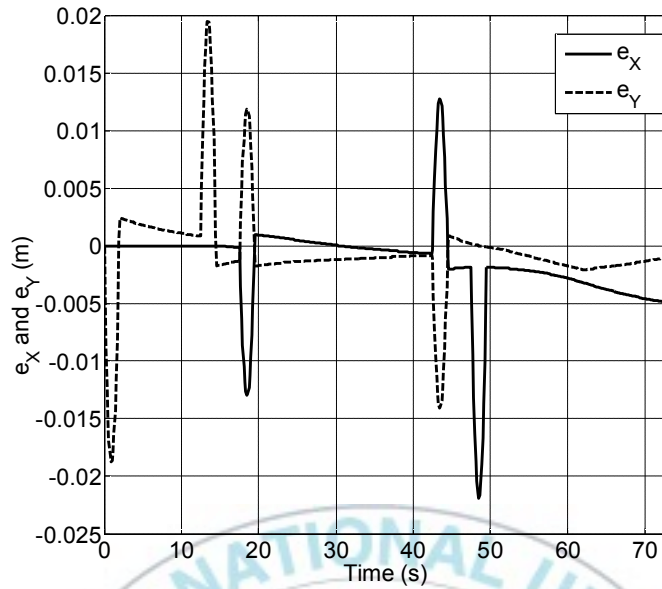


Fig. 4.12 Errors e_x and e_y

Fig. 4.13 shows the simulation results of the vehicle orientation during the tracking process and it can be seen that the orientation is kept $\pi/2$ rad to keep the AGV posture for parallel steering maneuver during the motion.

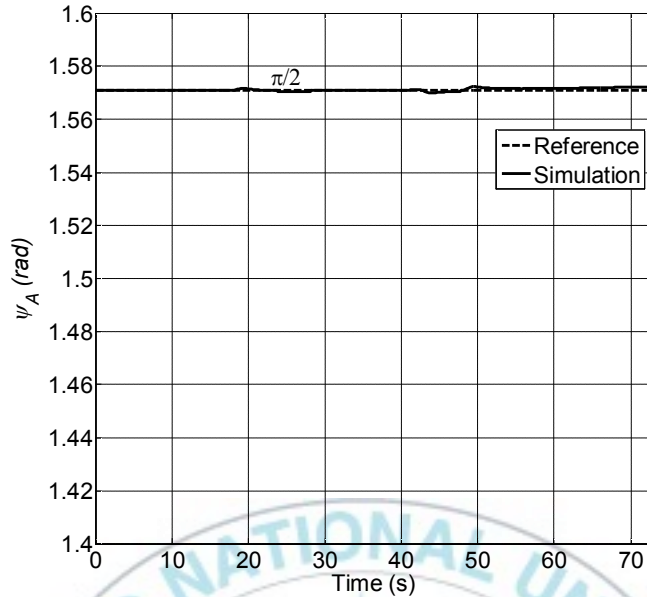


Fig. 4.13 Vehicle orientation reference and simulation

Fig. 4.14 shows the simulation result of the vehicle sideslip angle compared with its reference value. It can be seen that the vehicle is able to follow the reference sideslip angle very well. At the first section where the 4WIS-AGV has to track a 1 m line in the Y axis direction, the sideslip angles are made to be zero. After the 4WIS-AGV arrives at the first sharp edge point, the sideslip angles are adjusted to be $-\pi/4$ rad. Then, when the 4WIS-AGV reaches at the second sharp edge point, the sideslip angles are adjusted to be $-\pi/2$ rad. The wheel steering angle of the 4WIS-AGV, δ_i (for $i = 1, \dots, 4, fr, re$), is shown in Fig. 4.15. As introduced in Chapter 2, the wheel steering angles follow the sideslip angle, β_A , in parallel steering maneuver.

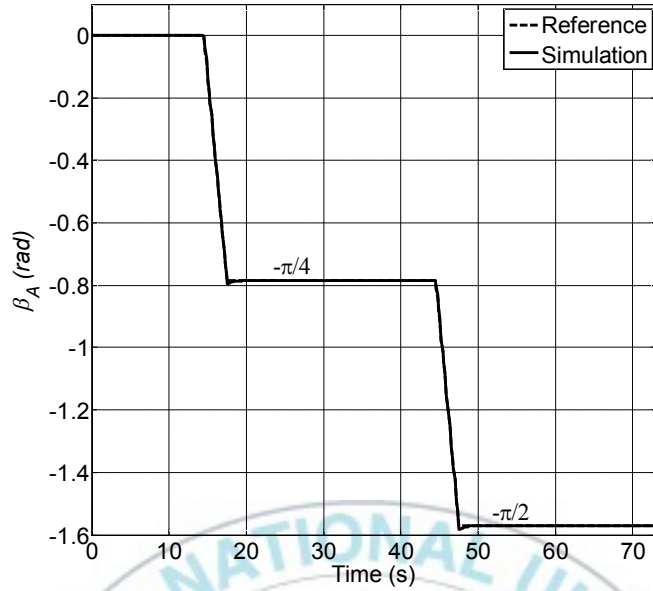


Fig. 4.14 Vehicle sideslip angle reference and simulation

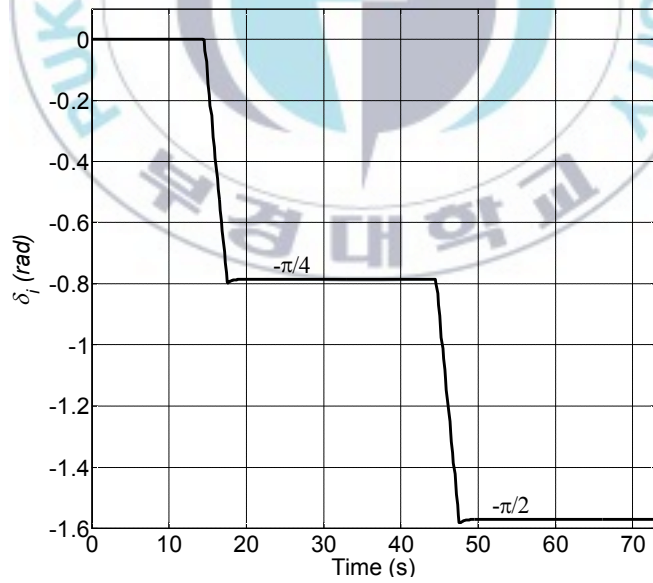


Fig. 4.15 Wheel steering angle δ_i

The linear and angular velocities of each wheel, v_i and ω_i (for $i = 1, \dots, 4, fr, re$), are shown in Figs. 4.16 and 4.17, respectively. As mentioned in Chapter 2, the linear velocity of each wheel, v_i , follows the vehicle linear velocity, v_A . Therefore, the linear velocity of each wheel as shown in Fig. 4.16 is same to v_A in Fig. 4.9. Fig. 4.17 shows that the angular velocity of each wheel is proportional to the vehicle linear velocity.

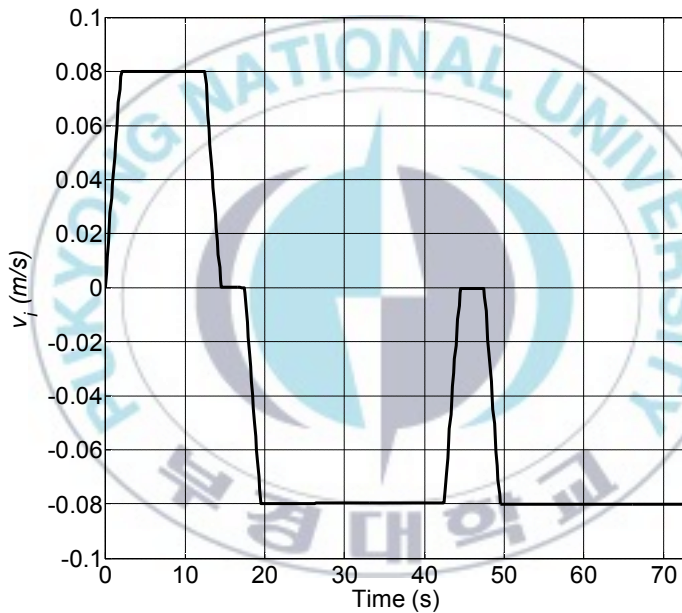


Fig. 4.16 Linear velocity of each wheel v_i

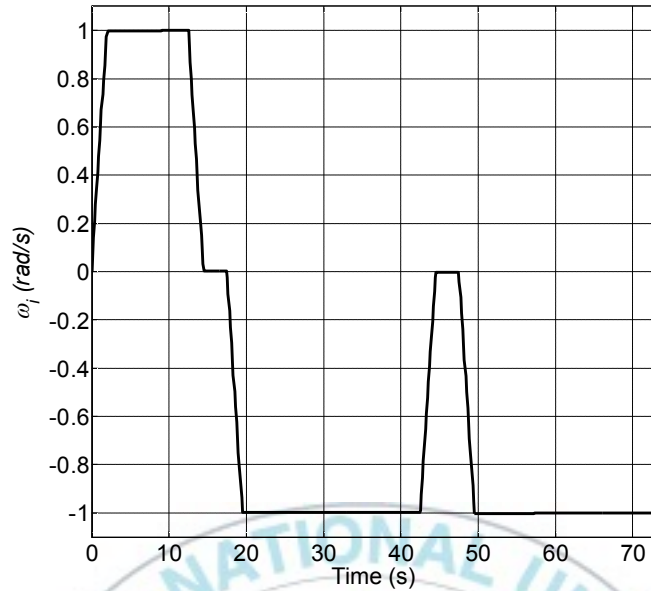


Fig. 4.17 Angular velocity of each wheel ω_i

4.1.2 Circular reference trajectory

In this section, the 4WIS-AGV is controlled to track a circular reference trajectory with the radius of 1 m. This case is taken to show the experimental 4WIS-AGV's ability to move with zero-sideslip maneuver. The circular reference trajectory is shown in Fig. 4.18. The simulation was conducted within 78.5 s.

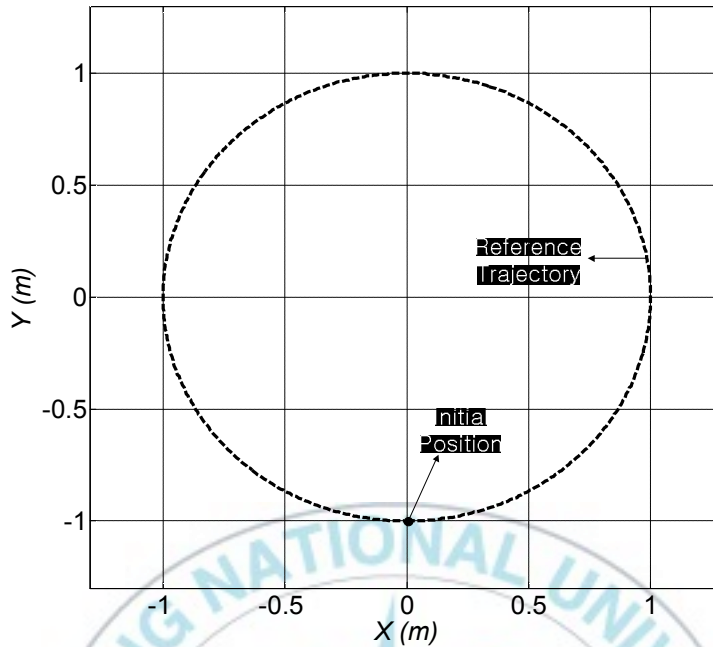


Fig. 4.18 Initial position and circular reference trajectory

In this simulation, the vehicle tracks the circular trajectory with the radius of 1 m. An illustration on how the vehicle is expected to move is shown in Fig. 4.19. In this instance, the vehicle sideslip angle, β_A , is kept zero. Parameters and initial values of the simulation are listed in Table 4.2.

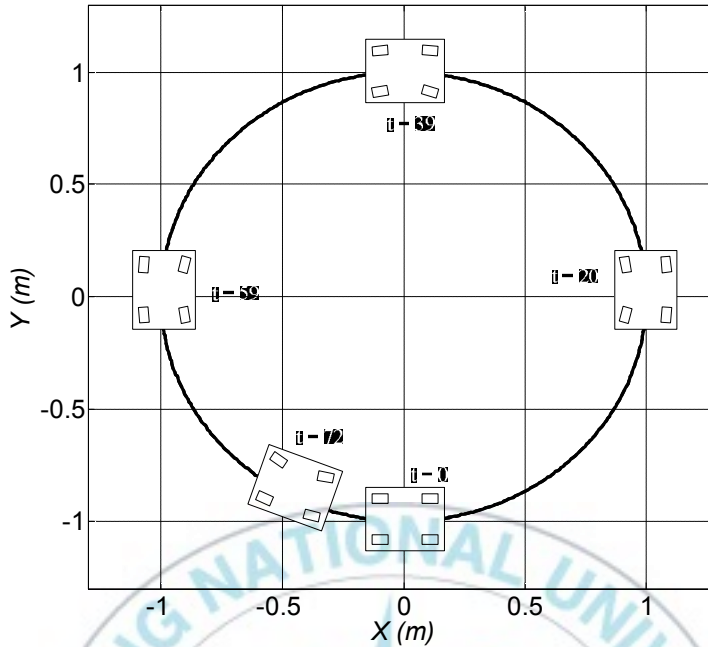


Fig. 4.19 Illustration of the expected motion

Table 4.2 Parameter and initial values of the simulation

Descriptions	Symbols	Values
Initial position of the vehicle	(X_0, Y_0)	(0, -1) m
Initial position of reference	(X_R, Y_R)	(0, -1) m
Initial value of vehicle orientation	$\psi_A(0)$	0
Initial value of sideslip angle	$\beta_A(0)$	0
Initial value of wheel steering angles	$\delta_i(0)$	0
Reference vehicle linear velocity	v_R	0.08 m/s
Reference vehicle orientation	ψ_R	$0.08t$ rad
Reference vehicle angular velocity	$\dot{\psi}_R$	0.08 rad/s
Reference vehicle sideslip angle	β_R	0
Reference vehicle sideslip angular velocity	$\dot{\beta}_R$	0
Limit value of vehicle linear velocity	v_A	± 0.2 m/s
Limit value of vehicle angular velocity	$\dot{\psi}_A$	± 0.15 rad/s

Limit value for vehicle sideslip angular velocity	$\dot{\beta}_A$	± 0.28 rad/s
Controller gain 1	k_1	4 s ⁻¹
Controller gain 2	k_2	20 rad/m ²
Controller gain 3	k_3	0.5 rad/s
Controller gain 4	k_4	1 s ⁻¹

Figs. 4.20 and 4.21 demonstrate X -axis and Y -axis reference trajectories for the 4WIS AGV to track the circular reference trajectory, respectively.

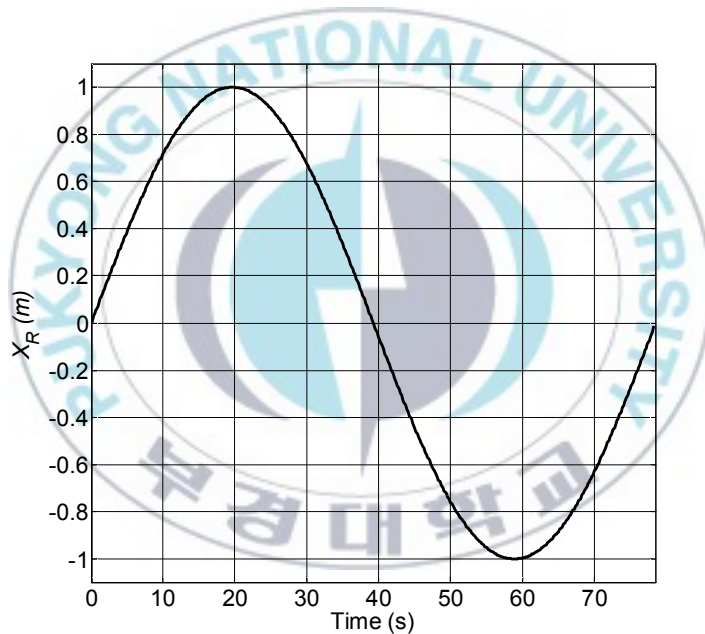


Fig. 4.20 X -axis reference trajectory

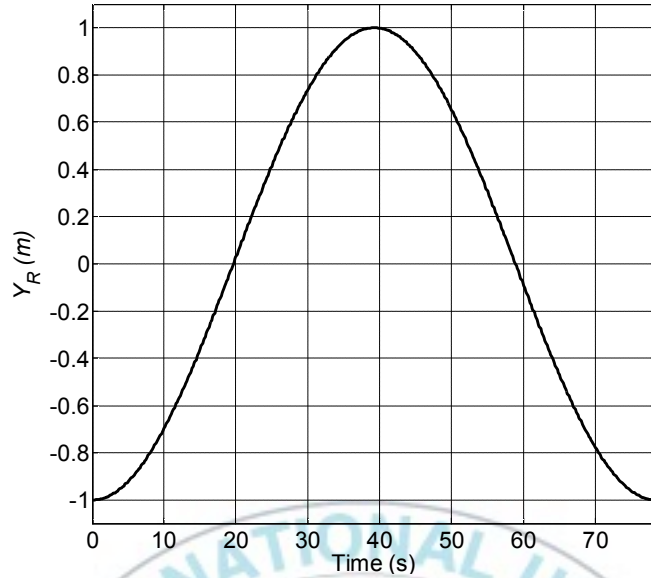


Fig. 4.21 Y-axis reference trajectory

The circular trajectory tracking result is shown in Fig. 4.22. It shows that the 4WIS-AGV can track the circular reference trajectory very well. The circular trajectory tracking errors are shown in Fig. 4.23. It shows that the errors go to zero at 25 s.

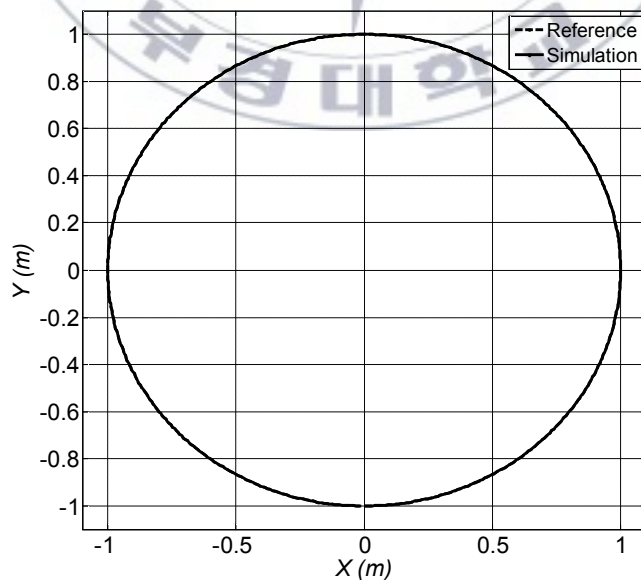


Fig. 4.22 Trajectory tracking result

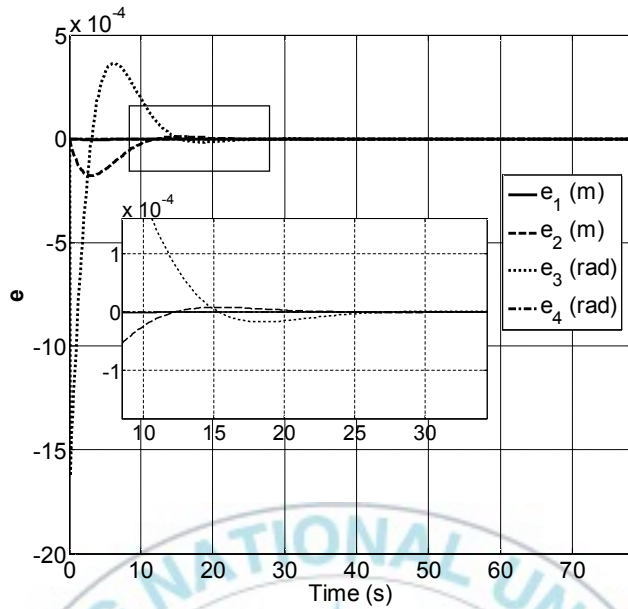


Fig. 4.23 Trajectory tracking errors

The control law for this circular trajectory tracking is shown in Fig. 4.24. This figure shows that the vehicle linear and angular velocities quickly goes to their reference values, 0.08 m/s and 0.08 rad/s, respectively. Vehicle sideslip angular velocity is kept constant at 0 rad/s.

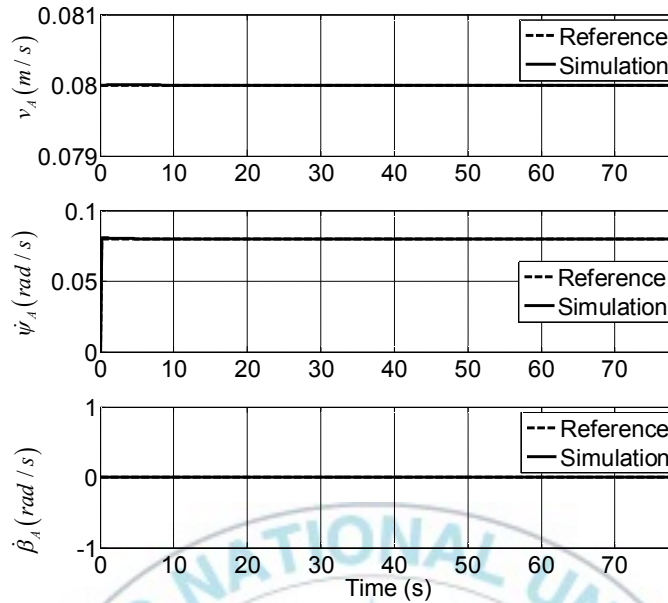


Fig. 4.24 Control law U

Figs. 4.25 and 4.26 show comparison of simulation results and references of X -axis and Y -axis trajectory tracking. It can be seen that the vehicle tracks the reference trajectories very well. The tracking errors in the X and Y directions, e_x and e_y , are shown in Fig. 4.27. At the initial time, the vehicle has small errors which go to zero at 25 s.

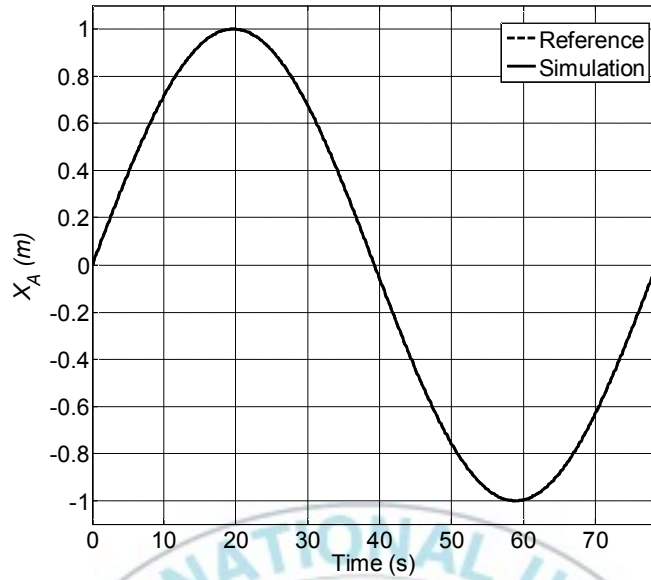


Fig. 4.25 X-axis reference and simulation

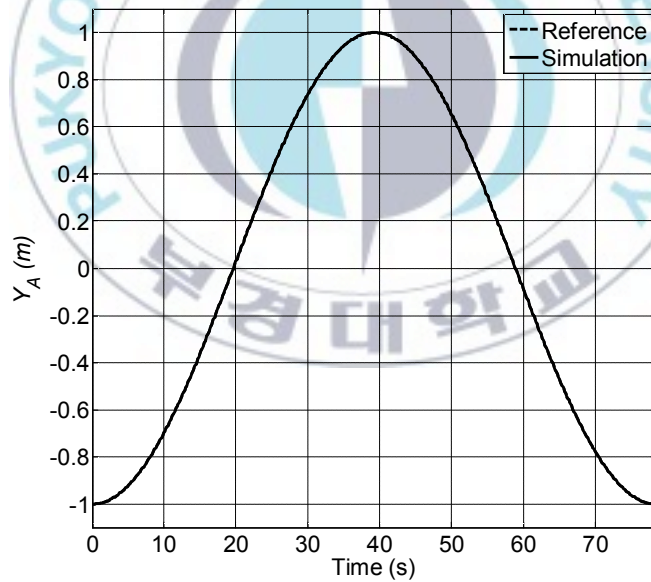


Fig. 4.26 Y-axis reference and simulation

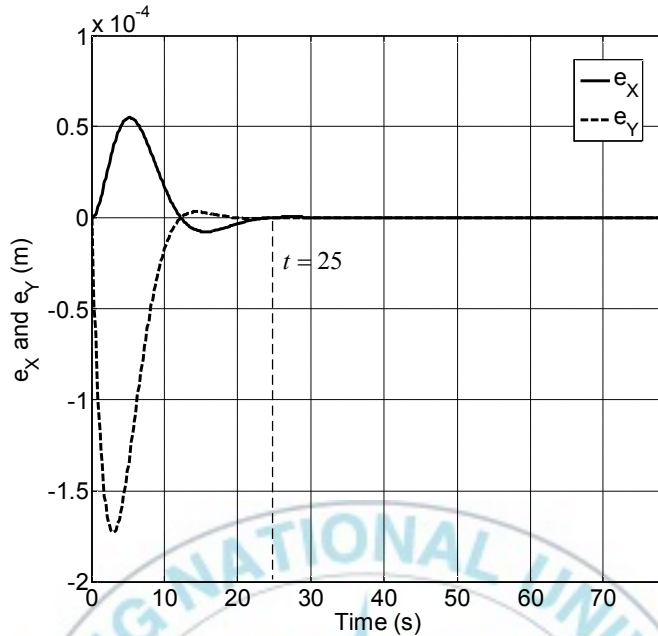


Fig. 4.27 Errors e_x and e_y

Fig. 4.28 shows comparison of simulation result and reference of the vehicle orientation. This figure shows that the simulation result is very close with the reference. The sideslip angle of the 4WIS-AGV is shown in Fig. 4.29. This figure shows that the vehicle sideslip angle is kept zero during the simulation and the vehicle has zero-sideslip maneuver. Figs. 4.30 - 4.31 show the steering angles of front and rear wheels which quickly go to 0.3277 rad and -0.3277 rad, respectively. Figs. 4.32 - 4.35 show the steering angles of front outer wheel, front inner wheel, rear inner wheel and rear outer wheel, which after 20 s, go to 0.2535 rad, 0.4592 rad, -0.4592 rad and -0.2535 rad, respectively. The steering angles of the front wheels are opposite to steering angles of the rear wheels. In addition, these figures show that the inner wheels have bigger steering angles than the outer wheels.

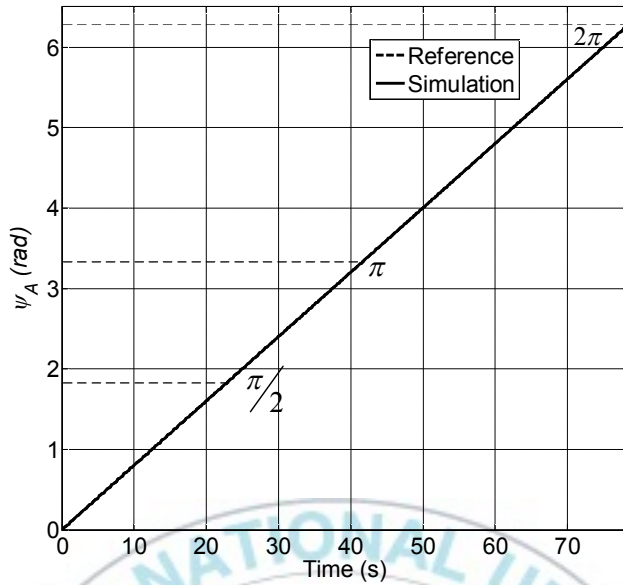


Fig. 4.28 Vehicle orientation reference and simulation

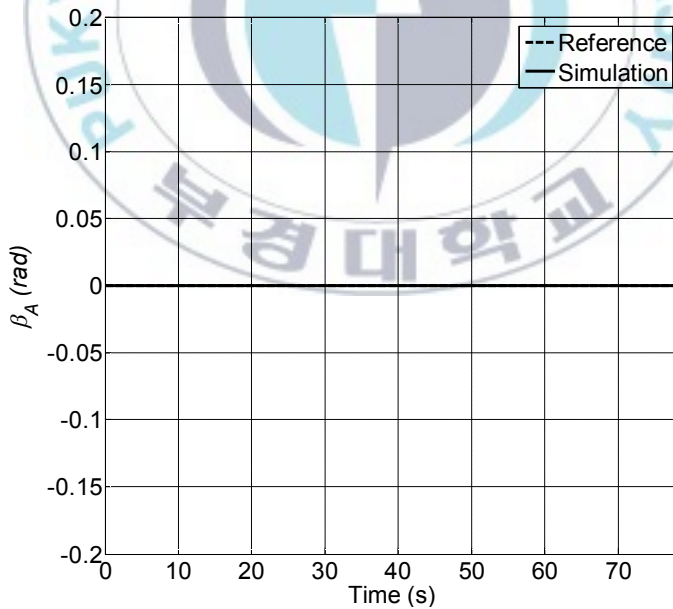


Fig. 4.29 Vehicle sideslip angle reference and simulation

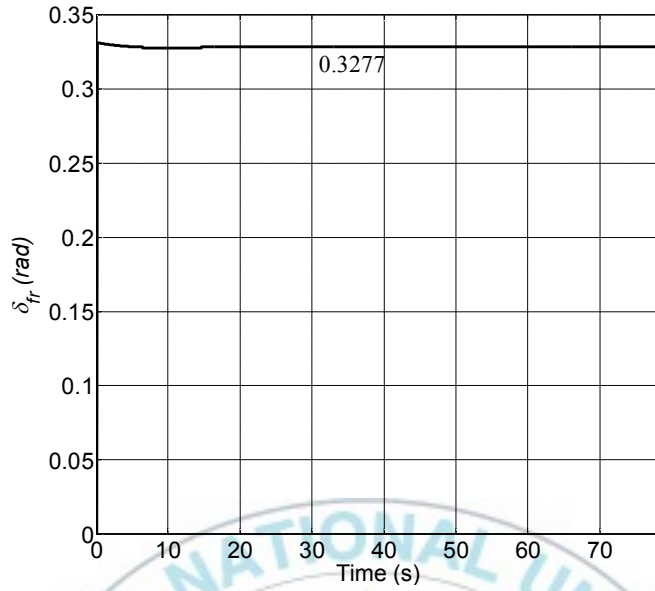


Fig. 4.30 Steering angle of the front wheel

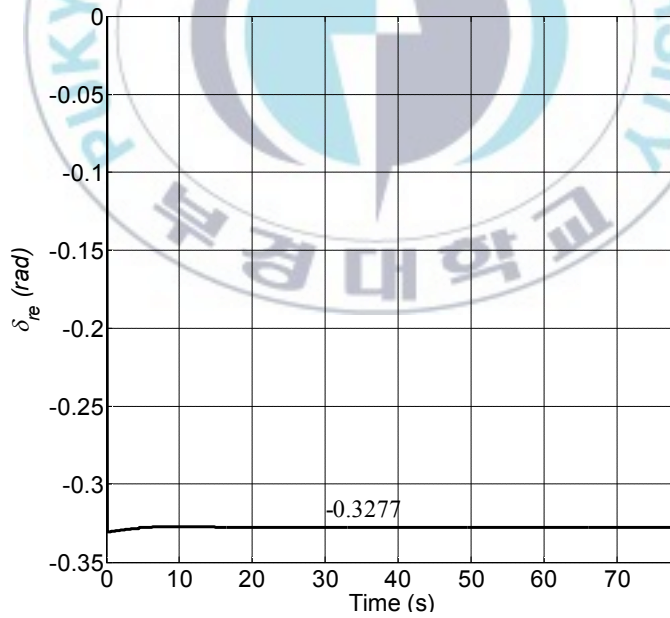


Fig. 4.31 Steering angle of the rear wheel



Fig. 4.32 Steering angle of the front outer wheel

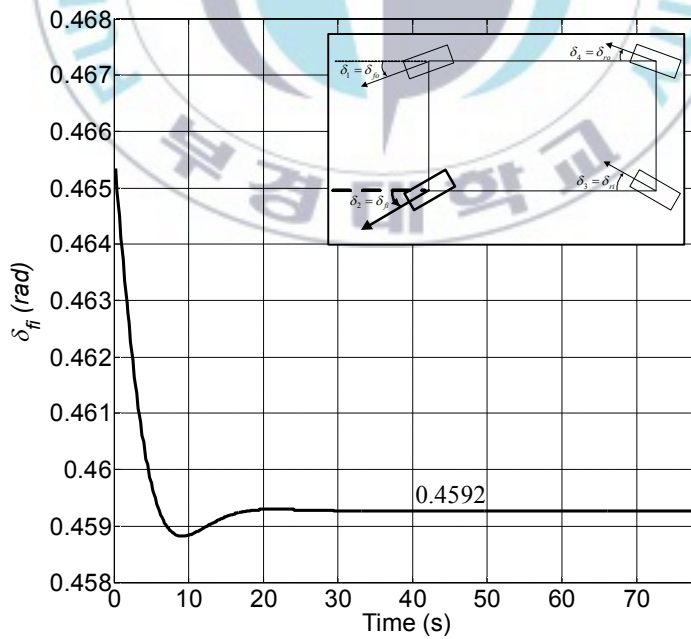


Fig. 4.33 Steering angle of the front inner wheel

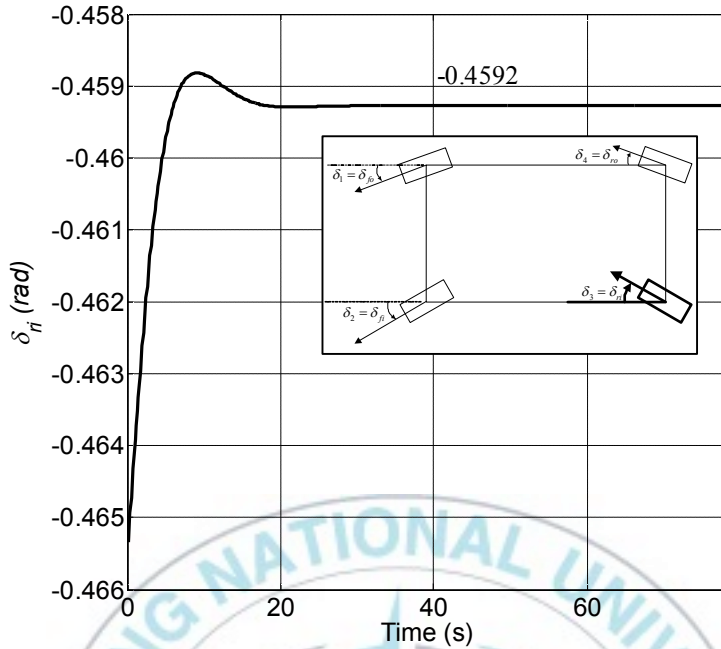


Fig. 4.34 Steering angle of the rear inner wheel



Fig. 4.35 Steering angle of the rear outer wheel

The linear velocities of the front outer wheel, the front inner wheel, the rear inner wheel and the rear outer wheel are shown in Figs. 4.36 - 4.39, respectively. The outer wheels have the same velocity of 0.10843 m/s after 20 s. Likewise the inner wheels have the same velocity, which is 0.06139 m/s after 20 s

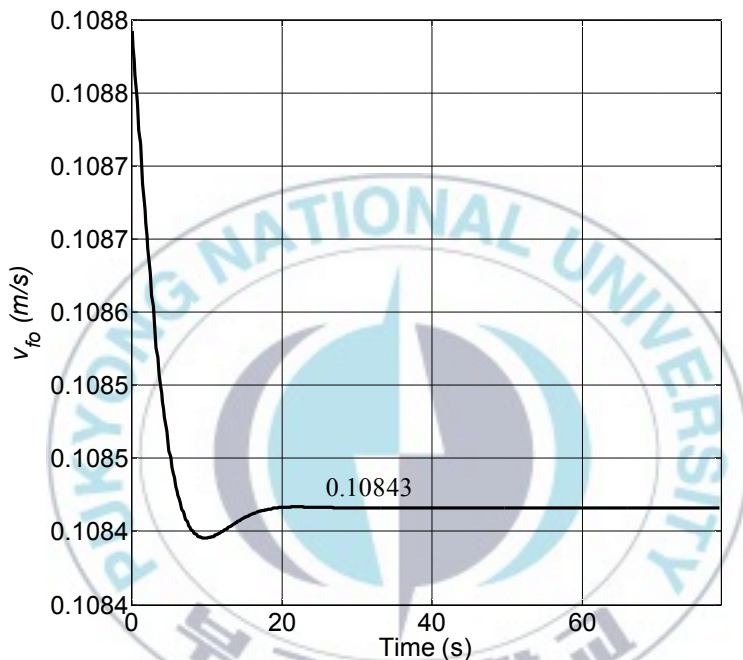


Fig. 4.36 Linear velocity of the front outer wheel

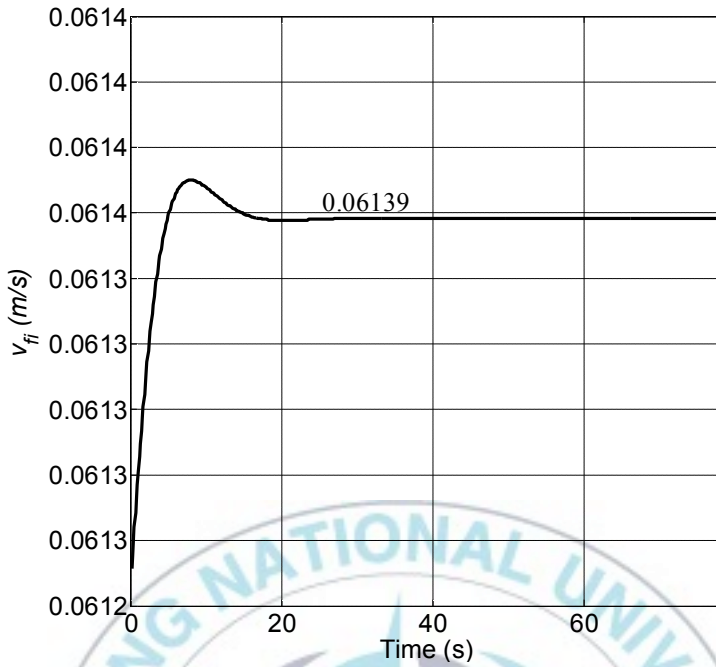


Fig. 4.37 Linear velocity of the front inner wheel

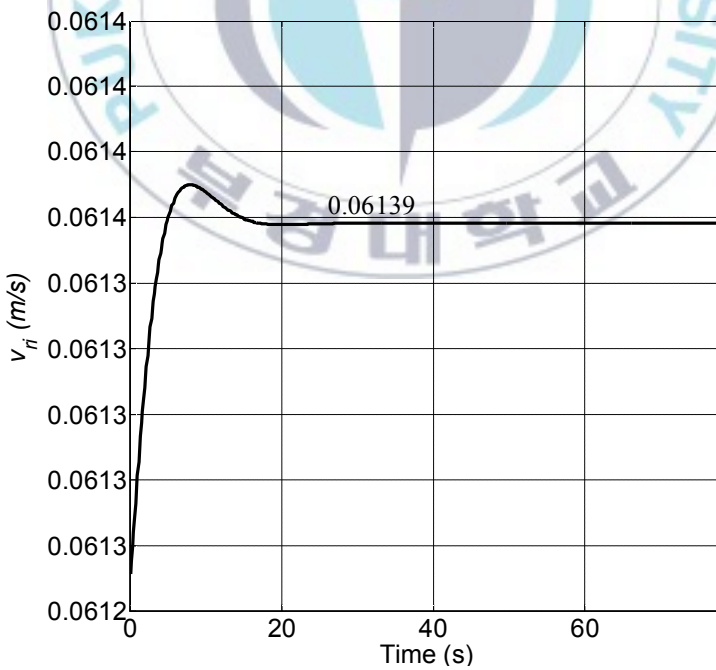


Fig. 4.38 Linear velocity of the rear inner wheel

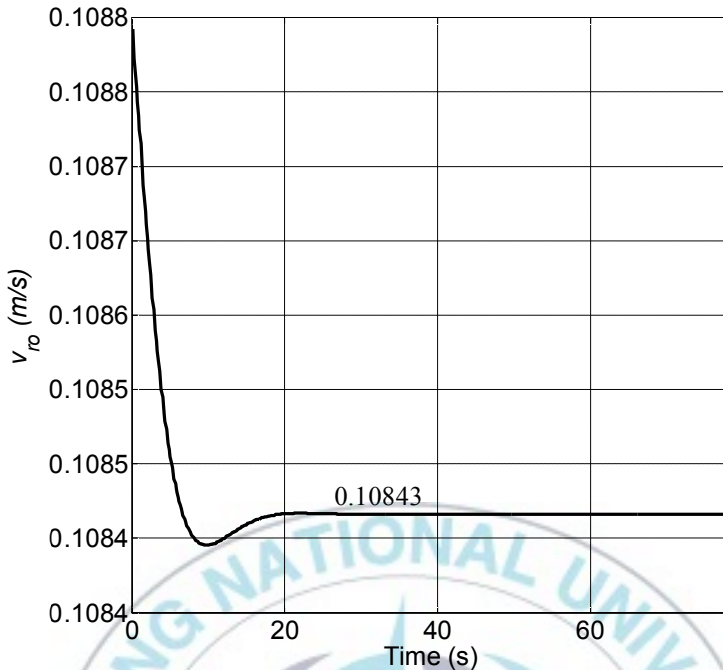


Fig. 4.39 Linear velocity of the rear outer wheel

The angular velocities of the front outer wheel, the front inner wheel, the rear inner wheel and the rear outer wheel are shown in Figs. 4.40 - 4.43, respectively. The inner wheels have the same angular velocity, which is 0.7669 rad/s after 20 s. Likewise the outer wheels have the same angular velocity of 1.3558 rad/s after 20 s. These figures show that the outer wheels have higher wheel angular velocities than the inner wheels.

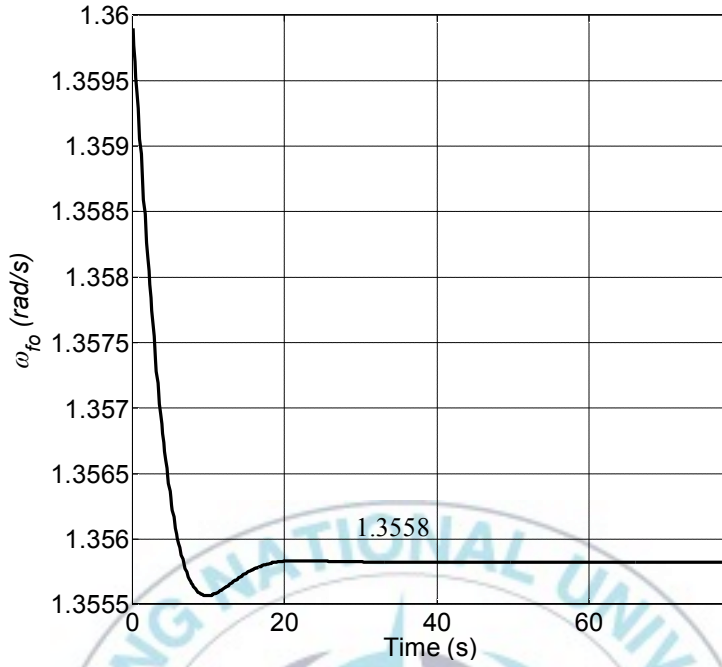


Fig. 4.40 Angular velocity of the front outer wheel

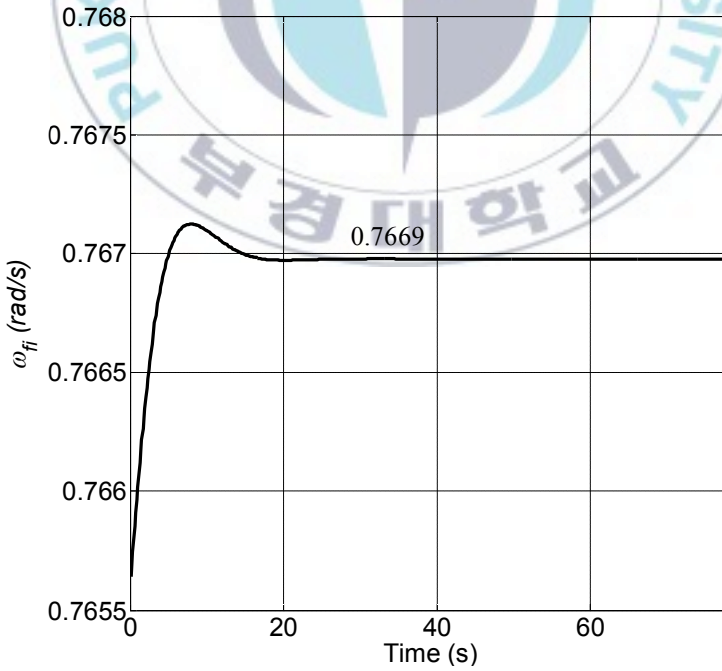


Fig. 4.41 Angular velocity of the front inner wheel

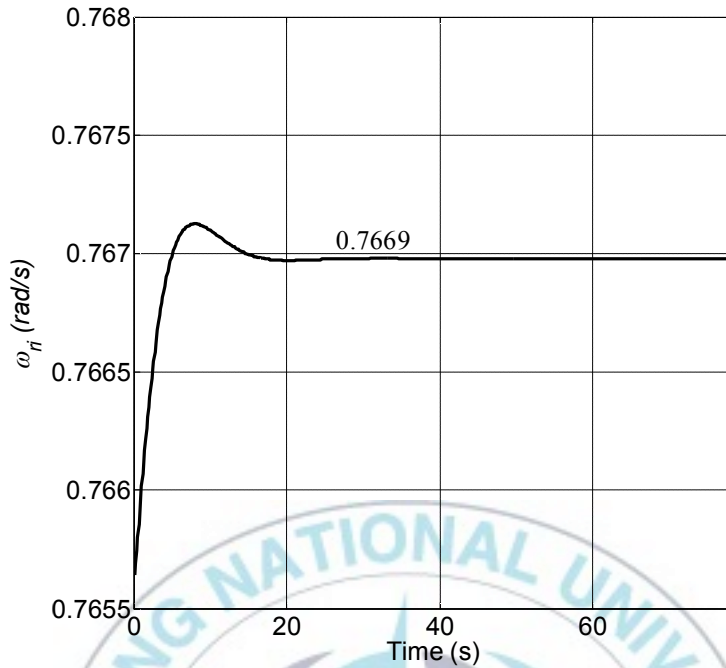


Fig. 4.42 Angular velocity of the rear inner wheel

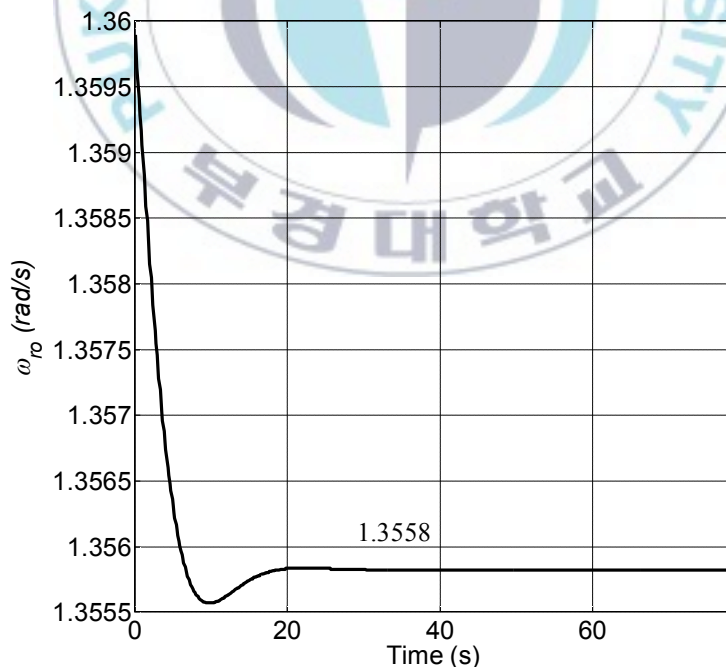


Fig. 4.43 Angular velocity of the rear outer wheel

4.2 Experimental results

This section shows the experimental results of the two trajectory tracking that have been simulated. In this section, the experimental results are compared with their simulation results to show the effectiveness of the proposed controller.

4.2.1 Reference trajectory with sharp edges

The experimental trajectory tracking result of the reference with sharp edges is shown in Fig. 4.44. This figure shows that experimental result is very close with the reference and simulation results. Fig. 4.45 shows the trajectory tracking errors. It shows that all trajectory tracking errors are relatively small within the range of $e_1 = \pm 0.02$ m, $e_2 = \pm 0.025$ m, $e_3 = \pm 0.01$ rad and $e_4 = \pm 0.015$ rad. The control law for this trajectory tracking is shown in Fig. 4.46. It can be seen that the experimental results of the control law are quite close with its simulation results and references. The experimental vehicle angular velocity is within ± 0.005 m along the simulation vehicle angular velocity.

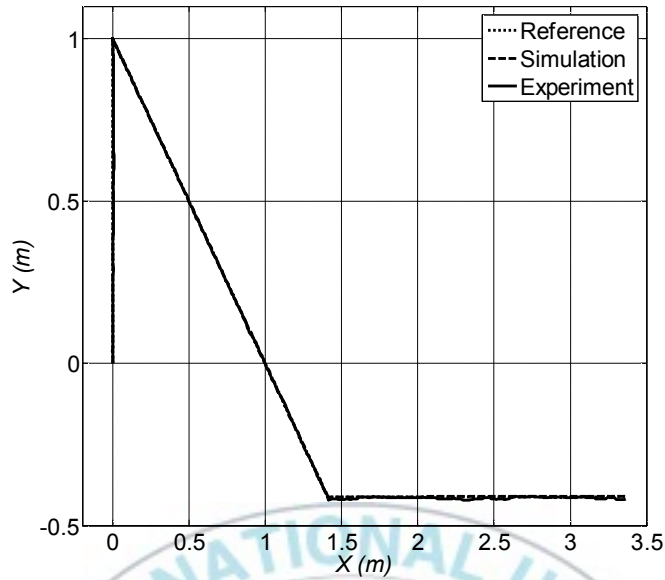


Fig. 4.44 Simulation and experimental trajectory tracking results

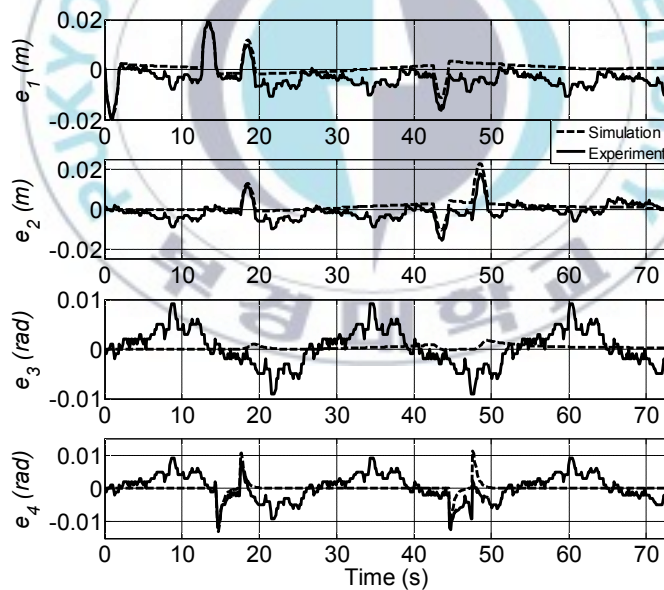


Fig. 4.45 Simulation and experimental trajectory tracking errors

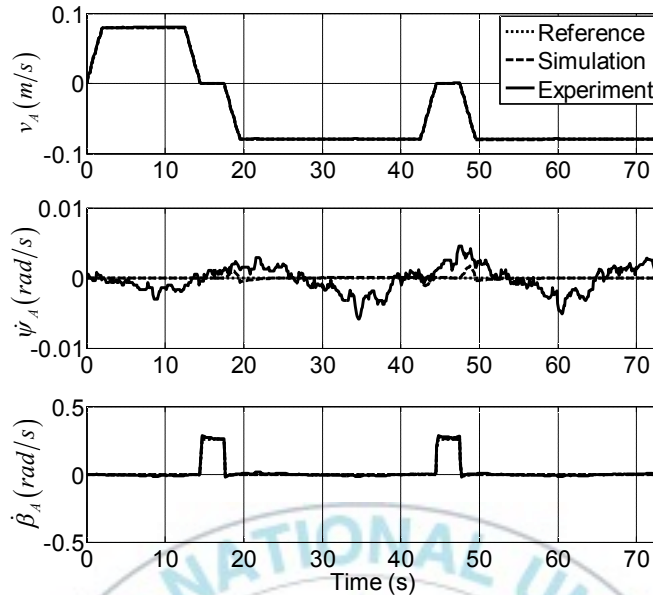


Fig. 4.46 Simulation and experimental control laws

Figs. 4.47 and 4.48 show comparison of the experimental and simulation results of the X -axis and Y -axis trajectory tracking, respectively. The experimental results show that the vehicle tracks the reference trajectories very well. The trajectory tracking errors is shown in Fig. 4.49 and it can be seen that the result is quite close with the simulation result. Fig. 4.50 shows the experimental results of the vehicle orientation during the trajectory tracking and it shows that the orientation, ψ_A , is kept $\pi/2$ rad to keep vehicle posture of zero-sideslip maneuver during the motion.

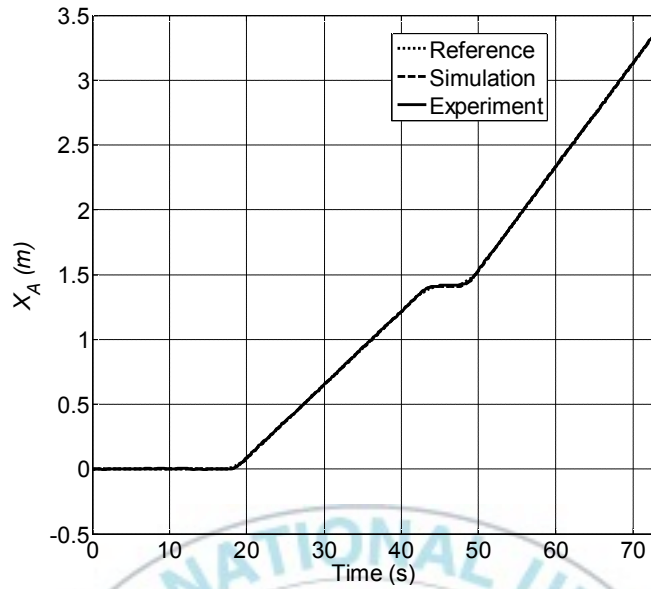


Fig. 4.47 Simulation and experimental results of X-axis trajectory tracking

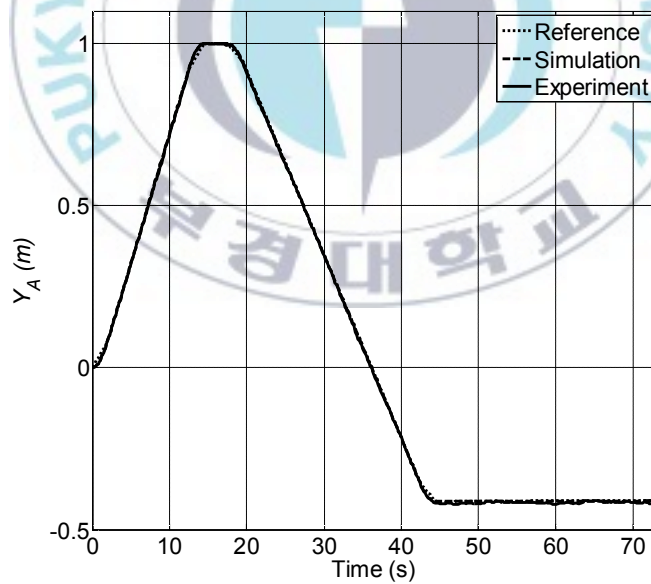


Fig. 4.48 Simulation and experimental results of Y-axis trajectory tracking

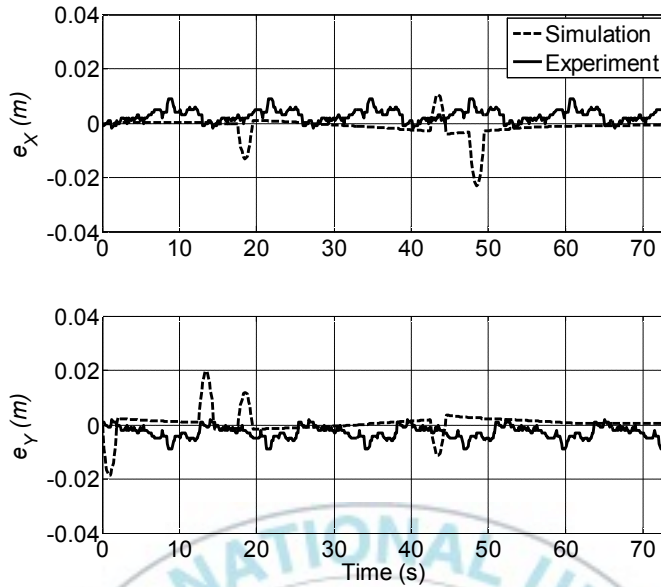


Fig. 4.49 Simulation and experimental errors e_x and e_y

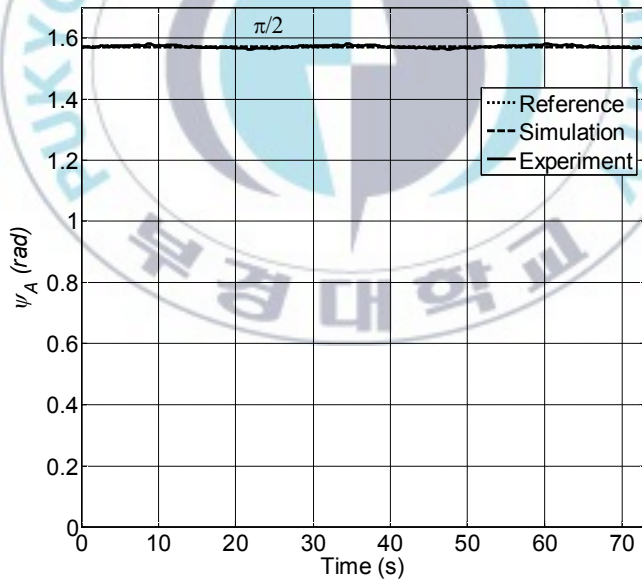


Fig. 4.50 Simulation and experimental vehicle orientation

Fig. 4.51 shows the experimental vehicle sideslip angle is close with its reference and simulation result due to parallel steering maneuver. Fig. 4.52 shows the wheel steering angles of the 4WIS-AGV in experiment and simulation during tracking the trajectory, δ_i for $i = 1, \dots, 4, fr, re$. Both figures show that the wheel steering angles of the 4WIS-AGV follows vehicle sideslip angle due to parallel steering maneuver. Figs. 4.53 and 4.54 demonstrate the experimental results of linear velocity and angular velocity of each wheel compared with its simulation result, respectively. It can be seen that the experimental and simulation results are very close.

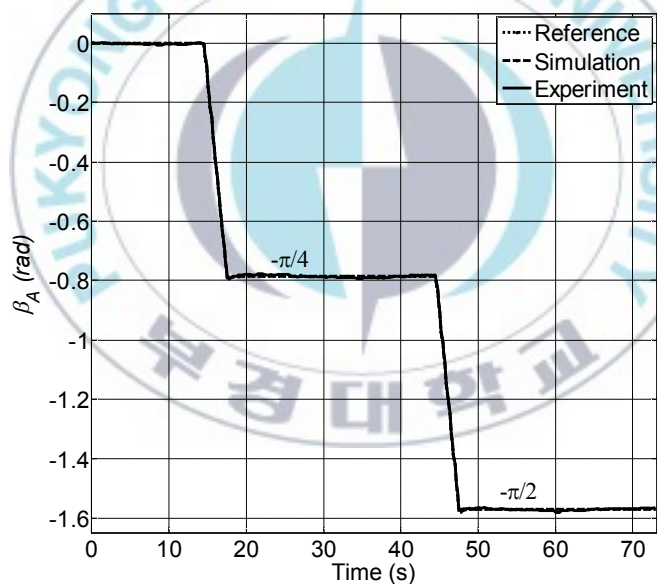


Fig. 4.51 Simulation and experimental vehicle sideslip angles

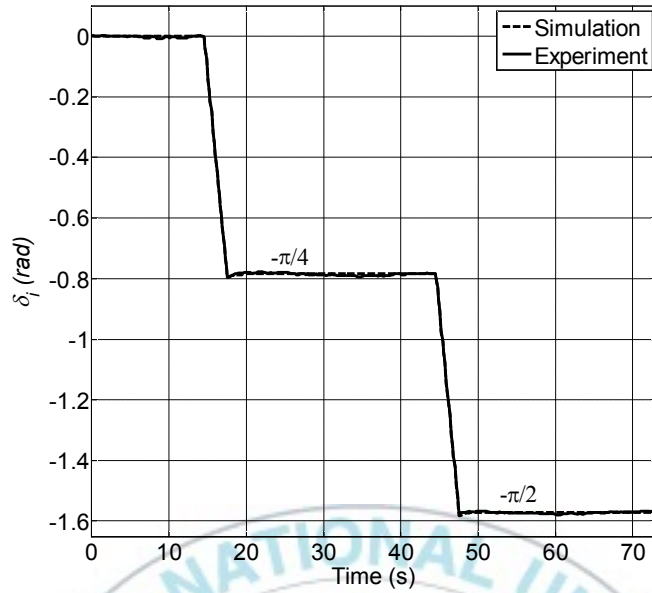


Fig. 4.52 Simulation and experimental wheel steering angles

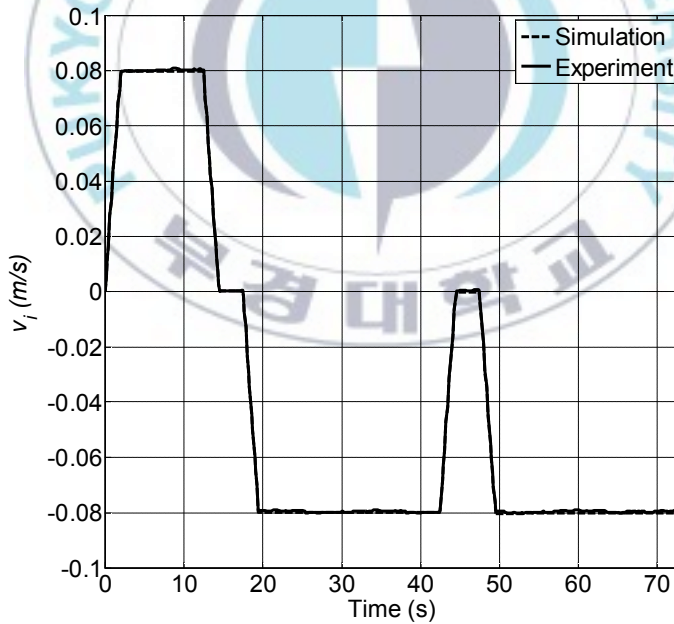


Fig. 4.53 Simulation and experimental linear velocities of each wheel

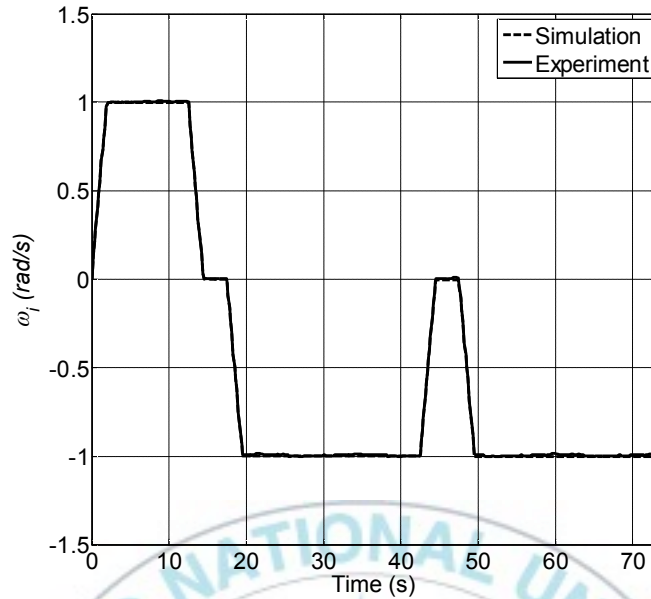


Fig. 4.54 Simulation and experimental angular velocities of each wheel

4.2.2 Circular reference trajectory

Fig. 4.55 shows the experimental result of the trajectory tracking of circular reference trajectory with the radius of 1 m for zero-sideslip maneuver. Fig. 4.56 shows the trajectory tracking errors within the range of $e_1 = \pm 0.02$ m, $e_2 = \pm 0.01$ m, $e_3 = \pm 0.015$ rad and $e_4 = \pm 0.005$ rad. It can be seen that the 4WIS-AGV tracks the trajectory very well. The control law of the trajectory tracking is shown in Fig. 4.57. The experimental vehicle linear velocity, vehicle angular velocity and sideslip angular velocity are $v_A = 0.08 \pm 0.06$ m/s, $\dot{\psi}_A = 0.08 \pm 0.02$ rad/s and $\dot{\beta}_A = 0 \pm 1 \times 10^{-4}$ rad/s, respectively. The experimental results are very close to simulation results.

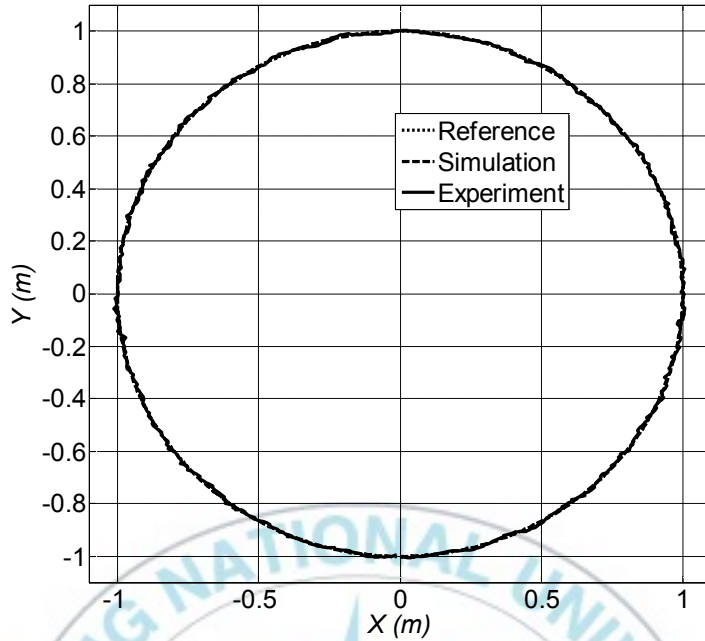


Fig. 4.55 Simulation and experimental results of circular reference trajectory tracking

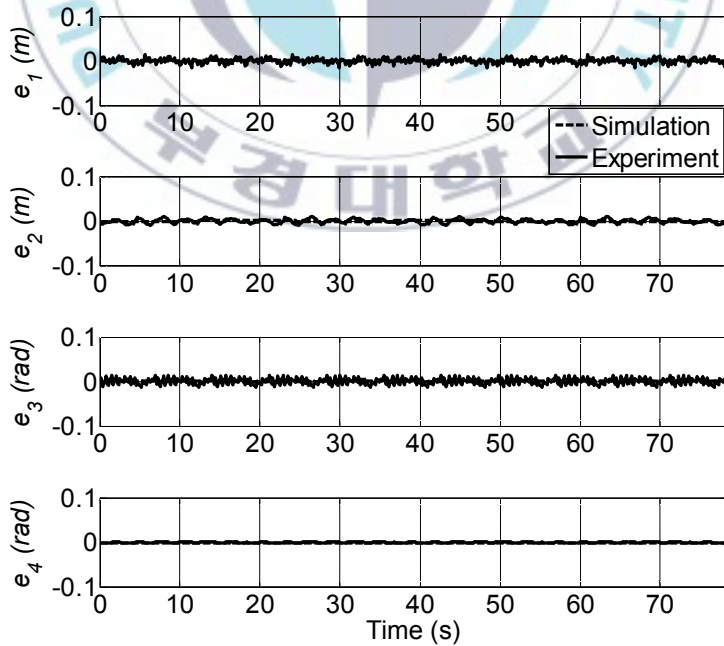


Fig. 4.56 Simulation and experimental trajectory tracking errors

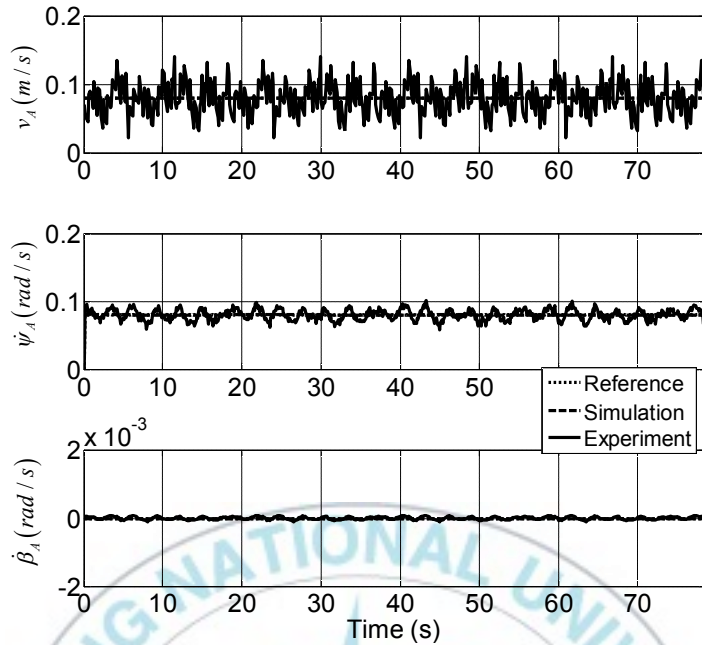


Fig. 4.57 Simulation and experimental control laws U

Figs. 4.58 and 4.59 present comparison of experimental and simulation results of the X -axis and Y -axis trajectory tracking, respectively. The experimental results show that the vehicle can track the reference trajectory in both X -axis and Y -axis very well. The trajectory tracking errors in X -axis and Y -axis is given in Fig. 4.60. It shows that the errors in experiment are bounded within ± 0.015 m along simulation result for e_x and ± 0.01 m along simulation result for e_y . Fig. 4.61 shows the experimental result of the vehicle orientation. The experimental result tracks the simulation result very well.

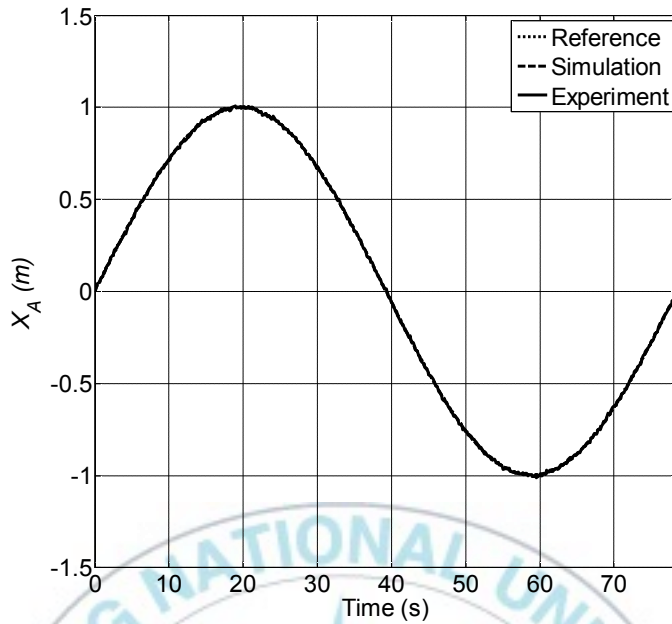


Fig. 4.58 Simulation and experimental results of X-axis trajectory tracking

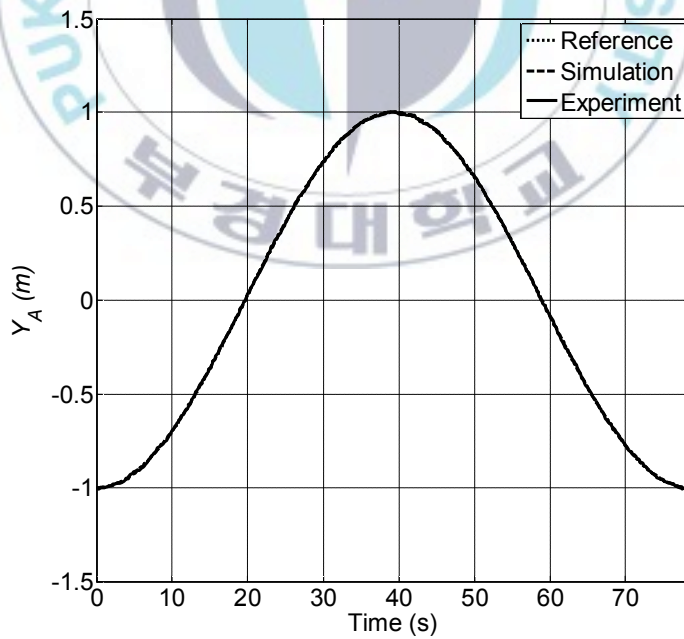


Fig. 4.59 Simulation and experimental results of Y-axis trajectory tracking

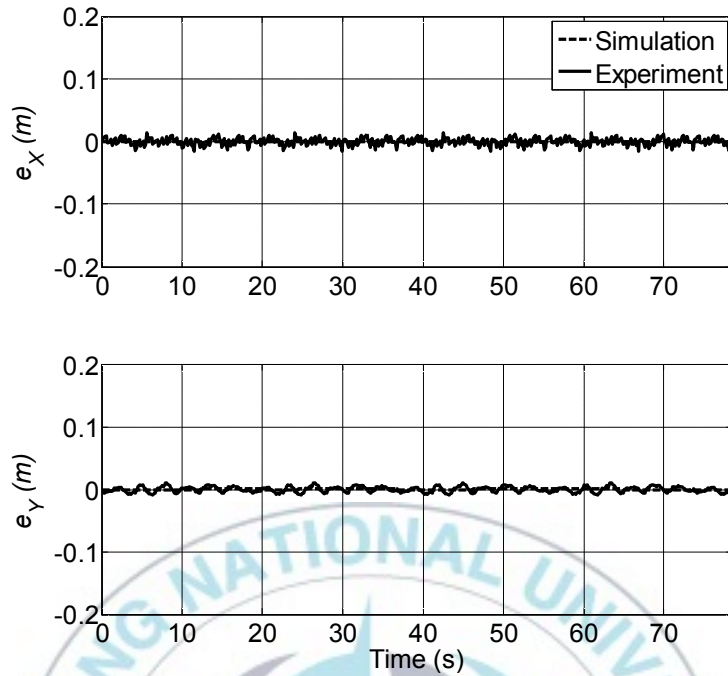


Fig. 4.60 Simulation and experimental errors e_x and e_y

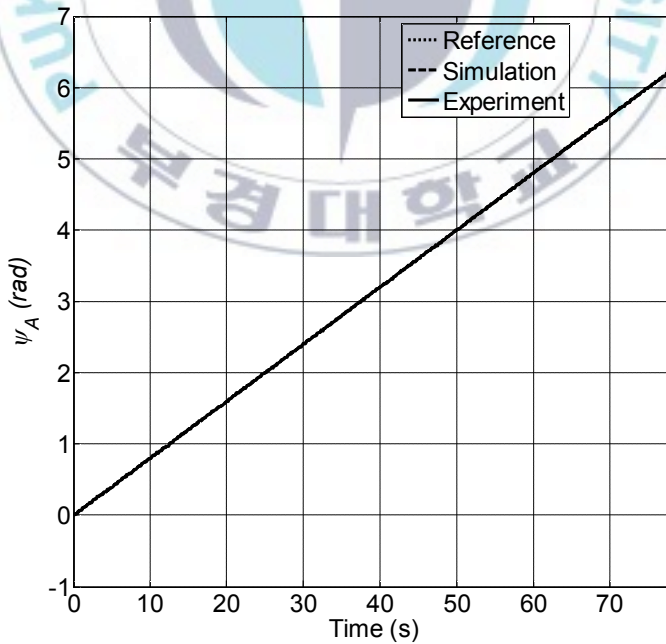


Fig. 4.61 Simulation and experimental vehicle orientation

The experimental result of the vehicle sideslip angle is shown in Fig. 4.62 and it can be seen that the experimental value is bounded within ± 0.0001 rad along the simulation value. The experimental results of the wheel steering angles are given in Figs. 4.63 - 4.68 which illustrate the steering angles of the front wheel, rear wheel, front outer wheel, front inner wheel, rear inner wheel and rear outer wheel, respectively. They show that the experimental results of the steering angles are very close with the simulation results. The experimental steering angles of the front wheel, rear wheel, front outer wheel, front inner wheel, rear inner wheel and rear outer wheel are 0.3277 ± 0.0127 rad, -0.3277 ± 0.0127 rad, 0.2535 ± 0.0085 rad, 0.4593 ± 0.0257 rad, -0.4593 ± 0.0257 rad and -0.2535 ± 0.0085 rad, respectively.

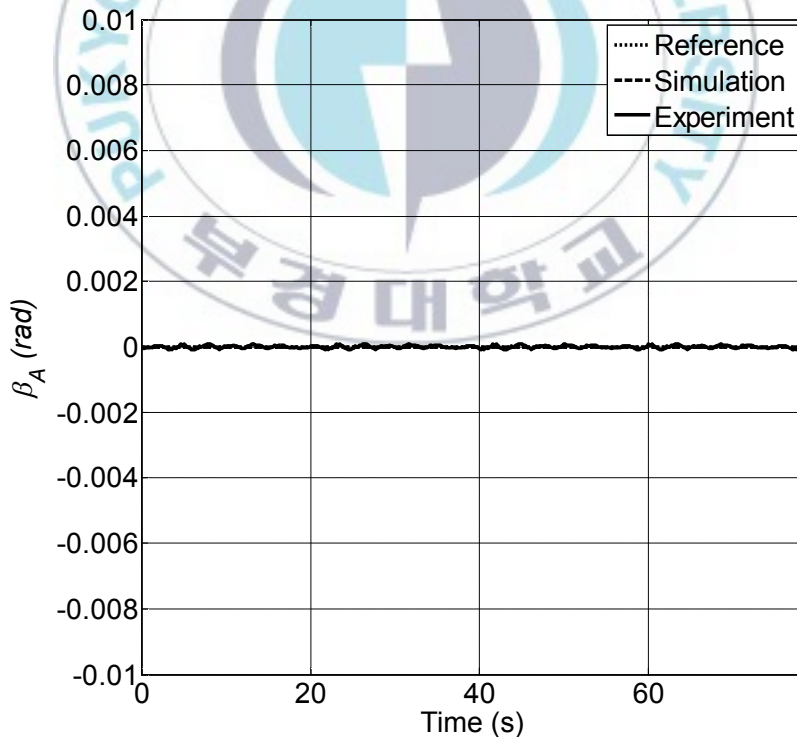


Fig. 4.62 Simulation and experimental vehicle sideslip angles

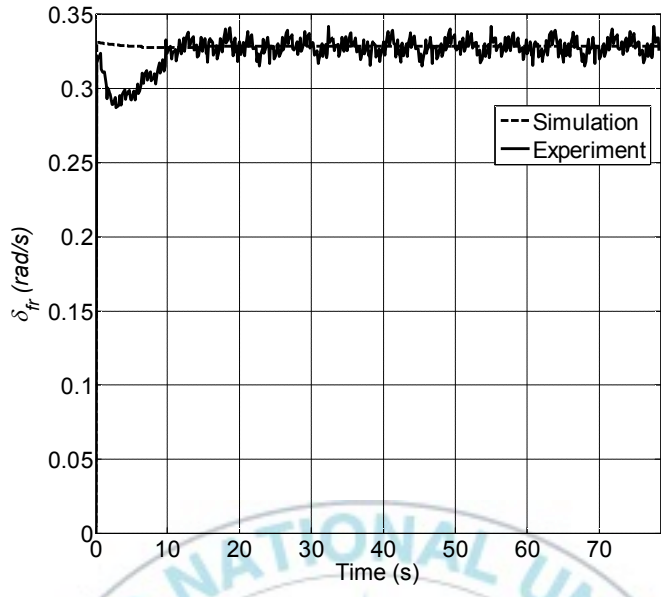


Fig. 4.63 Simulation and experimental front wheel steering angles

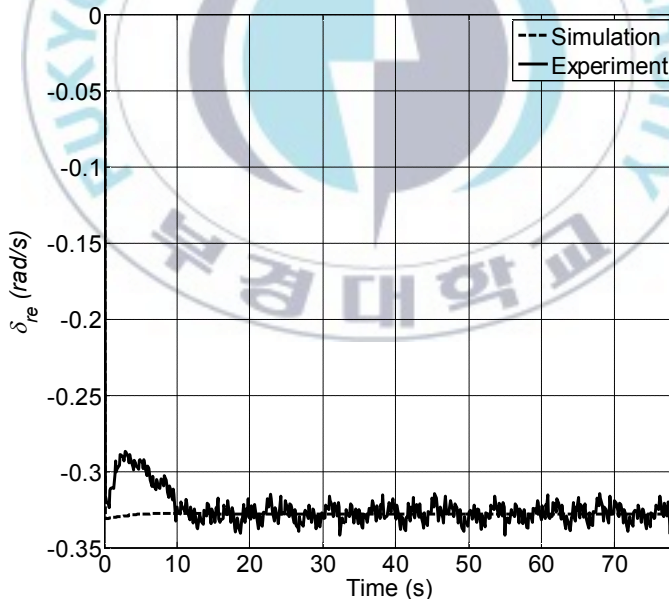


Fig. 4.64 Simulation and experimental rear wheel steering angles

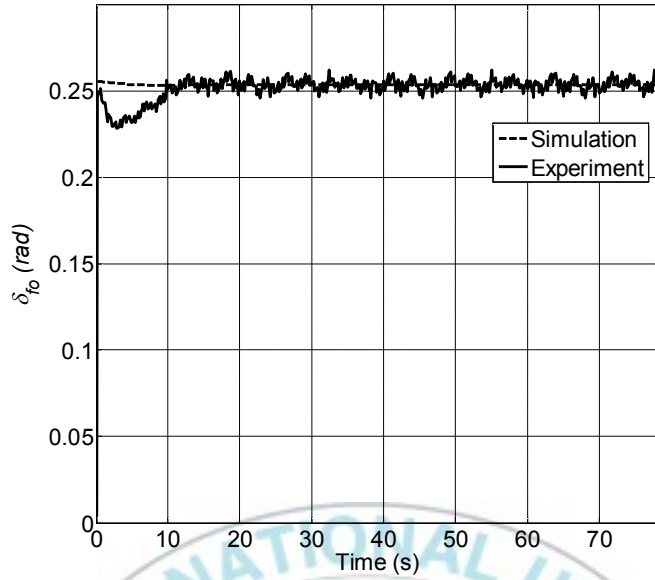


Fig. 4.65 Simulation and experimental steering angles of the front outer wheel

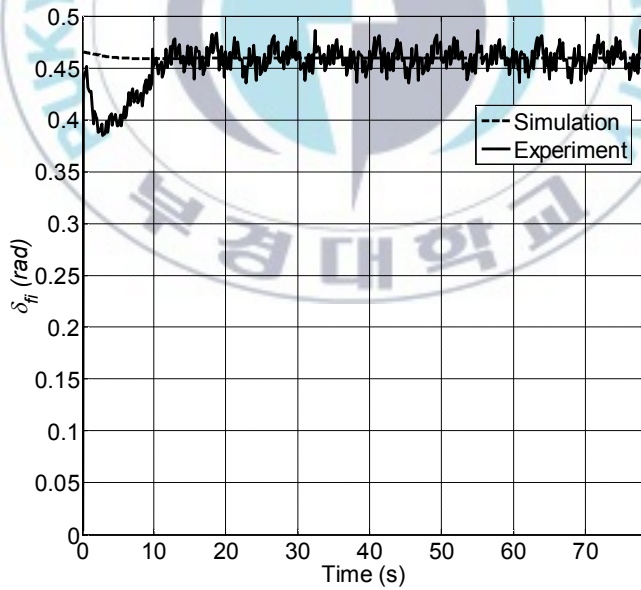


Fig. 4.66 Simulation and experimental steering angles of the front inner wheel

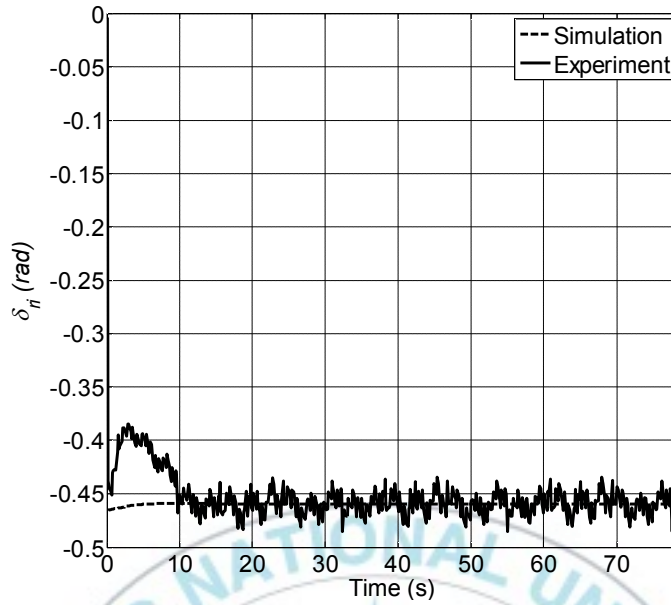


Fig. 4.67 Simulation and experimental steering angles of the rear inner wheel

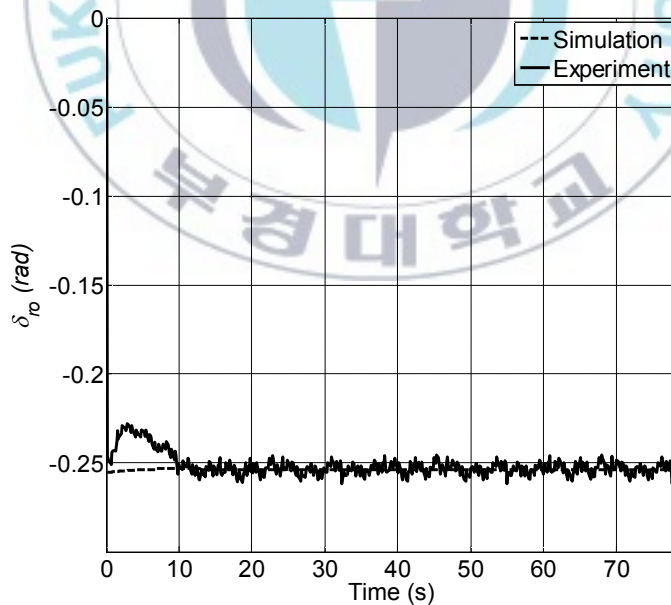


Fig. 4.68 Simulation and experimental steering angles of the rear outer wheel

The experimental results of wheel linear velocities are given in Figs. 4.69 - 4.72 which show the angular velocities of the front outer wheel, the front inner wheel, the rear inner wheel and the rear outer wheel, respectively. The experimental linear velocities of the front outer wheel, front inner wheel, rear inner wheel and rear outer wheel are 0.1085 ± 0.0075 m/s, 0.0613 ± 0.0057 m/s, 0.0613 ± 0.0057 m/s and 0.1085 ± 0.0075 m/s, respectively.

Likewise, Figs. 4.73 - 4.76 show the experimental results of wheel angular velocities of the front outer wheel, the front inner wheel, the rear inner wheel and the rear outer wheel, respectively. They show that the experimental results are very close to their simulation results. The experimental angular velocities of the front outer wheel, front inner wheel, rear inner wheel and rear outer wheel are 1.3558 ± 0.0942 rad/s, 0.7669 ± 0.0731 rad/s, 0.7669 ± 0.0731 rad/s and 1.3558 ± 0.0942 rad/s, respectively.

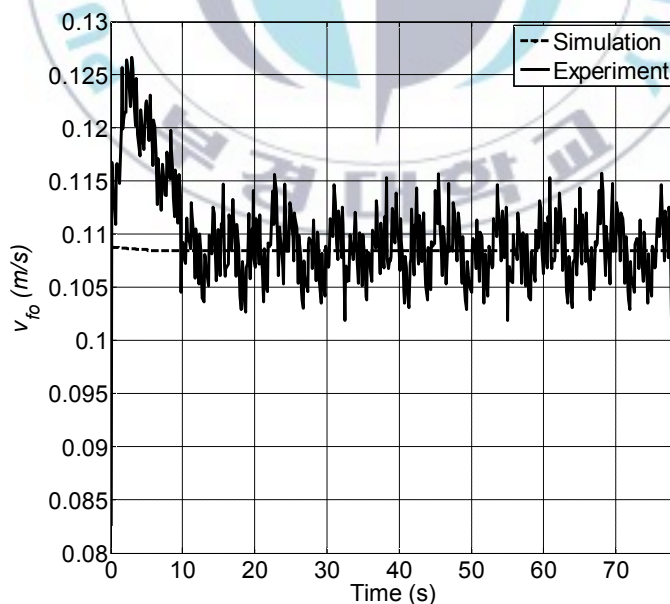


Fig. 4.69 Simulation and experimental linear velocities of the front outer wheel

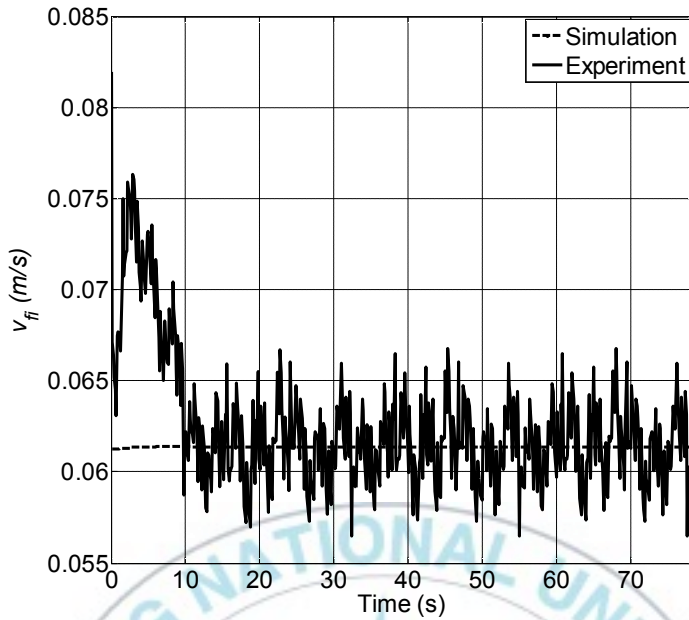


Fig. 4.70 Simulation and experimental linear velocities of the front inner wheel

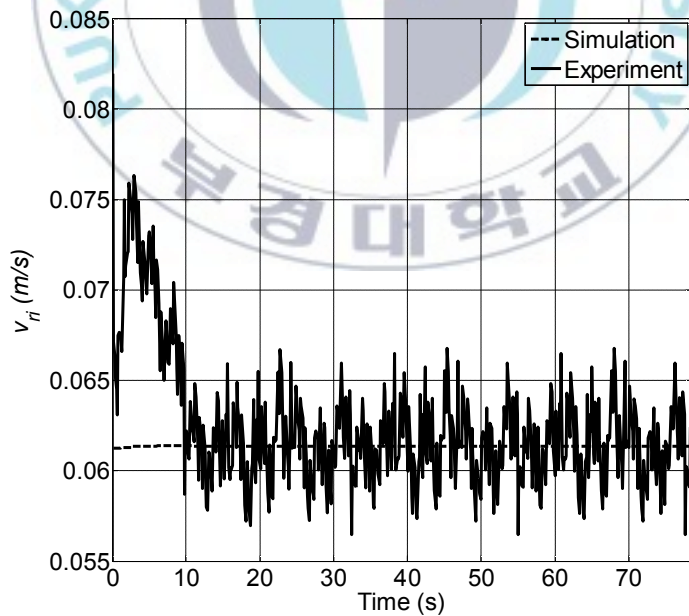


Fig. 4.71 Simulation and experimental linear velocities of the rear inner wheel

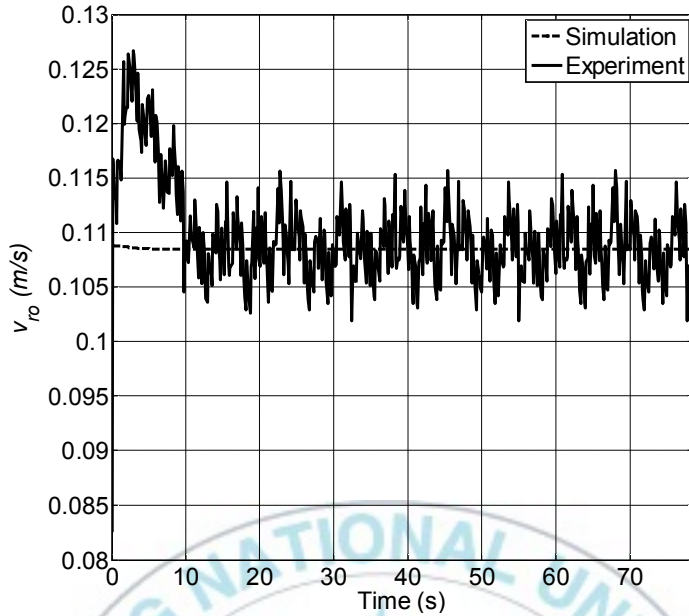


Fig. 4.72 Simulation and experimental linear velocities of the rear outer wheel

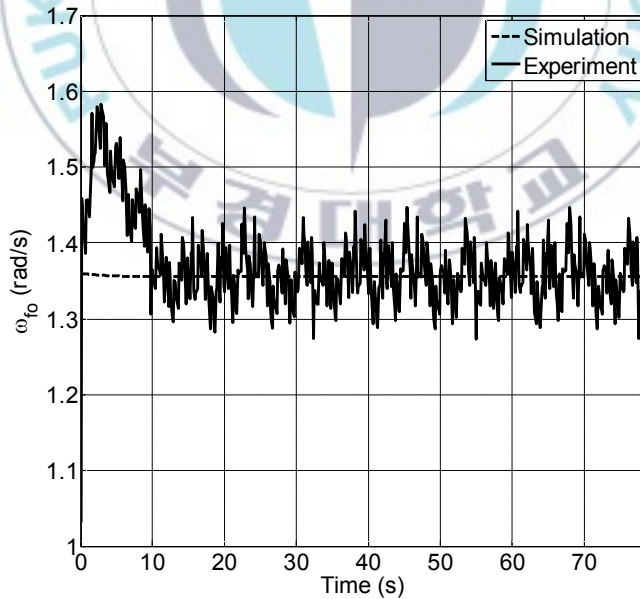


Fig. 4.73 Simulation and experimental angular velocities of the front outer wheel

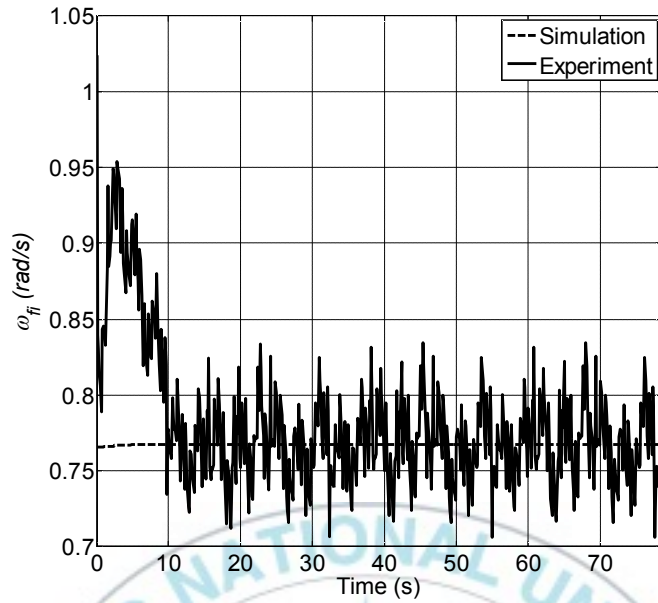


Fig. 4.74 Simulation and experimental angular velocities of the front inner wheel

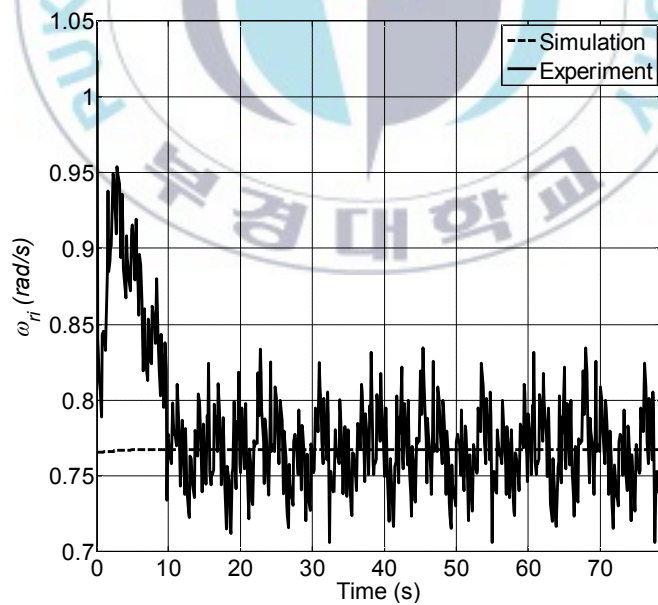


Fig. 4.75 Simulation and experimental angular velocities of the rear inner wheel

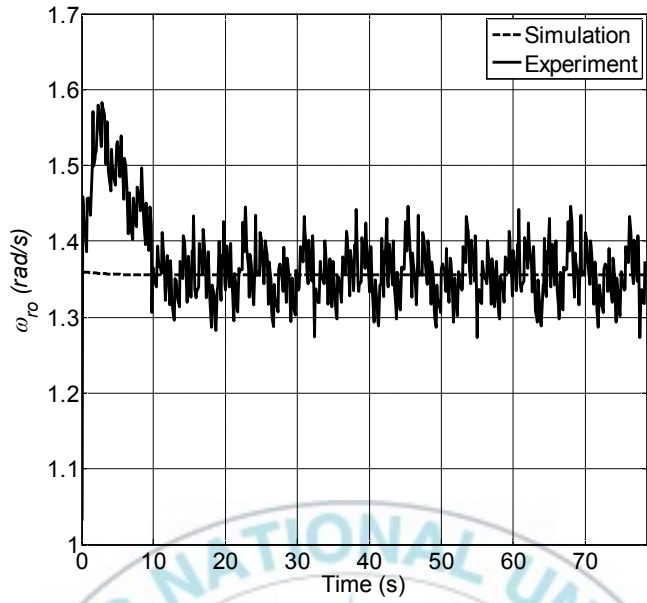
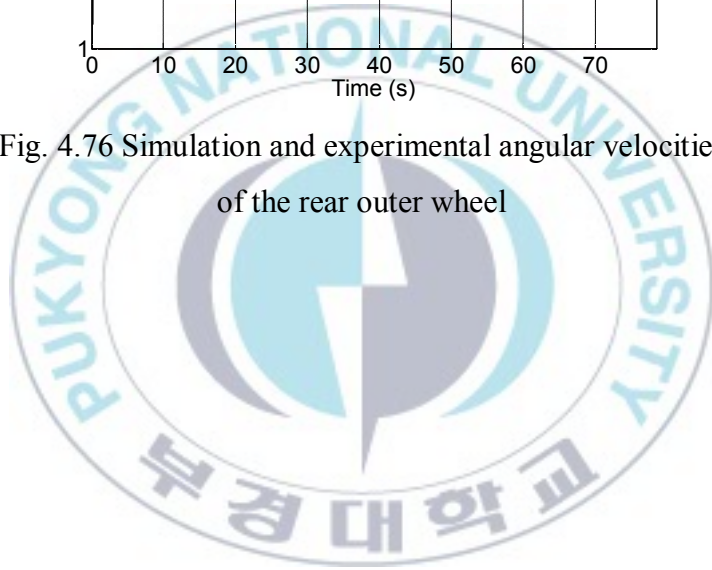


Fig. 4.76 Simulation and experimental angular velocities of the rear outer wheel



Chapter 5: Conclusions

5.1 Conclusion

This thesis is about a study on development and controlling a four wheel independent steering automatic guided vehicle. The conclusions of this thesis are summarized as follows:

- Two maneuvers for four wheel steering vehicles, i.e. parallel steering maneuver and zero-sideslip maneuver were introduced.
- A kinematic modeling of the 4WIS-AGV based on single track vehicle model was introduced by reducing an ordinary four wheel vehicle model into a two wheel vehicle model with the wheels at the centerline of the vehicle.
- A trajectory tracking controller was designed based on Backstepping method.
- Hardware configuration of the experimental 4WIS-AGV developed in this thesis were described. The system is comprised of body configuration, wheel configuration and laser navigation system NAV200. NAV200 was used to get vehicle position measurement. The body configuration consisted of body plate, body frame, electronic board, batteries, body plate, industrial PC and monitor. Industrial PC was used as the main controller of the system. It collected data from sensors, generated control signal and controlled Graphical User Interface (GUI) of the system. The monitor was used to display the GUI to users. The wheel configuration consisted of encoders, driving and steering motors, gear boxes, aluminum body cover plates and wheels.

- Simulations and experiments were conducted to verify the effectiveness and performances of the mathematical modeling and the designed controller for the 4WIS-AGV to track two reference trajectories: a reference trajectory with sharp edges for parallel steering maneuver and a circular reference trajectory for zero-sideslip maneuver.
- In the first case where the vehicle was controlled to track a reference trajectory with sharp edges for parallel steering maneuver, the vehicle tracked the reference well. The trajectory tracking errors are as follows: $e_1 = \pm 0.02$ m, $e_2 = \pm 0.02$ m, $e_3 = \pm 0.015$ rad and $e_4 = \pm 0.015$ rad.
- In the second case where the vehicle was controlled to track a circular reference trajectory for zero-sideslip maneuver, the vehicle quickly approaches the reference values and tracks the reference well. The trajectory tracking errors are as follows: $e_1 = \pm 0.02$ m, $e_2 = \pm 0.01$ m, $e_3 = \pm 0.015$ rad and $e_4 = \pm 0.005$ rad.
- The simulation and experimental results showed that the proposed controllers made the 4WIS-AGV track the reference trajectories such as a reference trajectory with sharp edges for parallel steering maneuver and a circular trajectory for zero-sideslip maneuver omnidirectionally very well.

Therefore, 4WIS-AGVs can be employed in warehouse material handling due to its omnidirectional ability and its performance mentioned above especially when material handling in narrow working space is needed.

5.2 Future works

In this thesis, the experimental 4WIS-AGV and the designed trajectory tracking controller were introduced. However, there are still some drawbacks found in the experiments, The future works are listed as follows:

- A dynamic controller will be designed based on dynamic modeling.
- Simultaneous, Localization and Mapping (SLAM) in the 4WIS-AGV will be applied.



References

- [1] T. Tsumura, “*AGV in Japan, Recent Trends of Advanced Research, Development and Industrial Applications*”, Proceedings of the IEEE/RSJ/GI International Conference on Intelligent Robots and Systems, pp. 1477 – 1484, 1994.
- [2] J. H. Chou, “*Automatic Guided Vehicle*”, Proceedings of the International IEEE/IAS Conference on Industrial Automation and Control: Emerging Technologies, pp. 241 – 245, 1995.
- [3] T. Tsumura, “*Survey of Automated Guided Vehicle in Japanese Factory*”, Proceedings of the IEEE International Conference on Robotics and Automation, pp. 1329 – 1334, 1986.
- [4] L. Schulze and A. Wullner, “*The Approach of Automated Guided Vehicle Systems*”, Proceedings of the IEEE International Conference on Service Operations and Logistics and Informatics, pp. 522 – 527, 2006.
- [5] D. Lecking, O. Wulf and B. Wagner, “*Variable Pallet Pick-Up for Automatic Guided Vehicles in Industrial Environments*”, Proceedings of the IEEE Conference on Emerging Technologies and Factory Automation, pp. 1169 – 1174, 2006.
- [6] K. Tanaka, K. Sawada, S. Shin, K. Kumagai and N. Yoneda, “*Modeling and Calibration of Automatic Guided Vehicle*”, Proceedings of the SICE Annual Conference, pp. 2485 – 2490, 2010.
- [7] F. L. Almeida, B. M. Terra, P. A. Dias and M. Goncalves, “*Transport with Automatic Guided Vehicles in the Factory of the Future*”, Proceedings of the IEEE Conference on Emerging Technologies and Factory Automation, pp. 1 – 4, 2010.

- [8] X. Cheng and R. Tao, “*Design of Automatic Guided Vehicles and Dinking Robot System*”, Proceedings of the Third International Conference on Intelligent Human-Machine Systems and Cybernetics, pp. 3 – 6, 2011.
- [9] B. Sert, J. Maddox and P. Veatch, “*Laser Assisted Intelligent Guidance for Automated Guided Vehicles*”, Proceedings of Symposium on Intelligent Vehicles, pp. 201 – 206, 1993.
- [10] L. Wang, J. Shu, T. Emura and M. Kumagai, “*A 3D Scanning Laser Rangefinder and its Application to an Autonomous Guided Vehicle*”, Proceedings of the 51st Vehicular Technology Conference, pp. 331 – 335, 2000.
- [11] C. C. Tsai, H. H. Lin and K. H. Wong, “*Laser-based Position Recovery of a Free-Ranging Automatic Guided Vehicle*”, Proceedings of the IEEE International Conference on Mechatronics, pp. 1 – 6, 2005.
- [12] G. Zhang and Z. Pan, “*The Application Research of Mobile Robots and Wireless Sensor Network in Laser Automatic Guided Vehicles*”, Proceedings of the Third International Conference on Measuring Technology and Mechatronics Automation, pp. 708 – 711, 2011.
- [13] K. Fan, Q. Yang, W. Yan and B. Lei, “*Fuzzy-PID based Deviation-correcting Control System for Laser Guided AGV*”, Proceedings of the International Conference on Modeling, Identification and Control, pp. 472 – 477, 2012.
- [14] H. Song, J. Kim, E. Jung, J. Lee and S. Kim, “*Path-Tracking Control of a Laser Guided Vehicle using Fuzzy Inference System*”, Proceedings of the International Conference on Control, Automation and Systems, pp. 1666 – 1668, 2012.

- [15] T. L. Bui, P. T. Doan, H. K. Kim and S. B. Kim, “*Trajectory Tracking Controller Design for AGV Using Laser Sensor Based Positioning System*”, Proceedings on 9th Asian Control Conference, pp. 1 – 5, 2013.
- [16] B. F. Buxton, D. A. Castelow, M. Rygol, P. F. McLauchlan and S. B. Pollard, “*Developing a Stereo Vision System for Control of an AGV*”, Proceedings of the Second International Specialist Seminar on the Design and Application of Parallel Digital Processors, pp. 79 – 83, 1991.
- [17] E. M. Petriu, N. Trif, W. S. McMath and S. K. Yeung, “*Environment Encoding for AGV Navigation Using Vision*”, Proceedings of the IEEE – IEE Vehicle Navigation and Information System Conference, pp. 525 – 528, 1993.
- [18] T. Y. Sun and S. J. Tsai, “*Fuzzy Adaptive Mechanism for Improving the Efficiency and Precision of Vision-based Automatic Guided Vehicle Control*”, Proceedings of the IEEE International Conference on Systems, Man and Cybernetics, pp. 263 – 269, 2005.
- [19] A. Ye, H. Zhu, Z. Xu, C. Sun and K. Yuan, “*A Vision-Based Guidance Method for Autonomous Guided Vehicles*”, Proceedings of IEEE International Conference on Mechatronics and Automation, pp. 2025 – 2030, 2012.
- [20] J. Kang, J. Lee, H. Eum, C. H. Hyun and M. Park, “*An Application of Parameter Extraction for AGV Navigation Based on Computer Vision*”, Proceedings of the 10th International Conference on Ubiquitous Robots and Ambient Intelligence, pp. 622 – 626, 2013.

- [21] B. Kotze, G. Jordaan and H. Vermaak, “*Reconfigurable navigation of an Automatic Guided Vehicle utilising omnivision*”, Proceedings of the 6th Robotics and Mechatronics Conference, pp. 80 – 86, 2013.
- [22] X. Liang, T. Tomizawa, H. M. Do, Y. S. Kim and K. Ohara, “*Multiple Robots Localization Using Large Planar Camera Array For Automated Guided Vehicle System*”, Proceedings of the IEEE International Conference on Information and Automation, pp. 984 – 990, 2008.
- [23] S. Borthwick and H. Durrant-Whyte, “*Dynamic Localisation of Autonomous Guided Vehicles*”, Proceedings of the IEEE International Conference on Multisensor Fusion and Integration for Intelligent Systems, pp. 92 – 97, 1994.
- [24] H. Wang and N. Liu, “*Design and Recognition of a Ring Code for AGV Localization*”, Proceedings of the Fourth International Conference on Information, Communications and Signal Processing, pp. 532 – 536, 2003.
- [25] X. Liang, Y. Sumi, B. K. Kim, H. M. Do and Y. S. Kim, “*A Large Planar Camera Array for Multiple Automated Guided Vehicles Localization*”, Proceedings of the IEEE/ASME International Conference on Advanced Intelligent Mechatronics, pp. 608 – 613, 2008.
- [26] A. Azenha and A. Carvalho, “*A Neural Network Approach for AGV Localization Using Trilateration*”, Proceedings of the 35th Annual Conference of IEEE Industrial Electronics, pp. 2699 – 2702, 2009.
- [27] D. Ronzoni, R. Olmi, C. Secchi and C. Fantuzzi, “*AGV Global Localization Using Indistinguishable Artificial Landmarks*”,

- IEEE International Conference on Robotics and Automation, pp. 287 – 292, 2011.
- [28] Q. Sun, H. Liu, Q. Yang and W. Yan, “*On the Design for AGVs: Modeling, Path Planning and Localization*”, Proceedings of the 2011 IEEE International Conference on Mechatronics and Automation, pp. 1515 – 1520, 2011.
- [29] C. Kirsch, F. Kunemund, D. Heb and C. Rohrig, “*Comparison of Localization Algorithms for AGVs in Industrial Environments*”, Proceedings of the 7th German Conference on Robotics, pp. 1 – 6, 2012.
- [30] J. Lategahn, M. Muller and C. Rohrig, “*Global Localization of Automated Guided Vehicles in Wireless Networks*”, Proceedings of the 1st IEEE International Symposium on Wireless Systems within the Conferences on Intelligent Data Acquisition and Advanced Computing Systems, pp. 7 -12, 2012.
- [31] H. Cho, H. Song, M. Parkm J. Kim, S. Woo and S. Kim, “*Independence Localization System for Mecanum Wheel AGV*”, Proceedings of the 22nd IEEE International Symposium on Robot and Human Interactive Communication, pp. 192 – 197, 2013.
- [32] M. D. Cecco, “*Self-Calibration of AGV Inertial-Odometric Navigation Using Absolute-Reference Measurements*”, Proceedings of the IEEE Instrumentation and Measurement Technology Conference, pp. 1513 – 1518, 2002.
- [33] R. Carelli, C. Soria, O. Nasisi and E. Freire, “*Stable AGV Corridor Navigation with Fused Vision-Based Control Signals*”, Proceedings of the 28th Annual Conference of the Industrial Electronics Society, pp. 2433 – 2438, 2002.

- [34] Z. Li, X. Weng and Z. Su, “*A Navigation Method of Information Fusion and Mutual Aid based on Map for Logistic AGV*”, Proceedings of the Sixth International Conference on Measuring Technology and Mechatronics Automation, pp. 21 – 24, 2014.
- [35] R. Rajagopalan, R. M. H. Cheng and S. Lequoc, “*Guidance Control Scheme Employing Knowledge-base for AGV Navigation*”, Proceedings of the American Control Conference, pp. 942 – 947, 1992.
- [36] R. Cucchiara, E. Perini and G. Pistoni, “*Efficient Stereo Vision for Obstacle Detection and AGV Navigation*”, Proceedings of the 14th International Conference on Image Analysis and Processing, pp. 291 – 296, 2007.
- [37] R. V. Bostelman, T. H. Hong and R. Madhavan, “*Towards AGV Safety and Navigation Advancement - Obstacle Detection using a TOF Range Camera*”, Proceedings of the 12th International Conference on Advanced Robotics, pp. 460 – 467, 2005.
- [38] A. K. Ray, M. Gupta, L. Behera and M. Jamshidi, “*Sonar Based Autonomous Automatic Guided Vehicle (AGV) Navigation*”, Proceedings of the IEEE International Conference on System of Systems Engineering, pp. 1 – 6, 2008.
- [39] G. G. Rigatos, “*Derivative-free distributed filtering for integrity monitoring of AGV navigation sensors*”, Proceedings of the IEEE International Conference on Multisensor Fusion and Integration for Intelligent Systems, pp. 299 – 304, 2012.

- [40] H. Wang, X. Zhang and J. Zhang, “*GPS/DR Information Fusion for AGV Navigation*”, Proceedings of the World Automation Congress (WAC), pp. 1 – 4, 2012.
- [41] N. Isozaki, D. Chugo, S. Yokota and K. Takase, “*Camera-based AGV Navigation System for Indoor Environment with Occlusion Condition*”, Proceedings of the IEEE International Conference on Mechatronics and Automation, pp. 778 – 783, 2011.
- [42] A. Lucas, C. Christo, M. P. Silva and C. Cardeira, “*Mosaic Based Flexible Navigation for AGVs*”, Proceedings of the IEEE International Symposium on Industrial Electronics (ISIE), pp. 3545 – 3550, 2010.
- [43] W. S. Wijesoma, P. P. Khaw and E. K. Teoh, “*Control and Navigation of an Outdoor AGV Using Fuzzy Reasoning*”, Proceedings of the IEEE/IEEJ/JSAI International Conference on Intelligent Transportation Systems, pp. 544 – 549, 1999.
- [44] Y. Du, X. Gao, Z. Liu and M. Sun, “*The new Navigation System for Automatic Guided Vehicle*”, Proceedings of the Control and Decision Conference, pp. 4653 – 4658, 2008.
- [45] P. S. Pratama, S. K. Jeong, S. S. Park and S. B. Kim, “*Moving Object Tracking and Avoidance Algorithm for Differential Driving AGV Based on Laser Measurement Technology*”, International Journal of Science and Engineering, vol. 4(1), pp. 11-15, 2013.
- [46] P. T. Doan, T. T. Nguyen, V. T. Dinh, H. K. Kim and S. B. Kim, “*Path Tracking Control of Automatic Guided Vehicle Using Camera Sensor*”, Proceedings of the 1st International

- Symposium on Automotive and Convergence Engineering, 2011.
- [47] B. Li and F. Yu, “*Optimal Model Following Control of Four-Wheel Active Steering Vehicle*”, Proceedings of the 2009 IEEE International Conference on Information and Automation, June 22 – 25, 2009, Macau, China, pp. 881-886, 2009.
- [48] R. H. Zhang, G. Y. Cheng, G. Q. Wang, H. G. Jia and T. Chen, “*Robust Optimal Control Technology for Four-Wheel Steering Vehicle*”, Proceedings of the 2007 IEEE International Conference on Mechatronics and Automation, Harbin, China, pp. 1513-1516, 2007.
- [49] I. Amdouni, N. Jeddi and L. E. Amraoui, “*Optimal Control Approach Developed to Four-Wheel Active Steering Vehicles*”, Proceedings of the 5th International Conference on Modeling, Simulation and Applied Optimization (ICMSAO), Hammamet, Tunisia, pp. 1-6, 2013.
- [50] T. L. Lam, H. Qian and Y. Xu, “*Behavior-Based Steering Control for Four Wheel Independent Steering Vehicle*”, Proceedings of the 2008 IEEE International Conference on Robotics and Biometrics, Bangkok, Thailand, pp. 536 – 541, 2008.
- [51] Z. Yang, Z. Wang, W. Su and J. Zhang, “*Multi-Mode Control Method Based on Fuzzy Selector in the Four Wheel Steering Control System*”, Proceedings of the 8th IEEE International Conference on Control and Automation, Xiamen, China, pp. 1221 – 1226, 2010.
- [52] A. Shaout, M. A. Jarrah, H. Al-Araji and K. Al-Tell, “*A Nonlinear Optimal Four-Wheels Steering Controller*”,

- Proceedings of the 43rd IEEE Midwest Symposium on Circuits and Systems, Lansing, Michigan, USA, pp. 1426-1429, 2000.
- [53] M. F. Selekwa and J. R. Nistler, “*Path Tracking Control of Four Wheel Independently Steered Ground Robotic Vehicles*”, Proceedings of the 50th IEEE Conference on Decision and Control and European Control Conference (CDC-ECC), pp. 6355 – 6360, 2011.
- [54] D. Wang and F. Qi, “*Trajectory Planning for a Four-Wheel-Steering Vehicle*”, Proceedings of the IEEE International Conference on Robotics & Automation, pp. 3320 – 3325, 2001.
- [55] Y. Wang, J. A. Linnett and J. W. Roberts, “*A Unified Approach to Inverse and Direct Kinematics for Four Kinds of Wheeled Mobile Robots and its Applications*”, Proceedings of the IEEE International Conference on Robotics and Automation, pp. 3458 – 3465, 1996.
- [56] R. Ronen and S. Arogeti, “*Coordinated Path Following Control for a Group of Car-like Vehicles*”, Proceedings of the 12th International Conference on Control, Automation, Robotics and Vision, pp. 719 – 724, 2012
- [57] N. Silva, L. Baglivo, A. Vale and M. D. Cecco, “*Four Path Following Controllers for Rhombic Like Vehicles*”, Proceedings of the IEEE International Conference on Robotics and Automation, pp. 3204 – 3211, 2013.
- [58] I. Kecskes, Z. Balogh and P. Odry, “*Modeling and Fuzzy Control of a Four-Wheeled Mobile Robot*”, Proceedings of the IEEE 10th Jubilee International Symposium on Intelligent Systems and Informatics, pp. 205 – 210, 2012.

- [59] R. Grepl, J. Vejlupěk, V. Lamberský, M. Jasanský, F. Vadlejš and P. Coupek, “*Development of 4WS/4WD Experimental Vehicle: Platform for Research and Education in Mechatronics*”, Proceedings of the IEEE International Conference on Mechatronics, pp. 893 – 898, 2011.
- [60] R. Solea, A. Filipescu, V. Minzu and S. Filipescu, “*Sliding-Mode Trajectory-tracking Control for a Four-Wheel-Steering Vehicle*”, Proceedings of the 8th IEEE International Conference on Control and Automation, Xiamen, China, pp. 382-387, 2010.
- [61] H. H. Lin and C. C. Tsai, “*Laser Pose Estimation and Tracking using Fuzzy Extended Information Filtering for an Autonomous Mobile Robot*”, Journal of Intelligent Robotic system, Vol. 53 (2), pp 119-143, 2008.
- [62] http://www.dnj.co.kr/2013_html/planetary_ig52gm_04_en.html



Publications and Conferences

A. Conferences

1. Yuhanes Dedy Setiawan, Pandu Sandi Pratama, Hak Kyeong Kim and Sang Bong Kim, “*Modeling and Control System Design of Four Wheel Independent Steering Automatic Guided Vehicle Based on Optimal Control Method*”, Proceedings of the Conference on Korea Logistic, Cheonan, South Korea, October 17, 2013.
2. Yuhanes Dedy Setiawan, Pandu Sandi Pratama, Sang Kwon Jeong, Vo Hoang Duy and Sang Bong Kim, “*Experimental Comparison of A* and D* Lite Path Planning Algorithms for Differential Drive Automated Guided Vehicle*”, AETA 2013: Recent Advances in Electrical Engineering and Related Sciences, Lecture Notes in Electrical Engineering 282, Springer-Verlag Berlin Heidelberg. vol. 282, pp. 555-564, 2014.
3. Yuhanes Dedy Setiawan, Pandu Sandi Pratama, Woo Young Jeong, Hak Kyeong Kim and Sang Bong Kim, “*Control System Design of Four Wheeled Independent Steering Automatic Guided Vehicles Based on Backstepping Control Method*”, Proceedings of the International Symposium on Advanced Engineering, pp. 85-88, Pukyong National University, Busan, South Korea, November 11-13, 2013.
4. Yuhanes Dedy Setiawan, Pandu Sandi Pratama, Jin Wook Kim, Dae Hwan Kim, Young Seok Jeong and Sang Bong Kim, “*Path Replanning and Control Design for Trajectory Tracking of Automated Guided Vehicles*”, Proceedings of the IEEE Second

- International Symposium on Control, Automation, Industrial Informatics and Smart Grid, Delhi, India, September 24-27, 2014.
5. Yuhanes Dedy Setiawan, Jin Wook Kim, Jung Hu Min, Hak Kyeong Kim and Sang Bong Kim, “*Pipe Inspection Robot Controller Design Based on Linear Quadratic Regulator*”, Proceedings of the Seventh Vietnam Conference on Mechatronics, Bien Hoa, Vietnam, November 21-22, 2014.
 6. Yuhanes Dedy Setiawan, Pandu Sandi Pratama, Dae Hwan Kim, Suk Min Yoon, Tae Kyoung Yeu, Sub Hong, Hak Kyeong Kim and Sang Bong Kim, “*Path Planning Based on A* Algorithm and Its Tracking Controller for Underwater Mining Robots*”, Proceedings of the Korean Society of Ocean Engineers (KSOE) Conference, Jeju Island, South Korea, October 16-17, 2014.
 7. Jung Hu Min, Yuhanes Dedy Setiawan, Pandu Sandi Pratama, Hak Kyeong Kim and Sang Bong Kim, “*Development and Controller Design of Wheeled-Type Pipe Inspection Robot*”, Proceedings of the IEEE Second International Symposium on Control, Automation, Industrial Informatics and Smart Grid, Delhi, India, September 24-27, 2014.
 8. Pandu Sandi Pratama, Yuhanes Dedy Setiawan, Dae Hwan Kim, Young Seok Jung, Sang Kwun Jeong, Jin Il Jeong, Hak Kyeong Kim and Sang Bong Kim, “*Fault Detection Algorithm for Automatic Guided Vehicle Based on Multiple Positioning Modules*”, Proceedings of the IEEE Second International Symposium on Control, Automation, Industrial Informatics and Smart Grid, Delhi, India, September 24-27, 2014.
 9. Jung Hu Min, Woo Young Jeong, Pandu Sandi Pratama, Yuhanes Dedy Setiawan, Hak Kyeong Kim and Sang Bong Kim,

“Fault Diagnosis System of Caterpillar Wheel Type Pipeline Inspection Robot”, Proceedings of International Symposium on Mechatronics and Robotics, pp. 74-78, Ho Chi Minh University of Technology, Vietnam, December 10-11, 2013.

10. Yuhanes Dedy Setiawan, Pandu Sandi Pratama, Hak Kyeong Kim and Sang Bong Kim, “*Trajectory Tracking Controller Design for Four Wheeled Independent Steering Automatic Guided Vehicles*”, Proceedings of the International Symposium on Advanced Mechanical and Power Engineering, Pukyong National University, Busan, South Korea, November 28, 2014.



Appendix A: Proof of Eq. (2.10)

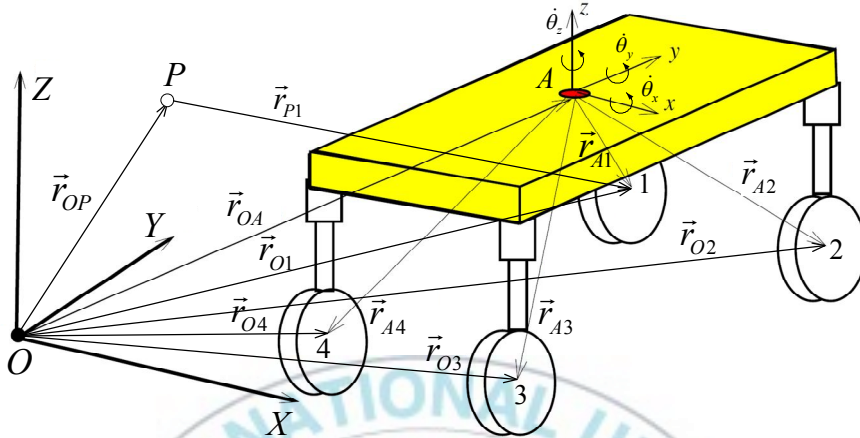


Fig. A.1 Coordinate system configuration of four wheel steering vehicles

Velocities at the wheel centers are expressed as [53]

$$\vec{v}_i = \vec{\Omega} \times \left[\vec{r}_{OP} - (\vec{r}_{OA} + \vec{r}_{Ai}) \right], i = 1, \dots, 4 \quad (\text{A.1})$$

where

\vec{r}_{OA} : relative position of the vehicle center of gravity (CG) in the XYZ global coordinate,

\vec{r}_{OP} : a turning point P in the inertial frame serving as the vehicle instantaneous center of zero velocity,

\vec{r}_{Ai} : position vectors of wheel i from the vehicle CG,

$\vec{\Omega}$: angular velocity vector of the xyz local coordinate in XYZ global coordinate defined as $\vec{\Omega} = [\dot{\theta}_x \quad \dot{\theta}_y \quad \dot{\theta}_z]^T$.

Eq. (A.1) can be written as

$$\vec{v}_1 = \vec{\Omega} \times \left[\vec{r}_{OP} - (\vec{r}_{OA} + \vec{r}_{A1}) \right] \quad (\text{A.2})$$

$$\vec{v}_2 = \vec{\Omega} \times \left[\vec{r}_{OP} - (\vec{r}_{OA} + \vec{r}_{A2}) \right] \quad (\text{A.3})$$

$$\vec{v}_3 = \vec{\Omega} \times \left[\vec{r}_{OP} - (\vec{r}_{OA} + \vec{r}_{A3}) \right] \quad (\text{A.4})$$

$$\vec{v}_4 = \vec{\Omega} \times \left[\vec{r}_{OP} - (\vec{r}_{OA} + \vec{r}_{A4}) \right] \quad (\text{A.5})$$

Since velocity of each wheel in Eqs. (A.2) - (A.5) are identical, only derivative of Eq. (A.2) is presented.

$$\dot{\vec{v}}_1 = \vec{\Omega} \times \left[\vec{r}_{OP} - (\vec{r}_{OA} + \vec{r}_{A1}) \right] = \vec{\Omega} \times \left[\vec{r}_{OP} - \vec{r}_{O1} \right] \quad (\text{A.6})$$

and

$$\begin{pmatrix} v_{1x} \\ v_{1y} \\ v_{1z} \end{pmatrix} = \begin{pmatrix} \dot{\theta}_x \\ \dot{\theta}_y \\ \dot{\theta}_z \end{pmatrix} \times \left[\begin{pmatrix} r_{OPx} \\ r_{OPy} \\ r_{OPz} \end{pmatrix} - \begin{pmatrix} r_{O1x} \\ r_{O2y} \\ r_{O3z} \end{pmatrix} \right] \quad (\text{A.7})$$

Since the vehicle does not move in z axis and rotate in x axis and y axis, $v_{1z} = \dot{\theta}_x = \dot{\theta}_y = 0$ and $\dot{\theta}_z = \dot{\psi}_A$, Eq. (A.7) becomes

$$\begin{pmatrix} v_{1x} \\ v_{1y} \\ 0 \end{pmatrix} = \begin{pmatrix} 0 \\ 0 \\ \dot{\psi}_A \end{pmatrix} \times \begin{pmatrix} r_{OPx} - r_{O1x} \\ r_{OPy} - r_{O2y} \\ r_{OPz} - r_{O3z} \end{pmatrix} = \begin{pmatrix} -\dot{\psi}_A (r_{OCx} - r_{O1x}) \\ \dot{\psi}_A (r_{OCy} - r_{O1y}) \\ 0 \end{pmatrix} \quad (\text{A.8})$$

From Eq. (A.8), v_1 can be obtained as follows:

$$\begin{aligned}
 v_1 &= \sqrt{v_{1x}^2 + v_{1y}^2} = \sqrt{\left(-\dot{\psi}_A (r_{OPx} - r_{O1x})\right)^2 + \left(\dot{\psi}_A (r_{OPy} - r_{O1y})\right)^2} \\
 &= \sqrt{\dot{\psi}_A^2 \left((r_{OPx} - r_{O1x})^2 + (r_{OPy} - r_{O1y})^2 \right)} \\
 &= \dot{\psi}_A \sqrt{\left((r_{OPx} - r_{O1x})^2 + (r_{OPy} - r_{O1y})^2 \right)} = \dot{\psi}_A r_{P1} \tag{A.9}
 \end{aligned}$$

where r_{P1} is the distance from turning point P to the center point of the wheel 1.

Likewise,

$$v_2 = \dot{\psi}_A r_{P2} \tag{A.10}$$

$$v_3 = \dot{\psi}_A r_{P3} \tag{A.11}$$

$$v_4 = \dot{\psi}_A r_{P4} \tag{A.12}$$

The distances from turning point P to each wheel center points can be calculated using two dimensional triangular relationships of the vehicle. Fig. A.2 illustrates the wheel configuration of the four wheel steering vehicles in two dimension.

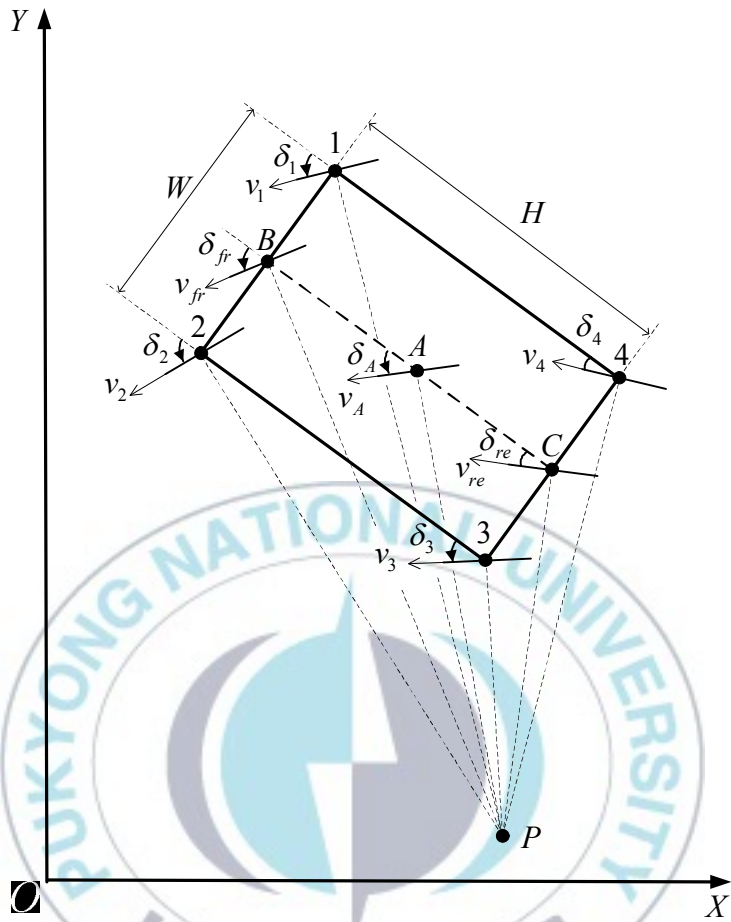


Fig. A.2 Wheel configuration in two dimension

In Figs. 2.1, 2.4 and A.2, vehicle width, $W = 2b$, and vehicle length, $H = l_{fr} + l_{re}$, are given. By considering the triangle relationship among points 1, 2, 3, 4, A, B, C and P in Fig. A.2, angle relationship between each wheel can be found.

Fig. A.3 shows triangle of points P, 4 and C (triangle P4C) that gives relationship between rear wheel 4 and rear wheel steering angles, δ_4 and δ_{re} , respectively.

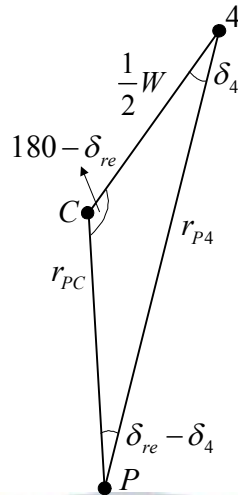


Fig. A.3 Triangle $PC4$

$\Delta PC4$

The distances (lengths) of points $P4$ and PC can be found using law of sines as follows:

$$\frac{r_{P4}}{\sin(180 - \delta_{re})} = \frac{1/2 W}{\sin(\delta_{re} - \delta_4)}$$

$$\Leftrightarrow r_{P4} = \frac{W \sin(180 - \delta_{re})}{2 \sin(\delta_{re} - \delta_4)} = \frac{W \sin \delta_{re}}{2 \sin(\delta_{re} - \delta_4)} \quad (\text{A.13})$$

$$\frac{r_{PC}}{\sin \delta_4} = \frac{1/2 W}{\sin(\delta_{re} - \delta_4)}$$

$$\Leftrightarrow r_{PC} = \frac{W \sin \delta_4}{2 \sin(\delta_{re} - \delta_4)} \quad (\text{A.14})$$

Since Eqs. (A.13) and (A.14) have sine functions, these equations have some constraints to apply such that these equations can work properly. The constraints are

- $\delta_4 \neq 0^\circ$
- $\delta_{re} \neq \delta_4$
- $\delta_{re} \neq 180^\circ$

Likewise, the equations for the other points can be obtained. Fig. A.4 shows triangle of points P , 3 and C (triangle $P3C$) that gives relationship between rear wheel 3 and rear wheel steering angles, δ_3 and δ_{re} , respectively.

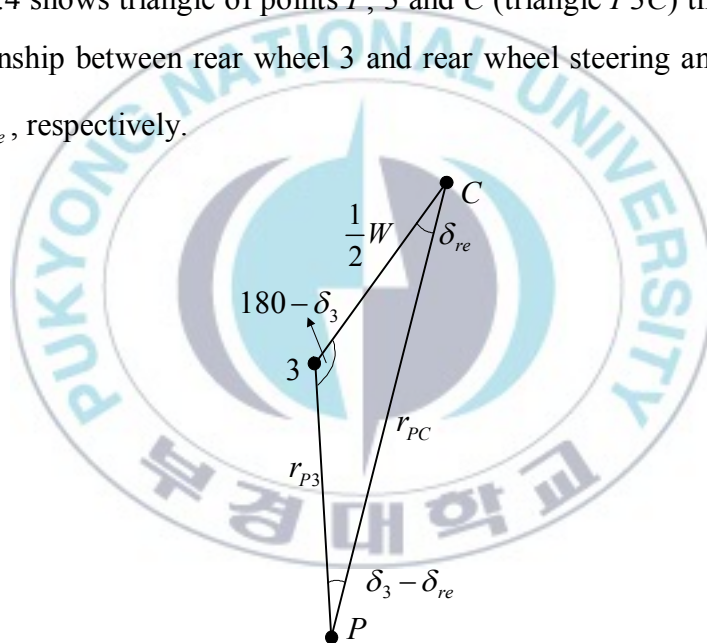


Fig. A.4 Triangle $P3C$

$\Delta P3C$

The distances (lengths) of points $P3$ and PC can be found using law of sines as follows:

$$\frac{r_{P3}}{\sin \delta_{re}} = \frac{1/2W}{\sin(\delta_3 - \delta_{re})}$$

$$\Leftrightarrow r_{P3} = \frac{W \sin \delta_{re}}{2 \sin(\delta_3 - \delta_{re})} \quad (\text{A.15})$$

$$\frac{r_{PC}}{\sin(180 - \delta_3)} = \frac{1/2W}{\sin(\delta_3 - \delta_{re})}$$

$$\Leftrightarrow r_{PC} = \frac{W \sin(180 - \delta_3)}{2 \sin(\delta_3 - \delta_{re})} = \frac{W \sin \delta_3}{2 \sin(\delta_3 - \delta_{re})} \quad (\text{A.16})$$

Since Eqs. (A.15) and (A.16) have sine functions, these equations have some constraints to apply such that these equations can work properly. The constraints are

- $\delta_{re} \neq 0^\circ$
- $\delta_{re} \neq \delta_3$
- $\delta_3 \neq 180^\circ$

Fig. A.5 shows triangle of points P , B and 1 (triangle $PB1$) that gives relationship between front wheel 1 and front wheel steering angles, δ_1 and δ_{fr} , respectively.

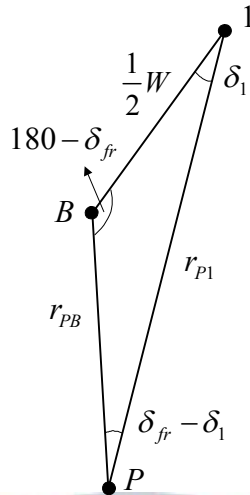


Fig. A.5 Triangle $PB1$

$\Delta PB1$

The distances (lengths) of points $P1$ and PB can be found using law of sines as follows:

$$\frac{r_{P1}}{\sin(180 - \delta_{fr})} = \frac{1/2 W}{\sin(\delta_{fr} - \delta_1)}$$

$$\Leftrightarrow r_{P1} = \frac{W \sin(180 - \delta_{fr})}{2 \sin(\delta_{fr} - \delta_1)} = \frac{W \sin \delta_{fr}}{2 \sin(\delta_{fr} - \delta_1)} \quad (\text{A.17})$$

$$\frac{r_{PB}}{\sin \delta_1} = \frac{1/2 W}{\sin(\delta_{fr} - \delta_1)}$$

$$\Leftrightarrow r_{PB} = \frac{W \sin \delta_1}{2 \sin(\delta_{fr} - \delta_1)} \quad (\text{A.18})$$

Since Eqs. (A.17) and (A.18) have sine functions, these equations have some constraints to apply such that these equations can work properly. The constraints are

- $\delta_1 \neq 0^\circ$
- $\delta_{fr} \neq \delta_1$
- $\delta_{fr} \neq 180^\circ$

Fig. A.6 shows triangle of points P , 2 and B (triangle $P2B$) that gives relationship between front wheel 2 and front wheel steering angles, δ_2 and δ_{fr} , respectively.

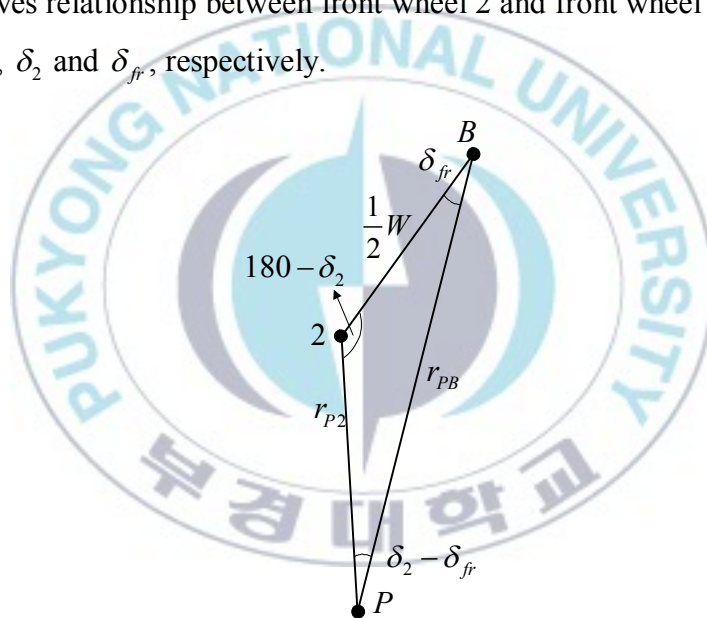


Fig. A.6 Triangle $P2B$

$\Delta P2B$

The distances (lengths) of points $P2$ and PB can be found using law of sines as follows:

$$\frac{r_{P_2}}{\sin \delta_{fr}} = \frac{1/2W}{\sin(\delta_2 - \delta_{fr})}$$

$$\Leftrightarrow r_{P_2} = \frac{W \sin \delta_{fr}}{2 \sin(\delta_2 - \delta_{fr})} \quad (\text{A.19})$$

$$\frac{r_{PB}}{\sin(180 - \delta_2)} = \frac{1/2W}{\sin(\delta_2 - \delta_{fr})}$$

$$\Leftrightarrow r_{PB} = \frac{W \sin(180 - \delta_2)}{2 \sin(\delta_2 - \delta_{fr})} = \frac{W \sin \delta_2}{2 \sin(\delta_2 - \delta_{fr})} \quad (\text{A.20})$$

Since Eqs. (A.19) and (A.20) have sine functions, these equations have some constraints to apply such that these equations can work properly. The constraints are

- $\delta_{fr} \neq 0^\circ$
- $\delta_{fr} \neq \delta_2$
- $\delta_2 \neq 180^\circ$

Fig. A.7 shows triangle of points P , C and B (triangle PBC) that gives relationship between front and rear wheel steering angles, δ_{fr} and δ_{re} , respectively.

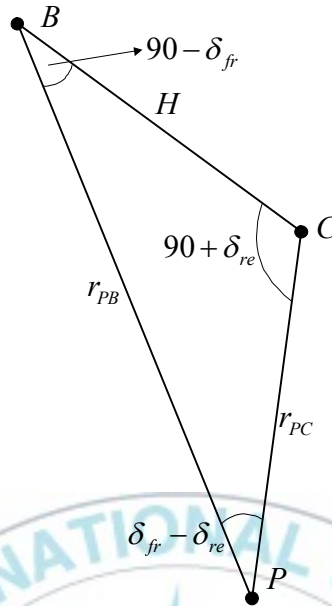


Fig. A.7 Triangle PBC

$\triangle PBC$

The distances (lengths) of points PC and PB can be found using law of sines as follows:

$$\frac{r_{PC}}{\sin(90 - \delta_{fr})} = \frac{H}{\sin(\delta_{fr} - \delta_{re})}$$

$$\Leftrightarrow r_{PC} = \frac{H \sin(90 - \delta_{fr})}{\sin(\delta_{fr} - \delta_{re})} = \frac{H \cos \delta_{fr}}{\sin(\delta_{fr} - \delta_{re})} \quad (\text{A.21})$$

$$\frac{r_{PB}}{\sin(90 + \delta_{re})} = \frac{H}{\sin(\delta_{fr} - \delta_{re})}$$

$$\Leftrightarrow r_{PB} = \frac{H \sin(90 + \delta_{re})}{\sin(\delta_{fr} - \delta_{re})} = \frac{H \cos \delta_{re}}{\sin(\delta_{fr} - \delta_{re})} \quad (\text{A.22})$$

Since Eqs. (A.21) and (A.22) have sine functions, these equations have some constraints to apply such that these equations can work properly. The constraints are

- $\delta_{fr} \neq 90^\circ$
- $\delta_{re} \neq -90^\circ$
- $\delta_{fr} \neq \delta_{re}$

Fig. A.8 shows triangle of points P , A and C (triangle PAC) that gives relationship between vehicle and rear wheel steering angles, δ_A and δ_{re} , respectively.

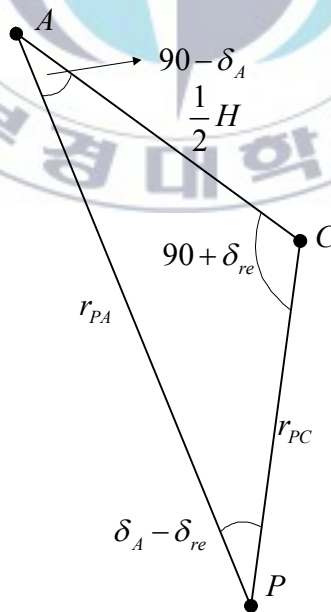


Fig. A.8 Triangle PAC

ΔPAC

The distances (lengths) of points PC and PA can be found using law of sines as follows:

$$\frac{r_{PC}}{\sin(90 - \delta_A)} = \frac{1/2 H}{\sin(\delta_A - \delta_{re})}$$
$$\Leftrightarrow r_{PC} = \frac{H \sin(90 - \delta_A)}{2 \sin(\delta_A - \delta_{re})} = \frac{H \cos \delta_A}{2 \sin(\delta_A - \delta_{re})} \quad (A.23)$$

Since Eq. (A.23) has sine functions, these equations have some constraints to apply such that these equations can work properly.

The constraints are

- $\delta_A \neq 90^\circ$
- $\delta_A \neq \delta_{re}$
- $\delta_{re} \neq -90^\circ$

By substituting Eq. (A.23) to Eq. (A.21), relationship among vehicle steering angle, δ_A , and front and rear wheel steering angles, δ_{fr} and δ_{re} , is obtained as follows:

$$\frac{H \cos \delta_A}{2 \sin(\delta_A - \delta_{re})} = \frac{H \cos \delta_{fr}}{\sin(\delta_{fr} - \delta_{re})}$$
$$\Leftrightarrow \cos \delta_A \sin(\delta_{fr} - \delta_{re}) = 2 \cos \delta_{fr} \sin(\delta_A - \delta_{re})$$
$$\Leftrightarrow \cos \delta_A \sin \delta_{fr} \cos \delta_{re} - \cos \delta_A \cos \delta_{fr} \sin \delta_{re} = 2 \cos \delta_{fr} \sin \delta_A \cos \delta_{re} - 2 \cos \delta_{fr} \cos \delta_A \sin \delta_{re}$$
$$\Leftrightarrow \cos \delta_A \sin \delta_{fr} \cos \delta_{re} - \cos \delta_A \cos \delta_{fr} \sin \delta_{re} + 2 \cos \delta_{fr} \cos \delta_A \sin \delta_{re}$$

$$\begin{aligned}
&= 2 \cos \delta_{fr} \sin \delta_A \cos \delta_{re} \\
\Leftrightarrow \cos \delta_A \sin \delta_{fr} \cos \delta_{re} + \cos \delta_{fr} \cos \delta_A \sin \delta_{re} &= 2 \cos \delta_{fr} \sin \delta_A \cos \delta_{re} \\
\Leftrightarrow \cos \delta_A (\sin \delta_{fr} \cos \delta_{re} + \cos \delta_{fr} \sin \delta_{re}) &= 2 \cos \delta_{fr} \sin \delta_A \cos \delta_{re} \\
\Leftrightarrow \frac{\sin \delta_A}{\cos \delta_A} &= \frac{\sin \delta_{fr} \cos \delta_{re} + \cos \delta_{fr} \sin \delta_{re}}{2 \cos \delta_{fr} \cos \delta_{re}}
\end{aligned}$$

where $\cos \delta_A \neq 0$ and $\cos \delta_{fr} \cos \delta_{re} \neq 0$

$$\begin{aligned}
\Leftrightarrow \tan \delta_A &= \frac{1}{2} (\tan \delta_{fr} + \tan \delta_{re}) \\
\Leftrightarrow \tan^2 \delta_A &= \frac{1}{4} (\tan \delta_{fr} + \tan \delta_{re})^2 \\
\Leftrightarrow \tan^2 \delta_A + 1 &= \frac{1}{4} (\tan \delta_{fr} + \tan \delta_{re})^2 + 1 \\
\Leftrightarrow \sec^2 \delta_A &= \frac{1}{4} (\tan \delta_{fr} + \tan \delta_{re})^2 + 1 \\
\Leftrightarrow \cos^2 \delta_A &= \frac{1}{\frac{1}{4} (\tan \delta_{fr} + \tan \delta_{re})^2 + 1} \\
\cos \delta_A &= \frac{1}{\sqrt{\frac{1}{4} (\tan \delta_{fr} + \tan \delta_{re})^2 + 1}} \tag{A.24}
\end{aligned}$$

Substituting Eqs. (A.19), (A.17), (A.15) and (A.12) to Eqs. (A.9) - (A.12) yields:

$$v_1 = \dot{\psi}_A r_{p1} = \frac{\dot{\psi}_A W \sin \delta_{fr}}{2 \sin(\delta_{fr} - \delta_1)} \tag{A.25}$$

$$v_2 = \dot{\psi}_A r_{p2} = \frac{\dot{\psi}_A W \sin \delta_{fr}}{2 \sin(\delta_2 - \delta_{fr})} \tag{A.26}$$

$$v_3 = \dot{\psi}_A r_{P3} = \frac{\dot{\psi}_A W \sin \delta_{re}}{2 \sin(\delta_3 - \delta_{re})} \quad (\text{A.27})$$

$$v_4 = \dot{\psi}_A r_{P4} = \frac{\dot{\psi}_A W \sin \delta_{re}}{2 \sin(\delta_{re} - \delta_4)} \quad (\text{A.28})$$

From Fig. A.2, kinematic and rigid body constraint shows that the longitudinal velocity at the vehicle centerline should be the same, and can be expressed mathematically as follows:

$$v_{fr} \cos \delta_{fr} = v_A \cos \delta_A = v_{re} \cos \delta_{re} \quad (\text{A.29})$$

In addition, inner, outer and centerline lateral velocities at the front and rear axles should be the same, and can be expressed mathematically as follows:

$$v_1 \sin \delta_1 = v_{fr} \sin \delta_{fr} = v_2 \sin \delta_2 \quad (\text{A.30})$$

$$v_3 \sin \delta_3 = v_{re} \sin \delta_{re} = v_4 \sin \delta_4 \quad (\text{A.31})$$

The triangular relationships of these equations are shown in Fig. A.9.

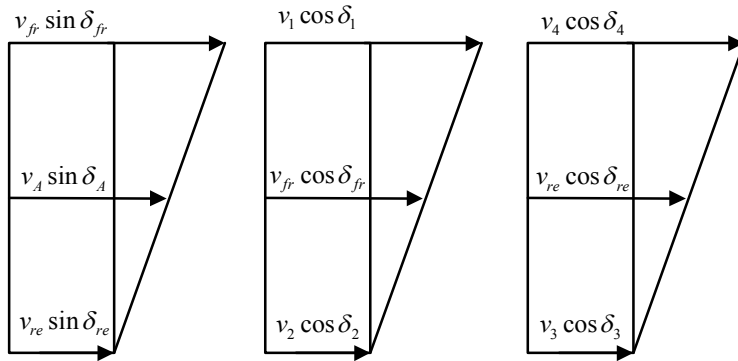


Fig. A.9 Triangular relationships

From the triangular relationships shown in Fig. A.9, the following equations are obtained.

$$v_A \sin \delta_A = \frac{v_{fr} \sin \delta_{fr} - v_{re} \sin \delta_{re}}{2} + v_{re} \sin \delta_{re} \quad (\text{A.32})$$

$$v_{fr} \cos \delta_{fr} = \frac{v_1 \cos \delta_1 - v_2 \cos \delta_2}{2} + v_2 \cos \delta_2 \quad (\text{A.33})$$

$$v_{re} \cos \delta_{re} = \frac{v_4 \cos \delta_4 - v_3 \cos \delta_3}{2} + v_3 \cos \delta_3 \quad (\text{A.34})$$

By simplification, these equations become as follows:

$$v_{fr} \sin \delta_{fr} - v_{re} \sin \delta_{re} = 2(v_A \sin \delta_A - v_{re} \sin \delta_{re}) = H\dot{\psi}_A \quad (\text{A.35})$$

$$v_1 \cos \delta_1 - v_2 \cos \delta_2 = 2(v_{fr} \cos \delta_{fr} - v_2 \cos \delta_2) = W\dot{\psi}_A \quad (\text{A.36})$$

$$v_4 \cos \delta_4 - v_3 \cos \delta_3 = 2(v_{re} \cos \delta_{re} - v_3 \cos \delta_3) = W\dot{\psi}_A \quad (\text{A.37})$$

By assuming that all angles δ_i , for $i = fr, A, re, 1, \dots, 4$ are limited to be less than $\pm\pi/2$ rad, velocities of each wheel can be formulated as follows:

$$v_1 = \frac{\dot{\psi}_A W \sin \delta_{fr}}{2 \sin(\delta_{fr} - \delta_1)} = \frac{(v_{fr} \cos \delta_{fr} - v_2 \cos \delta_2) \sin \delta_{fr}}{\sin(\delta_{fr} - \delta_1)} \quad (\text{A.38})$$

where $\delta_{fr} \neq \delta_1$

Then, the first part of Eq. (A.36) is obtained as follows:

$$\begin{aligned} v_1 \cos \delta_1 - v_2 \cos \delta_2 &= 2(v_{fr} \cos \delta_{fr} - v_2 \cos \delta_2) \\ \Leftrightarrow v_1 \cos \delta_1 - v_2 \cos \delta_2 &= 2v_{fr} \cos \delta_{fr} - 2v_2 \cos \delta_2 \\ \Leftrightarrow v_2 \cos \delta_2 &= 2v_{fr} \cos \delta_{fr} - v_1 \cos \delta_1 \end{aligned} \quad (\text{A.39})$$

By substituting Eq. (A.39) to Eq. (A.38), the following is obtained.

$$\begin{aligned} v_1 &= \frac{(v_{fr} \cos \delta_{fr} - (2v_{fr} \cos \delta_{fr} - v_1 \cos \delta_1)) \sin \delta_{fr}}{\sin(\delta_{fr} - \delta_1)} \\ &= \frac{(v_{fr} \cos \delta_{fr} - 2v_{fr} \cos \delta_{fr} + v_1 \cos \delta_1) \sin \delta_{fr}}{\sin(\delta_{fr} - \delta_1)} \\ &= \frac{(-v_{fr} \cos \delta_{fr} + v_1 \cos \delta_1) \sin \delta_{fr}}{\sin(\delta_{fr} - \delta_1)} \end{aligned} \quad (\text{A.40})$$

Then, substituting Eq. (A.29), $v_{fr} \cos \delta_{fr} = v_A \cos \delta_A$, to Eq. (A.40) yields:

$$v_1 = \frac{(-v_A \cos \delta_A + v_1 \cos \delta_1) \sin \delta_{fr}}{\sin(\delta_{fr} - \delta_1)} \quad (\text{A.41})$$

From Eq. (A.41), the following is obtained.

$$\begin{aligned} v_1 \sin(\delta_{fr} - \delta_1) &= (-v_A \cos \delta_A + v_1 \cos \delta_1) \sin \delta_{fr} \\ \Leftrightarrow v_1 (\sin \delta_{fr} \cos \delta_1 - \cos \delta_{fr} \sin \delta_1) &= (-v_A \cos \delta_A + v_1 \cos \delta_1) \sin \delta_{fr} \\ \Leftrightarrow v_1 \sin \delta_{fr} \cos \delta_1 - v_1 \cos \delta_{fr} \sin \delta_1 &= -v_A \cos \delta_A \sin \delta_{fr} + v_1 \cos \delta_1 \sin \delta_{fr} \\ \Leftrightarrow v_A \cos \delta_A \sin \delta_{fr} &= v_1 \cos \delta_1 \sin \delta_{fr} - v_1 \sin \delta_{fr} \cos \delta_1 + v_1 \cos \delta_{fr} \sin \delta_1 \\ \Leftrightarrow v_A \cos \delta_A \sin \delta_{fr} &= v_1 \cos \delta_{fr} \sin \delta_1 \\ \Leftrightarrow v_1 &= \frac{v_A \cos \delta_A \sin \delta_{fr}}{\cos \delta_{fr} \sin \delta_1} = v_A \cos \delta_A \tan \delta_{fr} \csc \delta_1 \end{aligned} \quad (\text{A.42})$$

where $\cos \delta_{fr} \sin \delta_1 \neq 0$

Substituting Eq. (A.24) to Eq. (A.42) yields

$$v_1 = \frac{v_A \tan \delta_{fr} \csc \delta_1}{\sqrt{\frac{1}{4} (\tan \delta_{fr} + \tan \delta_{re})^2 + 1}} \quad \text{for } \delta_{fr} \neq \delta_1, \cos \delta_{fr} \sin \delta_1 \neq 0 \quad (\text{A.43})$$

Likewise, v_2 , v_3 and v_4 can be obtained.

Using Eq. (A.24), Eq. (A.26) is as follows:

$$v_2 = \dot{\psi}_A r_{P2} = \frac{\dot{\psi}_A W \sin \delta_{fr}}{2 \sin(\delta_2 - \delta_{fr})} \quad \text{for } \delta_2 \neq \delta_{fr}$$

$$\begin{aligned}
&= \frac{2(v_{fr} \cos \delta_{fr} - v_2 \cos \delta_2) \sin \delta_{fr}}{2 \sin(\delta_2 - \delta_{fr})} \\
&= \frac{(v_A \cos \delta_A - v_2 \cos \delta_2) \sin \delta_{fr}}{\sin(\delta_2 - \delta_{fr})}
\end{aligned}$$

$$\begin{aligned}
&\Leftrightarrow v_2 \sin(\delta_2 - \delta_{fr}) = (v_A \cos \delta_A - v_2 \cos \delta_2) \sin \delta_{fr} \\
&\Leftrightarrow v_2 \sin \delta_2 \cos \delta_{fr} - v_2 \cos \delta_2 \sin \delta_{fr} = v_A \cos \delta_A \sin \delta_{fr} - v_2 \cos \delta_2 \sin \delta_{fr} \\
&\Leftrightarrow v_2 \sin \delta_2 \cos \delta_{fr} - v_2 \cos \delta_2 \sin \delta_{fr} + v_2 \cos \delta_2 \sin \delta_{fr} = v_A \cos \delta_A \sin \delta_{fr} \\
&\Leftrightarrow v_2 \sin \delta_2 \cos \delta_{fr} = v_A \cos \delta_A \sin \delta_{fr} \\
&\Leftrightarrow v_2 = \frac{v_A \cos \delta_A \sin \delta_{fr}}{\sin \delta_2 \cos \delta_{fr}} = v_A \cos \delta_A \tan \delta_{fr} \csc \delta_2
\end{aligned}$$

where $\sin \delta_2 \cos \delta_{fr} \neq 0$

$$v_2 = \frac{v_A \tan \delta_{fr} \csc \delta_2}{\sqrt{\frac{1}{4}(\tan \delta_{fr} + \tan \delta_{re})^2 + 1}} \quad \text{for } \delta_2 \neq \delta_{fr}, \sin \delta_2 \cos \delta_{fr} \neq 0 \quad (\text{A.44})$$

Using Eqs. (A.24) and (A.37), Eq. (A.27) is as follows:

$$\begin{aligned}
v_3 &= \dot{\psi}_A r_{P3} = \frac{\dot{\psi}_A W \sin \delta_{re}}{2 \sin(\delta_3 - \delta_{re})} \quad \text{for } \delta_3 \neq \delta_{re} \\
&= \frac{2(v_{re} \cos \delta_{re} - v_3 \cos \delta_3) \sin \delta_{re}}{2 \sin(\delta_3 - \delta_{re})} \\
&= \frac{(v_A \cos \delta_A - v_3 \cos \delta_3) \sin \delta_{re}}{\sin(\delta_3 - \delta_{re})}
\end{aligned}$$

$$\begin{aligned}
&\Leftrightarrow v_3 \sin(\delta_3 - \delta_{re}) = (v_A \cos \delta_A - v_3 \cos \delta_3) \sin \delta_{re} \\
&\Leftrightarrow v_3 \sin \delta_3 \cos \delta_{re} - v_3 \cos \delta_3 \sin \delta_{re} = v_A \cos \delta_A \sin \delta_{re} - v_3 \cos \delta_3 \sin \delta_{re}
\end{aligned}$$

$$\Leftrightarrow v_3 \sin \delta_3 \cos \delta_{re} - v_3 \cos \delta_3 \sin \delta_{re} + v_3 \cos \delta_3 \sin \delta_{re} = v_A \cos \delta_A \sin \delta_{re}$$

$$\Leftrightarrow v_3 \sin \delta_3 \cos \delta_{re} = v_A \cos \delta_A \sin \delta_{re}$$

$$\Leftrightarrow v_3 = \frac{v_A \cos \delta_A \sin \delta_{re}}{\sin \delta_3 \cos \delta_{re}} = v_A \cos \delta_A \tan \delta_{re} \csc \delta_3$$

where $\sin \delta_3 \cos \delta_{re} \neq 0$

$$v_3 = \frac{v_A \tan \delta_{re} \csc \delta_3}{\sqrt{\frac{1}{4}(\tan \delta_{fr} + \tan \delta_{re})^2 + 1}} \quad \text{for } \delta_3 \neq \delta_{re}, \sin \delta_3 \cos \delta_{re} \neq 0 \quad (\text{A.45})$$

Using Eqs. (A.24) and (A.37), Eq. (A.28) is as follows:

$$v_4 = \dot{\psi}_A r_{P4} = \frac{\dot{\psi}_A W \sin \delta_{re}}{2 \sin(\delta_{re} - \delta_4)} = \frac{2(v_{re} \cos \delta_{re} - v_3 \cos \delta_3) \sin \delta_{re}}{2 \sin(\delta_{re} - \delta_4)} \quad (\text{A.46})$$

where $\delta_{re} \neq \delta_4$

$$\Leftrightarrow v_4 \cos \delta_4 - v_3 \cos \delta_3 = 2(v_{re} \cos \delta_{re} - v_3 \cos \delta_3)$$

$$\Leftrightarrow v_4 \cos \delta_4 - v_3 \cos \delta_3 = 2v_{re} \cos \delta_{re} - 2v_3 \cos \delta_3$$

$$\Leftrightarrow v_3 \cos \delta_3 = 2v_{re} \cos \delta_{re} - v_4 \cos \delta_4 \quad (\text{A.47})$$

Substituting Eq. (A.47) into Eq. (A.46) yields:

$$\begin{aligned} v_4 &= \frac{(v_{re} \cos \delta_{re} - (2v_{re} \cos \delta_{re} - v_4 \cos \delta_4)) \sin \delta_{re}}{\sin(\delta_{re} - \delta_4)} \\ &= \frac{(v_{re} \cos \delta_{re} - 2v_{re} \cos \delta_{re} + v_4 \cos \delta_4) \sin \delta_{re}}{\sin(\delta_{re} - \delta_4)} \end{aligned}$$

$$= \frac{(-v_{re} \cos \delta_{re} + v_4 \cos \delta_4) \sin \delta_{re}}{\sin(\delta_{re} - \delta_4)}$$

$$= \frac{(-v_A \cos \delta_A + v_4 \cos \delta_4) \sin \delta_{re}}{\sin(\delta_{re} - \delta_4)}$$

$$\Leftrightarrow v_4 \sin(\delta_{re} - \delta_4) = (-v_A \cos \delta_A + v_4 \cos \delta_4) \sin \delta_{re}$$

$$\Leftrightarrow v_4 \sin \delta_{re} \cos \delta_4 - v_4 \cos \delta_{re} \sin \delta_4 = -v_A \cos \delta_A \sin \delta_{re} + v_4 \cos \delta_4 \sin \delta_{re}$$

$$\Leftrightarrow v_4 \cos \delta_4 \sin \delta_{re} - v_4 \sin \delta_{re} \cos \delta_4 + v_4 \cos \delta_{re} \sin \delta_4 = v_A \cos \delta_A \sin \delta_{re}$$

$$\Leftrightarrow v_4 \cos \delta_{re} \sin \delta_4 = v_A \cos \delta_A \sin \delta_{re}$$

$$v_4 = \frac{v_A \cos \delta_A \sin \delta_{re}}{\cos \delta_{re} \sin \delta_4}$$

where $\cos \delta_{re} \sin \delta_4 \neq 0$

$$v_4 = v_A \cos \delta_A \tan \delta_{re} \csc \delta_4$$

$$= \frac{v_A \tan \delta_{re} \csc \delta_4}{\sqrt{\frac{1}{4}(\tan \delta_{fr} + \tan \delta_{re})^2 + 1}} \quad \text{for } \delta_{re} \neq \delta_4, \cos \delta_{re} \sin \delta_4 \neq 0 \quad (\text{A.48})$$

Eqs. (A.43), (A.44), (A.45) and (A.48) can be written as

$$v_i = \begin{cases} \frac{v_A \tan \delta_{fr} \csc \delta_i}{\sqrt{1 + \frac{1}{4}(\tan \delta_{fr} + \tan \delta_{re})^2}}, & i = 1, 2; \cos \delta_{fr} \sin \delta_i \neq 0, \delta_i \neq \delta_{fr} \\ \frac{v_A \tan \delta_{re} \csc \delta_i}{\sqrt{1 + \frac{1}{4}(\tan \delta_{fr} + \tan \delta_{re})^2}}, & i = 3, 4; \cos \delta_{re} \sin \delta_i \neq 0, \delta_i \neq \delta_{re} \end{cases} \quad (2.10)$$

E.O.D.

Appendix B: Proof of Eqs. (2.12) - (2.15)

Eq. (A.18) and Eq. (A.22) are as follows:

$$r_{PB} = \frac{W \sin \delta_1}{2 \sin(\delta_{fr} - \delta_1)} \quad (\text{A.18})$$

$$r_{PB} = \frac{H \cos \delta_{re}}{\sin(\delta_{fr} - \delta_{re})} \quad (\text{A.22})$$

where $\delta_1 \neq \delta_{fr}$ and $\delta_{fr} \neq \delta_{re}$

From Eqs. (A.18) and (A.22), the followings are obtained:

$$\begin{aligned} \frac{H \cos \delta_{re}}{\sin(\delta_{fr} - \delta_{re})} &= \frac{W \sin \delta_1}{2 \sin(\delta_{fr} - \delta_1)} \\ \Leftrightarrow \frac{2H}{W} \cos \delta_{re} \sin(\delta_{fr} - \delta_1) &= \sin \delta_1 \sin(\delta_{fr} - \delta_{re}) \\ \Leftrightarrow \frac{2H}{W} \cos \delta_{re} \sin \delta_{fr} \cos \delta_1 - \frac{2H}{W} \cos \delta_{re} \cos \delta_{fr} \sin \delta_1 &= \sin \delta_1 \sin \delta_{fr} \cos \delta_{re} \\ &\quad - \sin \delta_1 \cos \delta_{fr} \sin \delta_{re} \\ \Leftrightarrow \frac{2H}{W} \cos \delta_{re} \sin \delta_{fr} \cos \delta_1 &= \sin \delta_1 \sin \delta_{fr} \cos \delta_{re} - \sin \delta_1 \cos \delta_{fr} \sin \delta_{re} \\ &\quad + \frac{2H}{W} \cos \delta_{re} \cos \delta_{fr} \sin \delta_1 \\ \Leftrightarrow \frac{2H}{W} \cos \delta_{re} \sin \delta_{fr} \cos \delta_1 & \\ &= \sin \delta_1 \left(\sin \delta_{fr} \cos \delta_{re} - \cos \delta_{fr} \sin \delta_{re} + \frac{2H}{W} \cos \delta_{re} \cos \delta_{fr} \right) \end{aligned}$$

$$\Leftrightarrow \frac{\cos \delta_1}{\sin \delta_1} = \frac{\sin \delta_{fr} \cos \delta_{re} - \cos \delta_{fr} \sin \delta_{re} + \frac{2H}{W} \cos \delta_{re} \cos \delta_{fr}}{\frac{2H}{W} \cos \delta_{re} \sin \delta_{fr}}$$

where $\sin \delta_1 \neq 0$ and $\cos \delta_{re} \sin \delta_{fr} \neq 0$

$$\Leftrightarrow \cot \delta_1 = \frac{W}{2H} - \frac{W}{2H} \cot \delta_{fr} \tan \delta_{re} + \cot \delta_{fr}$$

$$\cot \delta_1 = \cot \delta_{fr} + \frac{W}{2H} \cot \delta_{fr} (\tan \delta_{fr} - \tan \delta_{re}) \quad (\text{B.1})$$

Substituting $W = 2b$ and $H = l_{fr} + l_{re}$ into Eq. (B.1) and taking inverse cotangent of the angle δ_1 , this equation becomes

$$\delta_1 = \cot^{-1} \left(\cot \delta_{fr} + \frac{b}{l_{fr} + l_{re}} \cot \delta_{fr} [\tan \delta_{fr} - \tan \delta_{re}] \right) \quad (2.12)$$

for $\delta_1 \neq \delta_{fr}$, $\delta_{fr} \neq \delta_{re}$, $\sin \delta_1 \neq 0$, $\cos \delta_{re} \sin \delta_{fr} \neq 0$

Eqs. (A.20) and (A.22) are as follows:

$$r_{PB} = \frac{W \sin \delta_2}{2 \sin(\delta_2 - \delta_{fr})} \quad (\text{A.20})$$

$$r_{PB} = \frac{H \cos \delta_{re}}{\sin(\delta_{fr} - \delta_{re})} \quad (\text{A.22})$$

where $\delta_2 \neq \delta_{fr}$ and $\delta_{fr} \neq \delta_{re}$

From Eqs. (A.20) and (A.22), the followings are obtained:

$$\frac{H \cos \delta_{re}}{\sin(\delta_{fr} - \delta_{re})} = \frac{W \sin \delta_2}{2 \sin(\delta_2 - \delta_{fr})}$$

$$\Leftrightarrow \frac{2H}{W} \cos \delta_{re} \sin(\delta_2 - \delta_{fr}) = \sin \delta_2 \sin(\delta_{fr} - \delta_{re}) \quad (\text{B.2})$$

$$\Leftrightarrow \frac{2H}{W} \cos \delta_{re} \sin \delta_2 \cos \delta_{fr} - \frac{2H}{W} \cos \delta_{re} \cos \delta_2 \sin \delta_{fr} = \sin \delta_2 \sin \delta_{fr} \cos \delta_{re} - \sin \delta_2 \cos \delta_{fr} \sin \delta_{re}$$

$$\Leftrightarrow \frac{2H}{W} \cos \delta_{re} \sin \delta_2 \cos \delta_{fr} - \sin \delta_2 \sin \delta_{fr} \cos \delta_{re} + \sin \delta_2 \cos \delta_{fr} \sin \delta_{re}$$

$$= \frac{2H}{W} \cos \delta_{re} \cos \delta_2 \sin \delta_{fr}$$

$$\Leftrightarrow \sin \delta_2 \left(\frac{2H}{W} \cos \delta_{re} \cos \delta_{fr} - \sin \delta_{fr} \cos \delta_{re} + \cos \delta_{fr} \sin \delta_{re} \right)$$

$$= \frac{2H}{W} \cos \delta_{re} \cos \delta_2 \sin \delta_{fr}$$

$$\Leftrightarrow \frac{\cos \delta_2}{\sin \delta_2} = \frac{\frac{2H}{W} \cos \delta_{re} \cos \delta_{fr} - \sin \delta_{fr} \cos \delta_{re} + \cos \delta_{fr} \sin \delta_{re}}{\frac{2H}{W} \cos \delta_{re} \sin \delta_{fr}}$$

where $\sin \delta_2 \neq 0$ and $\cos \delta_{re} \sin \delta_{fr} \neq 0$

$$\Leftrightarrow \cot \delta_2 = \cot \delta_{fr} - \frac{W}{2H} + \frac{W}{2H} \cot \delta_{fr} \tan \delta_{re}$$

$$= \cot \delta_{fr} - \frac{W}{2H} \cot \delta_{fr} (\tan \delta_{fr} - \tan \delta_{re}) \quad (\text{B.2})$$

Substituting $W = 2b$ and $H = l_{fr} + l_{re}$ into Eq. (B.2) and taking inverse cotangent of the angle δ_2 , this equation becomes

$$\delta_2 = \cot^{-1} \left(\cot \delta_{fr} - \frac{b}{l_{fr} + l_{re}} \cot \delta_{fr} \left[\tan \delta_{fr} - \tan \delta_{re} \right] \right) \quad (2.13)$$

for $\delta_2 \neq \delta_{fr}$, $\delta_{fr} \neq \delta_{re}$, $\sin \delta_2 \neq 0$, $\cos \delta_{re} \sin \delta_{fr} \neq 0$

Eqs. (A.16) and (A.21) are as follows:

$$r_{PC} = \frac{W \sin \delta_3}{2 \sin(\delta_3 - \delta_{re})} \quad (A.16)$$

$$r_{PC} = \frac{H \cos \delta_{fr}}{\sin(\delta_{fr} - \delta_{re})} \quad (A.21)$$

where $\delta_3 \neq \delta_{fr}$ and $\delta_{fr} \neq \delta_{re}$

From Eqs. (A.16) and (A.21), the followings are obtained:

$$\begin{aligned} \frac{H \cos \delta_{fr}}{\sin(\delta_{fr} - \delta_{re})} &= \frac{W \sin \delta_3}{2 \sin(\delta_3 - \delta_{re})} \\ \Leftrightarrow \frac{2H}{W} \cos \delta_{fr} \sin(\delta_3 - \delta_{re}) &= \sin \delta_3 \sin(\delta_{fr} - \delta_{re}) \\ \Leftrightarrow \frac{2H}{W} \cos \delta_{fr} \sin \delta_3 \cos \delta_{re} - \frac{2H}{W} \cos \delta_{fr} \cos \delta_3 \sin \delta_{re} &= \sin \delta_3 \sin \delta_{fr} \cos \delta_{re} \\ &\quad - \sin \delta_3 \cos \delta_{fr} \sin \delta_{re} \end{aligned}$$

$$\Leftrightarrow \frac{2H}{W} \cos \delta_{fr} \sin \delta_3 \cos \delta_{re} - \sin \delta_3 \sin \delta_{fr} \cos \delta_{re} + \sin \delta_3 \cos \delta_{fr} \sin \delta_{re} =$$

$$\frac{2H}{W} \cos \delta_{fr} \cos \delta_3 \sin \delta_{re}$$

$$\Leftrightarrow \sin \delta_3 \left(\frac{2H}{W} \cos \delta_{fr} \cos \delta_{re} - \sin \delta_{fr} \cos \delta_{re} + \cos \delta_{fr} \sin \delta_{re} \right) =$$

$$\frac{2H}{W} \cos \delta_{fr} \cos \delta_3 \sin \delta_{re}$$

$$\Leftrightarrow \frac{\cos \delta_3}{\sin \delta_3} = \frac{\frac{2H}{W} \cos \delta_{fr} \cos \delta_{re} - \sin \delta_{fr} \cos \delta_{re} + \cos \delta_{fr} \sin \delta_{re}}{\frac{2H}{W} \cos \delta_{fr} \sin \delta_{re}}$$

where $\sin \delta_3 \neq 0$ and $\cos \delta_{fr} \sin \delta_{re} \neq 0$

$$\Leftrightarrow \cot \delta_3 = \cot \delta_{re} - \frac{W}{2H} \tan \delta_{fr} \cot \delta_{re} + \frac{W}{2H}$$

$$= \cot \delta_{re} - \frac{W}{2H} \cot \delta_{re} (\tan \delta_{fr} - \tan \delta_{re}) \quad (B.3)$$

Substituting $W = 2b$ and $H = l_{fr} + l_{re}$ into Eq. (B.3) and taking inverse cotangent of the angle δ_3 , this equation becomes

$$\delta_3 = \cot^{-1} \left(\cot \delta_{re} - \frac{b}{l_{fr} + l_{re}} \cot \delta_{re} [\tan \delta_{fr} - \tan \delta_{re}] \right) \quad (2.14)$$

for $\delta_3 \neq \delta_{re}$, $\delta_{fr} \neq \delta_{re}$, $\sin \delta_3 \neq 0$, $\cos \delta_{fr} \sin \delta_{re} \neq 0$

Eqs. (A.14) and (A.22) are as follows:

$$r_{PC} = \frac{W \sin \delta_4}{2 \sin(\delta_{re} - \delta_4)} \quad (\text{A.14})$$

$$r_{PC} = \frac{H \cos \delta_{fr}}{\sin(\delta_{fr} - \delta_{re})} \quad (\text{A.22})$$

where $\delta_4 \neq \delta_{re}$ and $\delta_{fr} \neq \delta_{re}$

From Eqs. (A.14) and (A.22), the followings are obtained:

$$\begin{aligned} \frac{H \cos \delta_{fr}}{\sin(\delta_{fr} - \delta_{re})} &= \frac{W \sin \delta_4}{2 \sin(\delta_{re} - \delta_4)} \\ \Leftrightarrow \frac{2H}{W} \cos \delta_{fr} \sin(\delta_{re} - \delta_4) &= \sin \delta_4 \sin(\delta_{fr} - \delta_{re}) \\ \Leftrightarrow \frac{2H}{W} \cos \delta_{fr} \sin \delta_{re} \cos \delta_4 - \frac{2H}{W} \cos \delta_{fr} \cos \delta_{re} \sin \delta_4 &= \sin \delta_4 \sin \delta_{fr} \cos \delta_{re} \\ &\quad - \sin \delta_4 \cos \delta_{fr} \sin \delta_{re} \\ \Leftrightarrow \frac{2H}{W} \cos \delta_{fr} \sin \delta_{re} \cos \delta_4 &= \sin \delta_4 \sin \delta_{fr} \cos \delta_{re} - \sin \delta_4 \cos \delta_{fr} \sin \delta_{re} \\ &\quad + \frac{2H}{W} \cos \delta_{fr} \cos \delta_{re} \sin \delta_4 \\ \Leftrightarrow \frac{2H}{W} \cos \delta_{fr} \sin \delta_{re} \cos \delta_4 &= \\ &\quad \sin \delta_4 \left(\sin \delta_{fr} \cos \delta_{re} - \cos \delta_{fr} \sin \delta_{re} + \frac{2H}{W} \cos \delta_{fr} \cos \delta_{re} \right) \\ \Leftrightarrow \frac{\cos \delta_4}{\sin \delta_4} &= \frac{\sin \delta_{fr} \cos \delta_{re} - \cos \delta_{fr} \sin \delta_{re} + \frac{2H}{W} \cos \delta_{fr} \cos \delta_{re}}{\frac{2H}{W} \cos \delta_{fr} \sin \delta_{re}} \end{aligned}$$

where $\sin \delta_4 \neq 0$ and $\cos \delta_{fr} \sin \delta_{re} \neq 0$

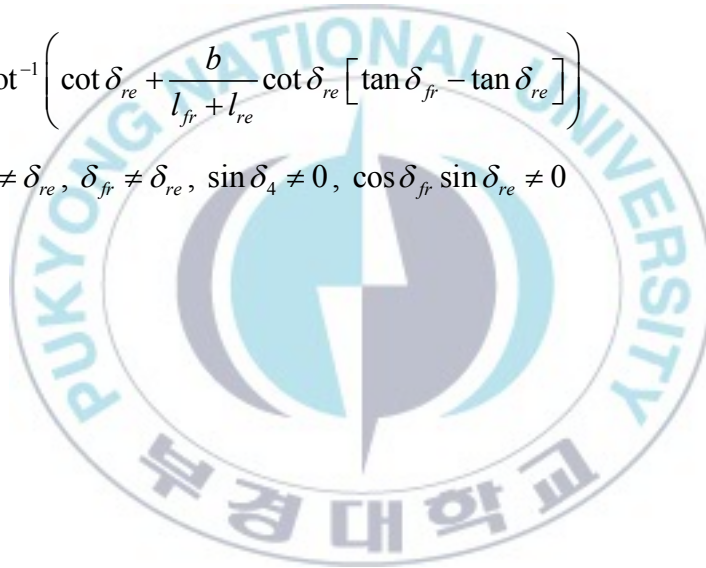
$$\begin{aligned} \Leftrightarrow \cot \delta_4 &= \frac{W}{2H} \tan \delta_{fr} \cot \delta_{re} - \frac{W}{2H} + \cot \delta_{re} \\ &= \cot \delta_{re} + \frac{W}{2H} \cot \delta_{re} (\tan \delta_{fr} - \tan \delta_{re}) \end{aligned} \quad (\text{B.4})$$

Substituting $W = 2b$ and $H = l_{fr} + l_{re}$ into Eq. (B.4) and taking inverse cotangent of the angle δ_4 , this equation becomes

$$\delta_4 = \cot^{-1} \left(\cot \delta_{re} + \frac{b}{l_{fr} + l_{re}} \cot \delta_{re} [\tan \delta_{fr} - \tan \delta_{re}] \right) \quad (2.15)$$

for $\delta_4 \neq \delta_{re}$, $\delta_{fr} \neq \delta_{re}$, $\sin \delta_4 \neq 0$, $\cos \delta_{fr} \sin \delta_{re} \neq 0$

E.O.D.



Appendix C: Proof of Eqs. (2.53) and (2.54)

Steering angles of the front and rear wheels of the vehicle in the single-track vehicle model can be obtained using Eqs. (2.44) and (2.45) as follows:

$$\beta_A = \tan^{-1} \left(\frac{l_{fr} \tan \delta_{re} + l_{re} \tan \delta_{fr}}{l_{fr} + l_{re}} \right) \quad (2.45)$$

$$\Leftrightarrow (l_{fr} + l_{re}) \tan \beta_A = l_{fr} \tan \delta_{re} + l_{re} \tan \delta_{fr}$$

$$\Leftrightarrow (l_{fr} + l_{re}) \tan \beta_A - l_{re} \tan \delta_{fr} = l_{fr} \tan \delta_{re}$$

$$\delta_{re} = \tan^{-1} \left(\frac{(l_{fr} + l_{re}) \tan \beta_A - l_{re} \tan \delta_{fr}}{l_{fr}} \right) \quad (C.1)$$

In zero-sideslip maneuver, $\beta_A = 0$, thus Eq. (C.1) becomes

$$\delta_{re} = \tan^{-1} \left(\frac{-l_{re} \tan \delta_{fr}}{l_{fr}} \right) \quad (2.53)$$

Then, by using Eq. (2.44), δ_{fr} can be calculated as follows:

$$\dot{\psi}_A = \frac{v_A \cos \beta_A (\tan \delta_{fr} - \tan \delta_{re})}{l_{fr} + l_{re}} \quad (2.44)$$

$$\Leftrightarrow \tan \delta_{fr} - \tan \delta_{re} = \frac{\dot{\psi}_A (l_{fr} + l_{re})}{v_A \cos \beta_A} \quad (C.2)$$

where $v_A \cos \beta_A \neq 0$

Substituting Eq. (C.1) to Eq. (C.2) yields

$$\begin{aligned}
 \tan \delta_{fr} - \tan \left(\tan^{-1} \left(\frac{(l_{fr} + l_{re}) \tan \beta_A - l_{re} \tan \delta_{fr}}{l_{fr}} \right) \right) &= \frac{\dot{\psi}_A (l_{fr} + l_{re})}{v_A \cos \beta_A} \\
 \Leftrightarrow \tan \delta_{fr} - \left(\frac{(l_{fr} + l_{re}) \tan \beta_A - l_{re} \tan \delta_{fr}}{l_{fr}} \right) &= \frac{\dot{\psi}_A (l_{fr} + l_{re})}{v_A \cos \beta_A} \\
 \Leftrightarrow \tan \delta_{fr} - \frac{(l_{fr} + l_{re}) \tan \beta_A}{l_{fr}} + \frac{l_{re}}{l_{fr}} \tan \delta_{fr} &= \frac{\dot{\psi}_A (l_{fr} + l_{re})}{v_A \cos \beta_A} \\
 \Leftrightarrow \left(1 + \frac{l_{re}}{l_{fr}} \right) \tan \delta_{fr} - \frac{(l_{fr} + l_{re}) \tan \beta_A}{l_{fr}} &= \frac{\dot{\psi}_A (l_{fr} + l_{re})}{v_A \cos \beta_A} \\
 \Leftrightarrow \left(\frac{l_{re} + l_{fr}}{l_{fr}} \right) \tan \delta_{fr} - \frac{(l_{fr} + l_{re}) \tan \beta_A}{l_{fr}} &= \frac{\dot{\psi}_A (l_{fr} + l_{re})}{v_A \cos \beta_A} \\
 \Leftrightarrow \left(\frac{l_{re} + l_{fr}}{l_{fr}} \right) (\tan \delta_{fr} - \tan \beta_A) &= \frac{\dot{\psi}_A (l_{fr} + l_{re})}{v_A \cos \beta_A} \\
 \Leftrightarrow \tan \delta_{fr} - \tan \beta_A &= \frac{\dot{\psi}_A l_{fr}}{v_A \cos \beta_A} \\
 \Leftrightarrow \tan \delta_{fr} &= \frac{\dot{\psi}_A l_{fr}}{v_A \cos \beta_A} + \tan \beta_A \\
 \Leftrightarrow \delta_{fr} &= \tan^{-1} \left(\frac{\dot{\psi}_A l_{fr}}{v_A \cos \beta_A} + \tan \beta_A \right) \tag{C.2}
 \end{aligned}$$

In zero-sideslip maneuver, $\beta_A = 0$, thus Eq. (C.2) becomes

$$\delta_{fr} = \tan^{-1} \left(\frac{\dot{\psi}_A l_{fr}}{v_A} \right) \tag{2.54}$$

for $v_A \neq 0$

E.O.D.

Appendix D: Proof of Eq. (2.62)

From Eq. (2.56), the following is obtained as:

$$e_1 = (X_A - X_R) \cos \psi_A + (Y_A - Y_R) \sin \psi_A \quad (D.1)$$

From Eq. (D.1), the time derivative of e_1 is reduced as:

$$\begin{aligned} \dot{e}_1 &= (\dot{X}_A - \dot{X}_R) \cos \psi_A + (\dot{Y}_A - \dot{Y}_R) \sin \psi_A \\ &\quad - (X_A - X_R) \dot{\psi}_A \sin \psi_A + (Y_A - Y_R) \dot{\psi}_A \cos \psi_A \\ &= \dot{X}_A \cos \psi_A - \dot{X}_R \cos \psi_A + \dot{Y}_A \sin \psi_A \\ &\quad - \dot{Y}_R \sin \psi_A + \dot{\psi}_A \{ -(X_A - X_R) \sin \psi_A + (Y_A - Y_R) \cos \psi_A \} \\ &= (\dot{X}_A \cos \psi_A + \dot{Y}_A \sin \psi_A) - \dot{X}_R \cos \psi_A - \dot{Y}_R \sin \psi_A + \dot{\psi}_A e_2 \end{aligned} \quad (D.2)$$

From Eq. (2.57), following is obtained as:

$$e_3 = \psi_A - \psi_R \rightarrow \dot{\psi}_A = \dot{\psi}_R + \dot{e}_3 \quad (D.3)$$

From Eq. (D.3), Eq. (D.2) is reduced into:

$$\begin{aligned} \dot{e}_1 &= v_A + \dot{\psi}_A e_2 - \dot{X}_R \cos(\psi_R + e_3) - \dot{Y}_R \sin(\psi_R + e_3) \\ &= v_A + \dot{\psi}_A e_2 - \dot{X}_R (\cos \psi_R \cos e_3 - \sin \psi_R \sin e_3) \\ &\quad - \dot{Y}_R (\sin \psi_R \cos e_3 + \cos \psi_R \sin e_3) \\ &= v_A + \dot{\psi}_A e_2 - \dot{X}_R \cos \psi_R \cos e_3 + \dot{X}_R \sin \psi_R \sin e_3 \\ &\quad - \dot{Y}_R \sin \psi_R \cos e_3 - \dot{Y}_R \cos \psi_R \sin e_3 \\ &= v_A + \dot{\psi}_A e_2 - \cos e_3 (\dot{X}_R \cos \psi_R + \dot{Y}_R \sin \psi_R) \end{aligned}$$

$$+ \sin e_3 (\dot{X}_R \sin \psi_R - \dot{Y}_R \cos \psi_R) \quad (D.4)$$

Recalling that Eq. (2.55) and Eq. (2.61), Eq. (D.4) becomes

$$\dot{e}_1 = v_A + \dot{\psi}_A e_2 - v_R \cos e_3 \quad (D.5)$$

In the same way, the derivatives of e_2 , e_3 and e_4 can be obtained. From Eq. (2.57), the following is obtained as:

$$e_2 = -(X_A - X_R) \sin \psi_A + (Y_A - Y_R) \cos \psi_A \quad (D.6)$$

From Eqs. (2.55), (2.57) and (2.61), the time derivative of Eq. (D.6) is reduced into:

$$\begin{aligned} \dot{e}_2 &= -(\dot{X}_A - \dot{X}_R) \sin \psi_A + (\dot{Y}_A - \dot{Y}_R) \cos \psi_A \\ &\quad - (X_A - X_R) \dot{\psi}_A \cos \psi_A - (Y_A - Y_R) \dot{\psi}_A \sin \psi_A \\ &= -\dot{X}_A \sin \psi_A + \dot{X}_R \sin \psi_A + \dot{Y}_A \cos \psi_A - \dot{Y}_R \cos \psi_A \\ &\quad - \dot{\psi}_A \{ (X_A - X_R) \cos \psi_A + (Y_A - Y_R) \sin \psi_A \} \\ &= (-\dot{X}_A \sin \psi_A + \dot{Y}_A \cos \psi_A) + \dot{X}_R \sin \psi_A - \dot{Y}_R \cos \psi_A - \dot{\psi}_A e_1 \\ &= \dot{X}_R \sin(\psi_R + e_3) - \dot{Y}_R \cos(\psi_R + e_3) - \dot{\psi}_A e_1 \\ &= \dot{X}_R (\sin \psi_R \cos e_3 + \cos \psi_R \sin e_3) \\ &\quad - \dot{Y}_R (\cos \psi_R \cos e_3 - \sin \psi_R \sin e_3) - \dot{\psi}_A e_1 \\ &= \dot{X}_R \sin \psi_R \cos e_3 + \dot{X}_R \cos \psi_R \sin e_3 \\ &\quad - \dot{Y}_R \cos \psi_R \cos e_3 + \dot{Y}_R \sin \psi_R \sin e_3 - \dot{\psi}_A e_1 \\ &= \cos e_3 (\dot{X}_R \sin \psi_R - \dot{Y}_R \cos \psi_R) + \sin e_3 (\dot{X}_R \cos \psi_R + \dot{Y}_R \sin \psi_R) - \dot{\psi}_A e_1 \\ &= v_R \sin e_3 - \dot{\psi}_A e_1 \quad (D.7) \end{aligned}$$

From Eqs. (2.58) and (2.59), the followings are obtained as:

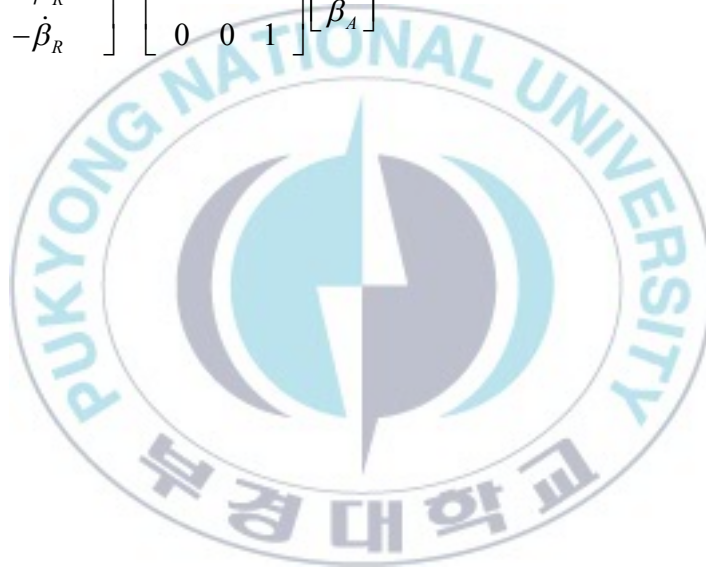
$$\dot{e}_3 = \dot{\psi}_A - \dot{\psi}_R \quad (D.8)$$

$$\dot{e}_4 = \dot{\beta}_A - \dot{\beta}_R \quad (D.9)$$

Eqs. (D.5), (D.7) - (D.9) can be written in vector form as follows:

$$\dot{\mathbf{e}} = \begin{bmatrix} -v_R \cos e_3 \\ v_R \sin e_3 \\ -\dot{\psi}_R \\ -\dot{\beta}_R \end{bmatrix} + \begin{bmatrix} 1 & e_2 & 0 \\ 0 & -e_1 & 0 \\ 0 & 1 & 0 \\ 0 & 0 & 1 \end{bmatrix} \begin{bmatrix} v_A \\ \dot{\psi}_A \\ \dot{\beta}_A \end{bmatrix} \quad (2.62)$$

E.O.D.



Appendix E: Mechanical design drawing

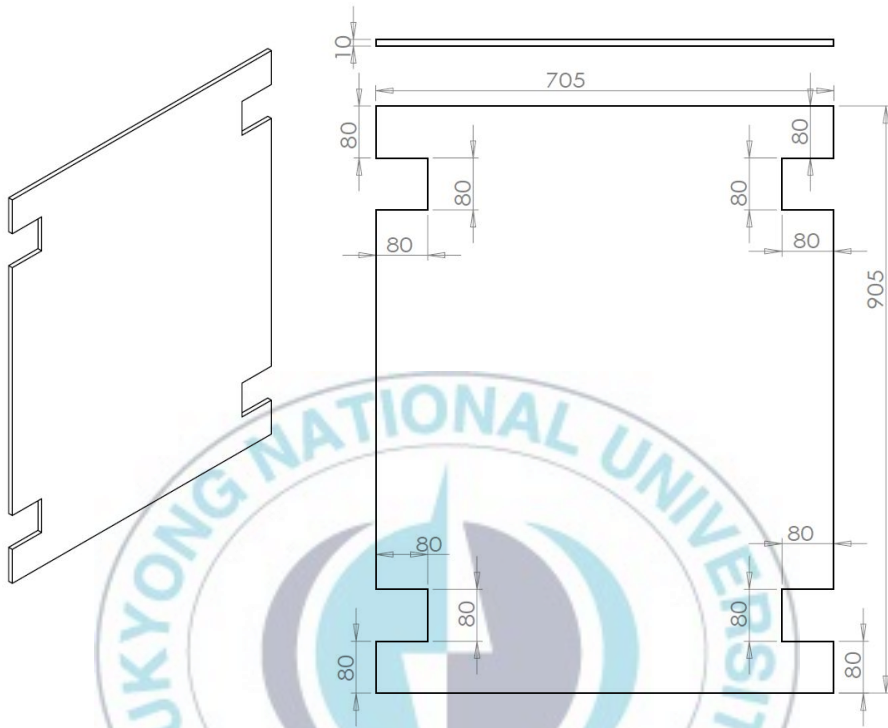


Fig. E.1 Body plate

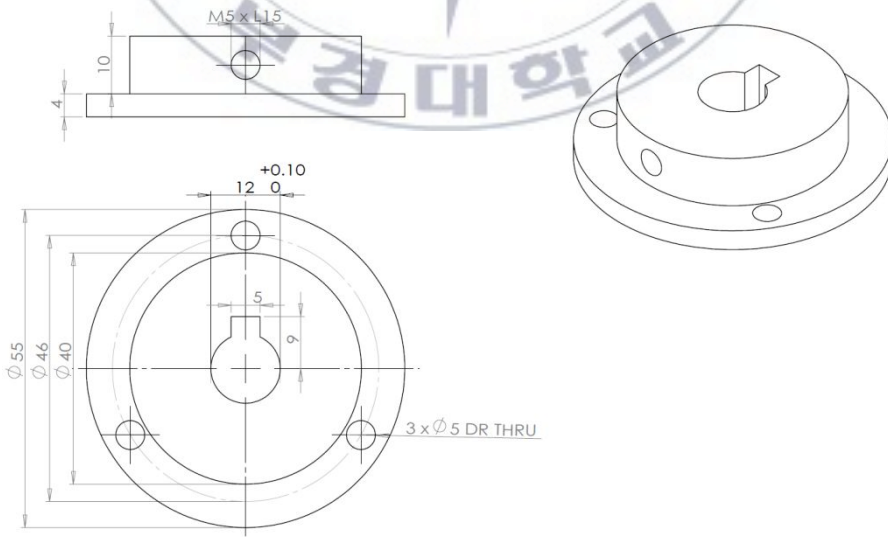


Fig. E.2 Wheel hub

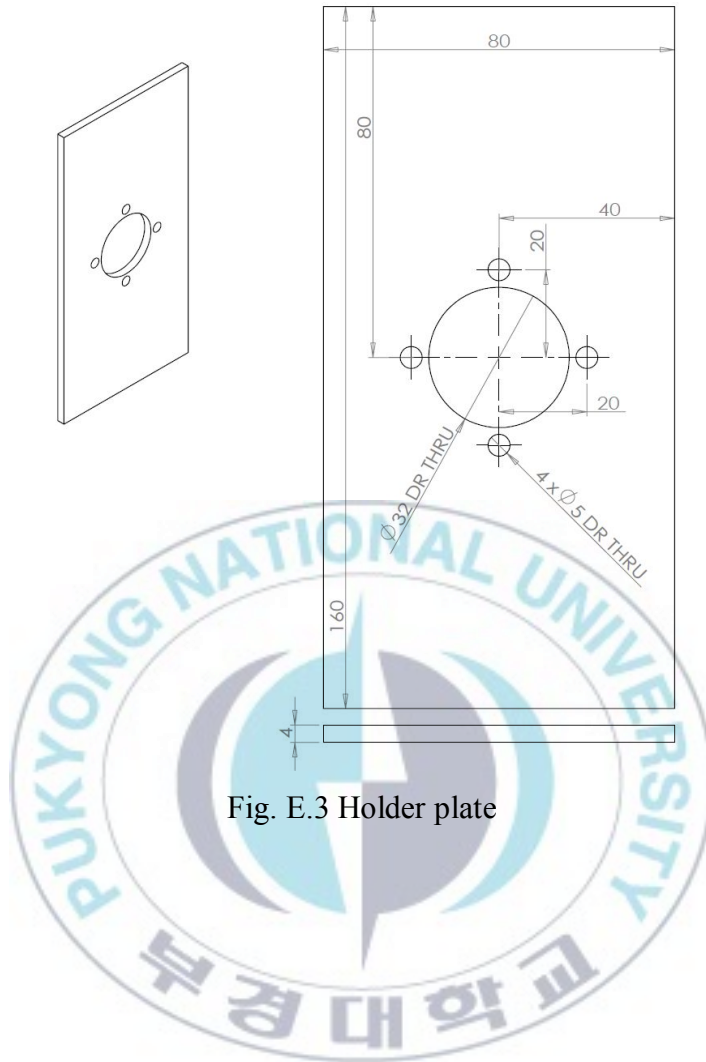


Fig. E.3 Holder plate

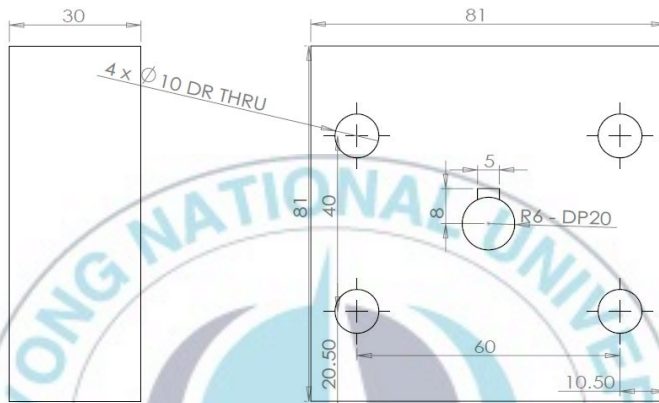
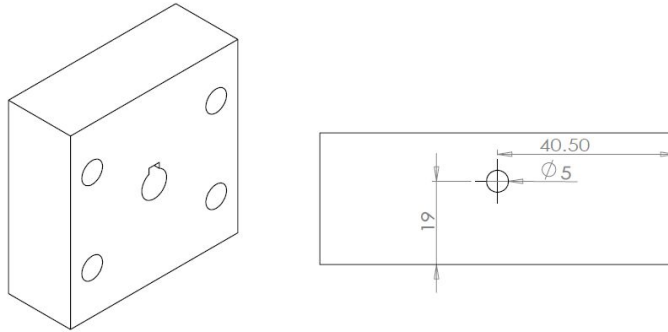
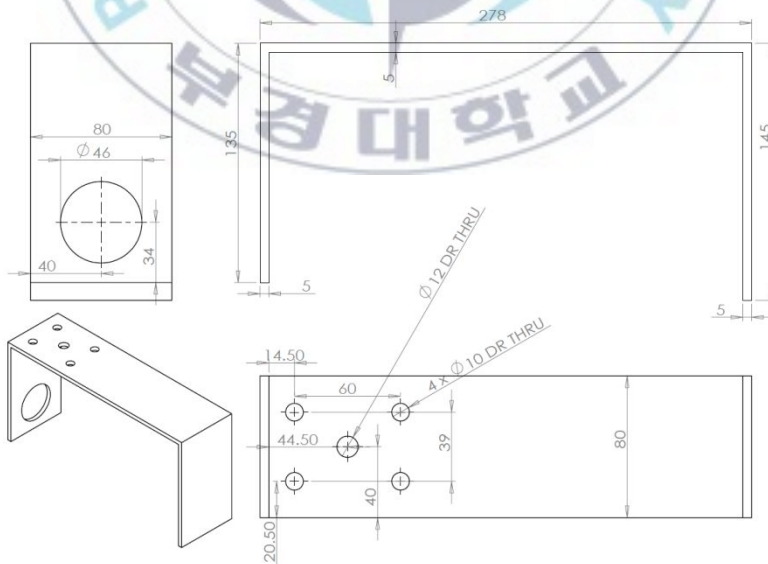
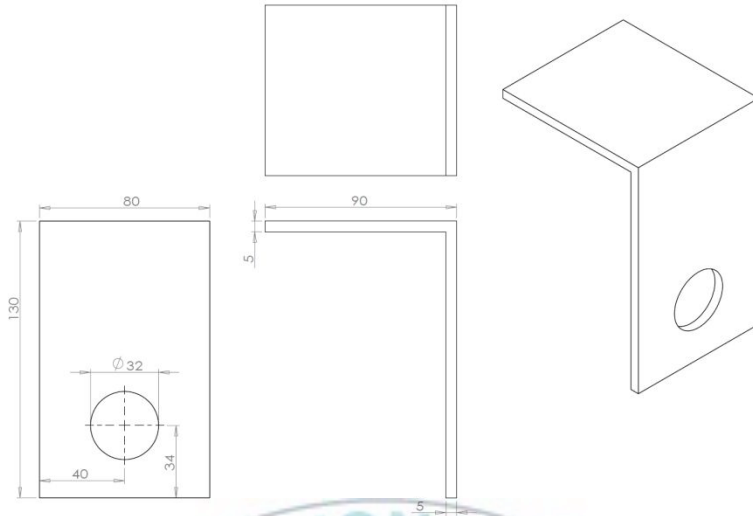


Fig. E.4 Nylon plate



(a) Plate A



(b) Plate B

Fig. E.5 Steering steel plate

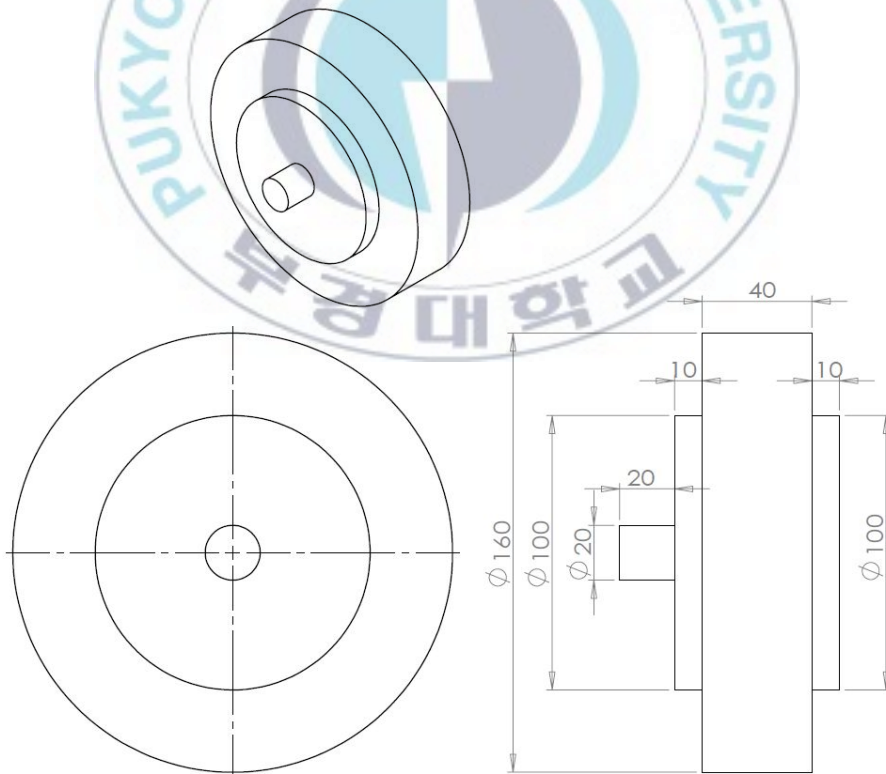


Fig. E.6 Nylon wheel

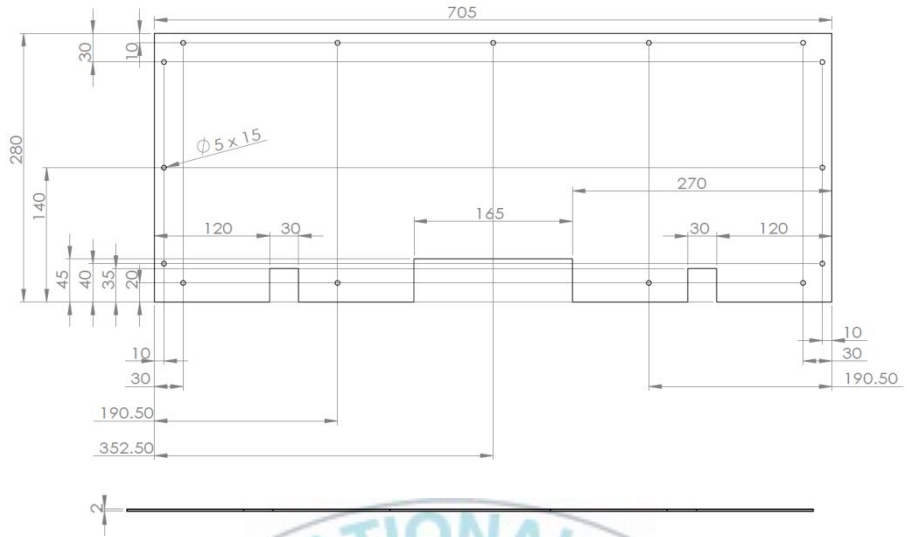


Fig. E.7 Front cover plate

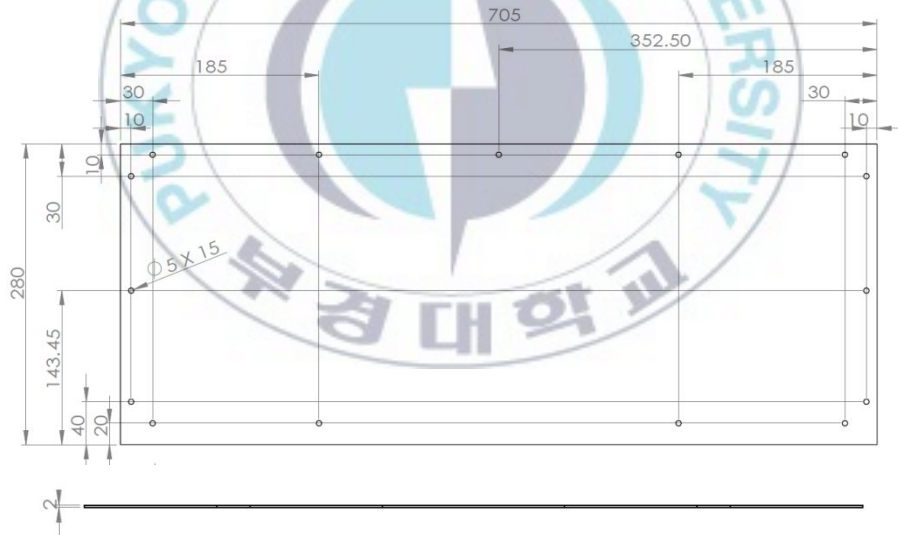


Fig. E.8 Rear cover plate

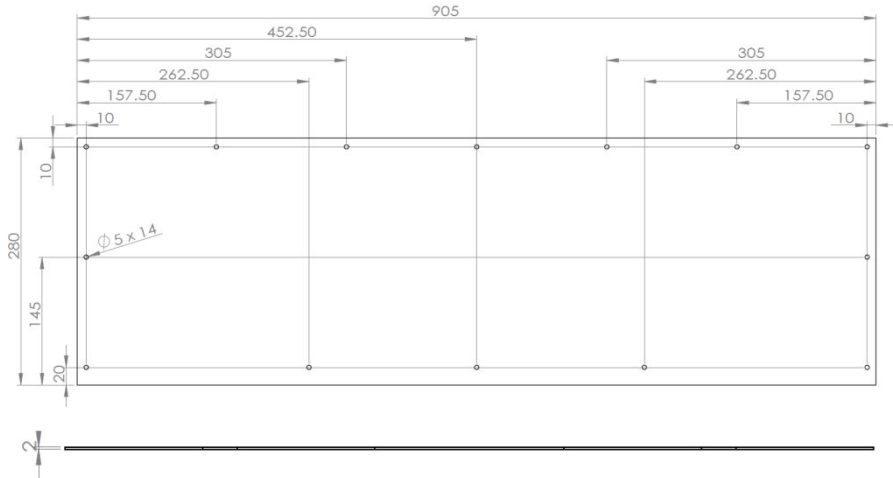


Fig. E.9 Side cover plate

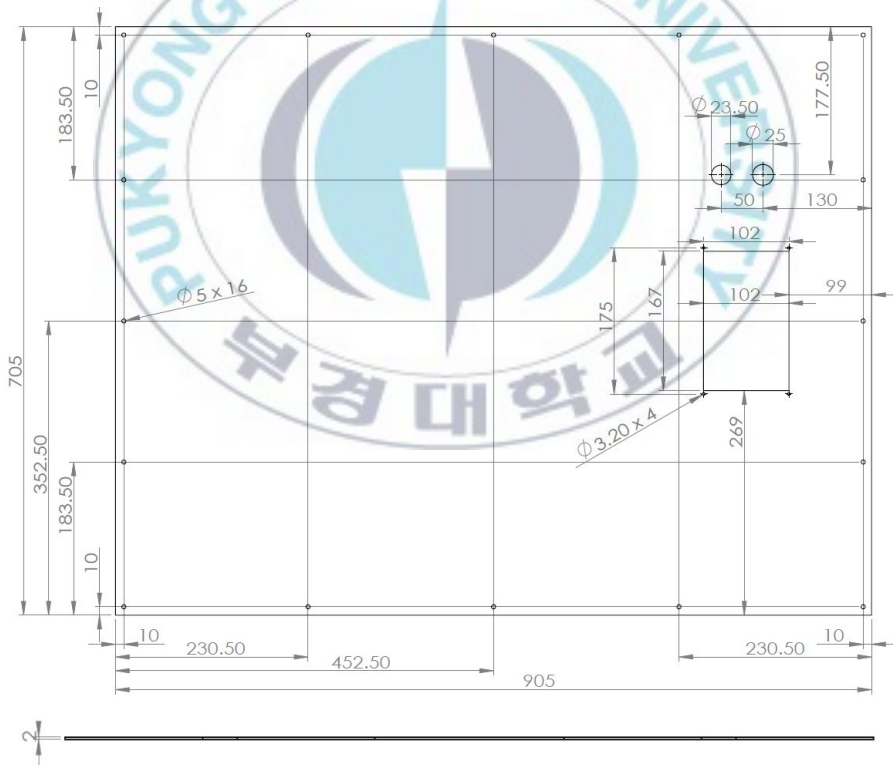


Fig. E.10 Top cover plate